AD-759 118

ANALYSIS OF MH-1A LOSS OF COOLANT ACCIDENT

Henry C. Gignilliat, et al

Army Engineer Reactors Group Group
Fort Belvoir, Virginia

9 November 1972

DISCLAIMER NOTICE

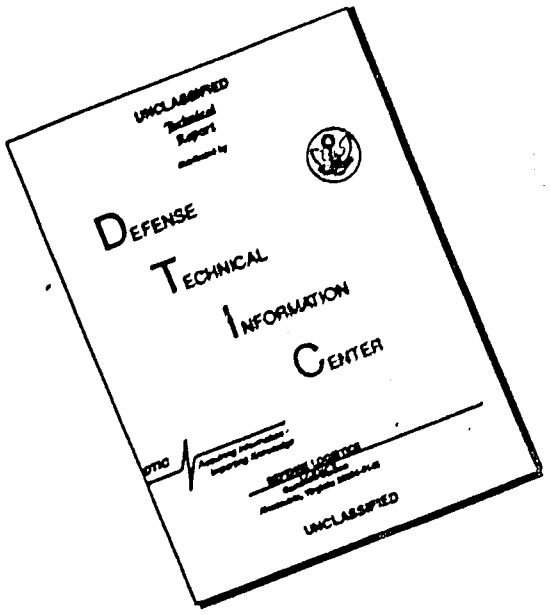

THIS DOCUMENT IS BEST QUALITY AVAILABLE. THE COPY FURNISHED TO DTIC CONTAINED A SIGNIFICANT NUMBER OF PAGES WHICH DO NOT REPRODUCE LEGIBLY.

ENGINEERING DIVISION
U.S. ARMY ENGINEER REACTORS GROUP
CORPS OF ENGINEERS
FT. BELVOIR, VA. 22060

ED-7212

ANALYSIS OF MH-1A LOSS OF COOLANT ACCIDENT

HENRY C. GIGNILLIAT
GEORGE JOHNSON
JAMES D. FRANSON, SP4 CE
PAUL M. TERPOLILLI, SP4 CE

9 NOVEMBER 1972

125

UNCLASSIFIED

Security Classification

DOCUMENT CONTROL DATA - R & D

(Security classification of title, body of abstract and indexing annotation must be entered when the overall report is classified)

1. ORIGINATING ACTIVITY (Corporate author)

Engineering Division
U. S. A. Engineer Power Group
Fort Belvoir, Virginia

2a. REPORT SECURITY CLASSIFICATION

UNCLASSIFIED

2b. GROUP

3. REPORT TITLE

ANALYSIS OF MH-1A LOSS OF COOLANT ACCIDENT

4. DESCRIPTIVE NOTES (Type of report and inclusive dates)

Final Report

5. AUTHOR(S) (First name, middle initial, last name)

Henry C. Gignilliat
George Johnson
James D. Franson, SP4 CE
Paul M. Terpolilli, SP4 CE

6. REPORT DATE	7a. TOTAL NO. OF PAGES	7b. NO. OF REFS
9 November 1972	126	30

8a. CONTRACT OR GRANT NO	9a. ORIGINATOR'S REPORT NUMBER(S)
In-house	
b. PROJECT NO.	ED 7212
c.	9b. OTHER REPORT NO(S) (Any other numbers that may be assigned this report)
d.	None

10. DISTRIBUTION STATEMENT

This document has been approved for public release and sale; its distribution is unlimited.

11. SUPPLEMENTARY NOTES	12. SPONSORING MILITARY ACTIVITY
	U. S. Army Engineer Power Group Corps of Engineers

13. ABSTRACT

Analyses of a postulated loss of coolant accident (LOCA) for the MH-1A Nuclear Power Plant are presented for large and intermediate size breaks in the primary system. Methods and assumptions consistent with AEC Interim Acceptance Criteria were used in evaluating the performance of the Emergency Core Cooling System (ECCS). The computer codes RELAP-3 for reactor system blowdown and THETA1-B for fuel element heatup were used to perform these calculations at a core power of 49.5 MW_t. The results of the core temperature transient for various break conditions are presented and the required cooling capability of a system meeting the AEC interim criteria is discussed.

DD FORM 1 NOV 68 1473 REPLACES DD FORM 1473, 1 JAN 64, WHICH IS OBSOLETE FOR ARMY USE.

UNCLASSIFIED

Security Classification

ACKNOWLEDGEMENT

The work reported herein represents contributions of several individuals associated with the early phase of the project. Particular acknowledgement is due R. S. Saunders, CPT CE who co-ordinated the initial work on the project and W. R. Jackson, SP5 CE who performed various computer analyses.

ED-7212

ANALYSIS OF MH-1A LOSS OF COOLANT ACCIDENT

HENRY C. GIGNILLIAT
GEORGE JOHNSON
JAMES D. FRANSON, SP4 CE
PAUL M. TERPOLILLI, SP4 CE

9 NOVEMBER 1972

ENGINEERING DIVISION
U. S. ARMY ENGINEER POWER GROUP
CORPS OF ENGINEERS

ib

TABLE OF CONTENTS

LIST OF TABLES

LIST OF FIGURES

LIST OF FIGURES (cont'd)

LIST OF FIGURES (cont'd)

LIST OF FIGURES (cont'd)

I. INTRODUCTION

A loss of coolant accident (LOCA) is defined as a failure of the reactor coolant system resulting in a partial or complete release of coolant to the containment vessel, thereby interrupting the normal mechanism for removing heat from the reactor core. If emergency coolant were not provided, clad and fuel melting would eventually occur as a result of residual heat generation in the fuel and possible metal water and other chemical reactions. The purpose of the Emergency Core Cooling System (ECCS) is to provide adequate core cooling for the period immediately following a break and to assure that the core is recovered and remains covered so that the residual heat can be removed.

The present MH-1A Emergency Core Cooling System consists of an emergency coolant injection tank and two high pressure coolant charging pumps. Emergency operation of the injection tank and one coolant charging pump is initiated by a coincident signal of low pressurizer pressure and high containment building pressure. Cooling water from the injection tank is delivered through a check valve to the reactor vessel downcomer region when the pressure in the inlet plenum drops below approximately 240 psia. Driving head for this injection consists of a regulated gas pressure within the injection tank plus the elevation head. The injection tank is designed to recover the core by bottom flooding within approximately ten minutes. The coolant charging pumps serve to make up coolant lost due to a small leak or as a result of boil-off after recovering of the core and provide long term emergency cooling to remove decay heat. Table 1 summarizes the characteristics of these systems which are described in more detail in Appendix A and References 3 and 5.

This report evaluates the effectiveness of the present MH-1A ECCS during a postulated loss of coolant accident and presents information to establish the required performance of a system meeting the AEC's "Interim Acceptance Criteria for Emergency Core Cooling Systems" (Reference 1) published in the Federal Register June 29, 1971. All calculations were performed in accordance with the AEC evaluation model Appendix A, Part 1 of the above reference using the recommended computer codes RELAP-3 (Reference 7) for reactor blowdown calculations and THETA 1-B (Reference 8) for the fuel element heat up transients. Analyses reported herein cover break sizes from 0.18 ft^2 up to the double ended severance of the largest reactor coolant pipe. The analyses were performed at 110 percent of rated power (49.5 MW_t) and at a peak linear heat rate of 21.1 kw/ft.

TABLE 1

SUMMARY OF MH-1A EMERGENCY CORE COOLING SYSTEM CHARACTERISTICS

Coolant Charging Pumps

Number of pumps	2
Capacity per pump	8.5 gpm
Actuation (coincident)	High cont. pressure (1/2) Low pressurizer press (1/2)
Emergency power source	Diesel generator
Startup delay for diesel	∿ 30 sec
Point of Injection	Reactor Vessel downcomer
Coolant source	Emergency water storage tank
Capacity of tank	10,000 gallons

Emergency Injection System

Number of injection lines	1
Emergency injection tanks	1
Method of injection	pressurized gas
Operating pressure	240 psia
Injection tank capacity	2600 gal
Minimum emergency coolant	1000 gal
Coolant temperature	85°F
Check valves in injection line	2
Isolation valves in injection line	2
Isolation valves in nitrogen pressurizing line	2
Method of actuation (coincident)	High cont. pressure (1/2) Low Pressurizer press (1/2)
Design injection rate	∿ 100 gpm
Point of injection	Reactor Vessel downcomer

II. SUMMARY AND CONCLUSIONS

The performance of the ECCS presently installed at the MH-1A has been analyzed for large and intermediate size breaks within the reactor primary system using the methods and assumptions specified in the AEC Interim Policy Statement on Emergency Core Cooling Syscems (Reference 1).

The parameters used in the analyses are consistent with the data reported in the MH-1A SAR (Reference 3) and MH-1A Core 4 Nuclear Analysis (Reference 9). Table 2 summarizes the MH-1A thermal parameters related to the LOCA. The computer programs and methods used in analyzing the effectiveness of the ECCS are discussed in Section IV. The major input parameters and additional data developed for the LOCA analysis are reported in the Appendices A through H and the results of the analyses for the present system are given in Section V. Based on these results it is concluded that the criteria identified in Section IV-A of the AEC Interim Policy Statement are not met by the present MH-1A ECCS. Further parametric analyses were performed to establish the basic performance criteria necessary for the improvement of the ECCS to meet the AEC interim criteria. The main conclusions regarding the improvement of the MH-1A ECCS as a result of these analyses are discussed in Section VI.

TABLE 2

SUMMARY OF MH-1A THERMAL DESIGN PARAMETERS

Thermal power rating, MW_t	45
Number of fuel assemblies	32
Fuel rods per assembly	104
Cladding outside diameter, in	.507
Fuel pellet diameter, in	.4565
Fuel rod pitch, in	.654
Cladding material	348 stainless steel
Average fuel specific power	
kw/kg of UO_2	13.6
kw/ft of rod	4.35
Adiabatic heating rate of fuel at average specific power °F/sec	66.5
Average rod power, kw	13.1
Peak to average heat flux ratios	
Axial	1.98
Radial	1.95
Total	3.86
Average fuel temperature at highest heat flux position, °F	2510
Core average fuel temperature at rated power, °F	1060

III. CONFORMANCE WITH AEC INTERIM POLICY STATEMENT

A. GENERAL

The analysis of the MH-1A LOCA was performed in accordance with the AEC Policy Statement for emergency core cooling systems (Reference 1). The criteria for the acceptance of the ECCS as contained in the AEC policy statement are met if the results of the LOCA are limited as follows:

> "1. The calculated maximum fuel element cladding temperature does not exceed 2300°F. This limit has been chosen on the basis of available data for embrittlement and possible subsequent shattering of the cladding. The results of further detailed experiments could be the basis for future revision of this limit.
>
> 2. The amount of fuel element cladding that reacts chemically with water or steam does not exceed 1 percent of the total amount of cladding in the reactor.
>
> 3. The clad temperature transient is terminated at a time when the core geometry is still amenable to cooling, and before the cladding is so embrittled as to fail during or after quenching.
>
> 4. The core temperature is reduced and decay heat is removed for an extended period of time, as required by the long-lived radioactivity remaining in the core."

This section discusses the application of the AEC evaluation model contained in Appendix A, Part I of the interim policy statement to the analysis of MH-1A ECCS and summarizes the analytical procedures and assumptions used in the evaluation model.

The analyses were performed for the entire break spectrum, from 0.18 ft^2 up to and including the double-ended severance of the largest pipe of the reactor coolant pressure boundary. Various break sizes and locations were analyzed to identify the most severe case. Table 3 summarizes the spectrum of breaks analyzed. Evaluation of the present MH-1A ECCS in terms of the single failure criterion is discussed in Reference 5.

In accordance with the AEC evaluation model the analyses were performed in three parts consisting of system blowdown, refill and reflooding, and core heat up phases. The thermal hydraulic calculations during blowdown were performed using the RELAP-3 computer program. Four nodes were used to describe the reactor core, nine nodes for the primary side of the steam generator and one node for the containment. The reflood transient was performed using a series of engineering calculations and the fuel element heat up calculations were performed using the THETA 1-B computer code. Six radial fuel nodes, two radial cladding nodes and eleven axial fluid nodes were used.

TABLE 3

BREAK SPECTRUM FOR MH-1A LOSS OF COOLANT ANALYSIS

1. Double-ended hot leg break (guillotine)
2. Double-ended hot leg break (slot)
3. Single-ended hot leg break (slot)
4. Double-ended break at the pump discharge (guillotine)
5. Double-ended break at the pump discharge (slct)
6. 0.6 Double-ended break at the pump discharge (slot)
7. 0.6 Double-ended break at the pump inlet (slot)
8. 0.5 ft^2 Break at the pump discharge (slot)
9. 0.18 ft^2 Pressurizer surge line break

B. ASSUMPTIONS AND PROCEDURES

The assumptions and procedures specified with respect to the AEC evaluation model are repeated below along with the section in this report in which their application to the MH-1A analysis is discussed:

"1. Pump model - The pump resistance, K, used for analysis should be fully justified. The effect of pump speed upon K should be considered. The more conservative of two assumptions (locked or running) should be used for the pump during the blowdown calculation (Section IV-B-4).

"2. Break characteristics - For large breaks in the range 0.6 to 1.0 times the total area of the double-ended break of the largest cold-leg pipe, two break models should be used. The first model should be the double-ended severance (guillotine), which assumes that there is break flow from both ends of the broken pipe, but no communication between the broken ends. The second model should assume discharge from a single node (split) (Section IV-B-2).

"3. A break discharge coefficient (C_D) of 1.0 should be used for all break sizes (Section IV-B-2).

"4. Decay heat - The decay heat curve described in the proposed ANS Standard, with a 20 percent allowance for uncertainty, should be used. The fraction of decay heat generated in the hot rod should be considered to be 100 percent of this value unless a smaller value is justified (Section IV-D-5).

"5. Time to departure from nucleate boiling - use any calculated option in the code (Section IV-D-3).

"6. Heat transfer after departure from nucleate boiling - use programmed transition boiling correlation option (Section IV-D-3).

"7. Film boiling heat transfer - use Groeneveld correlation (equation 5.7 of AECL - 3281, December 1969 (Section IV-D-3).

"8. Metal-water reaction rate - use the Baker-Just equation, with a coefficient of 1.0 (Section IV-D-8).

"9. Core flow - use 0.8 x RELAP smoothed flow at the junction which is entering core. If flows are opposed, use zero flow (Section IV-D-4).

"10. Enthalpy and pressure - use entering plenum conditions (Section IV-D-4).

"11. Accumulator bypass - for cold leg breaks, all of the water injected by the accumulators prior to end-of-blowdown shall be assumed to be lost. In this context the end-of-blowdown shall be specified as the time at which zero break flow is first computed (Section IV-B-6).

"12. Reflood - A calculation for the reflooding heat transfer should be performed. The containment back pressure assumed for the analysis should not be higher than the initial pre-break pressure plus 80 percent of the increase in pressure calculated for the accident (Section IV-C). The following items should be constraints on the calculations:

"a. No steam flow should be permitted in intact loops during the time period that accumulators are injecting.

"b. Core exit quality should be calculated from entering mass flow rate and nominal FLECHT heat transfer.

"c. Pump resistance, K, should be calculated on the basis of a locked rotor.

"d. The effects of the nitrogen gas in the accumulator, which is discharged following accumulator water discharge, should be taken into account in calculating steam flow as a function of time.

"e. The pressure drop in the steam generator should be calculated with the existing fluid conditions and associated loss coefficients.

"f. All effects of cold injection water, in either a hot or cold leg, on steam flow and ΔP, should be included in the calculation.

"g. The heat transfer coefficient during reflood should be derived from FLECHT data."

IV. METHOD OF ANALYSIS

A. GENERAL

The major events occurring during a LOCA are (1) system depressurization, (2) emergency coolant injection and core reflooding and (3) fuel and cladding heat up until core cooling becomes effective. The analysis considers each of these three aspects during the accident. First, the blowdown calculation determines the primary system hydraulic response and core power transient during system depressurization. This analysis provides input for the calculation of the core cooling during blowdown and basic information regarding the operation of the safety injection system. The blowdown analysis is performed with the RELAP-3 computer program. A reflooding analysis is initiated at the end of blowdown which considers rate of coolant injection, core reflooding rate, and heat transfer rates following blowdown. The core temperature transient is then analyzed with THETA-1B to determine the cladding temperature response and the extent of metal-water reaction. Input for this analysis is determined from the blowdown and reflooding analyses.

B. BLOWDOWN CALCULATION

The RELAP-3 computer program (Reference 7) is used to calculate the behavior of the primary system during subcooled and saturated blowdown. The code calculates transient pressures, flow rates, enthalpies and mass inventories throughout the primary system, and determines the core power transient and energy removal rates during system depressurization. The code employs a one dimensional analysis of the entire reactor loop requiring a geometric description in terms of a series of volumes and junctions. Pump characteristics, core and steam generator heat transfer, reactor kinetics, and emergency injection are included in the model.

Before the break occurs, the plant is assumed to be operating in an equilibrium condition with a system pressure of 1500 psia, a reactor coolant outlet temperature of 532°F, and a primary coolant flow rate of 3.88×10^6 lb/hr (9750 gpm). A reactor power level of 110 percent of rated power is assumed for all cases.

1. Primary System Representation. In the RELAP-3 model for the MH-1A, the primary system is divided into nodes with flow paths connecting the nodes. The reactor vessel downcomer region is represented by an annulus extending from the upper plenum region to the bottom of the inlet plenum. The lower plenum connects to the downcomer region and extends up to the bottom of the active fuel. The active core region is divided into four nodes of equal volume. Each volume is initialized at the proper fluid temperature based on the assumed power distribution. The power input to each of the axial core regions is based on the relative power generated

in that region and the segment length. The upper plenum and hot leg are each represented by separate nodes. The primary side of the steam generator is represented by nine nodes; one node represents the steam generator inlet plenum and another the outlet plenum. Seven nodes represent the active heat transfer portion of the steam generator tubes. The cold leg is represented by a node in which the primary coolant pumps are located. Additional nodes are assigned for the pressurizer, pressurizer surge line, and containment. A fill junction is provided in the reactor vessel downcomer to simulate emergency coolant injection. Figure 1 shows the representation for the single ended hot leg break. Other models are similar except for break type and location. Further details of the primary system representation are discussed in Appendix A.

2. Break Characteristics. The limiting mass flow through the break junction in RELAP-3 is defined by Moody's two-phase choked flow model (Reference 10). The flow through the junction is chosen as the smaller of the inertial flow or the choked flow. For choking to occur the containment pressure must be less than the throat pressure. A discharge coefficient of 1.0 is used in RELAP-3 for all break sizes.

Two break models were used for the analysis of large breaks. The first model was a double-ended severance of the pipe (guillotine), which assumed that there was break flow from both ends of the pipe but no communication between the broken ends. This type of break was simulated by assuming leakage from the adjacent nodes with a valve in the junction joining them. This valve is closed at the time the break occurs. The second model assumed discharge from a single node (slot).

3. Reactor Trip. Reactor trip setpoints with appropriate instrument delays to the beginning of rod motion can be included in the RELAP-3 model. For the LOCA, reactor trip was assumed to be initiated by low pressurizer pressure signal (1250 psia including error) with a .500 second delay to rod insertion. However, reactor shutdown due to voids occurred in general before control rod motion was initiated, for the break sizes analyzed.

4. Pump Representation. The pump head versus flow curve for the primary coolant pumps input into RELAP-3 was established from the manufacturer's test data on the as-built pumps. The test data was used to develop a nominal speed characteristic curve for the range of flow encountered in the LOCA. At flow rates greater than the flow corresponding to zero pump head, the pump head was conservatively assumed to be zero. Flow coastdown following a pump trip was approximated with a pump coastdown multiplier consistent with the loss of flow transient reported in Reference 11. Pump input data is discussed in Appendix C.

The effect of pump assumptions on the core heat removal rate during blowdown was evaluated. The most conservative assumptions are those which result in the least pump resistance and hence the most rapid blowdown. For all cases except the cold leg break at the pump inlet, the pumps were assumed to remain running with the pump head following the characteristic curve until cavitation occurred. Zero pump head occurred after cavitation. For the break at the pump inlet the pumps were assumed to trip at the time the break occurred due to loss of off-site power. After coastdown the resistance corresponding to a free spinning rotor was assumed. Comparison of results indicates that the assumption of pumps running is conservative, resulting in higher fuel temperatures at the end of the blowdown.

5. Reactor Kinetics. Reactor power during blowdown is determined from the standard point kinetics equations, using six delayed neutron groups as programmed into RELAP-3. The value of β^*/ℓ^*, the effective delayed neutron fraction over prompt neutron lifetime, for MH-1A is provided. Nonlinear Doppler feedback in the form of reactivity versus fuel temperature is input into RELAP-3 along with constant moderator temperature and void reactivity coefficients corresponding to BOL conditions. The primary shutdown mechanism during the LOCA is void formation in the core. For conservatism the calculated void reactivity coefficient is reduced by 25 percent to account for uncertainties. The spatial distribution of the moderator temperature and void reactivity feedback is assumed to be proportional to the product of the square of the axial power shape and the fraction of core volume in each region.

Heat generated during blowdown is calculated from the fission and residual heat-generation in the core in RELAP-3. A heat balance is performed in each axial region. Heat transfer rate is determined based on correlations built into RELAP-3 and calculated local conditions.

6. Safety Injection. A provision for safety injection into the reactor vessel downcomer region was included in the MH-1A model. A constant flow rate of 100 gpm was assumed consistent with the design value for the injection system. For cold leg breaks, it was assumed that all water injected prior to the end of blowdown was lost out of the break. In this context the end of blowdown was taken as the time when zero break flow was first computed. This assumption has negligible effect on the blowdown in the MH-1A because coolant injection on the order of 100 gpm is insignificant compared to the blowdown flow rates for large breaks. Details of the present injection system design are presented in Appendix A.

C. REFILL CALCULATION

1. General. The refilling phase of the LOCA is begun at the end of blowdown which is defined as the time when zero break flow is first computed. In the case of a guillotine break, zero break flow must be computed from both ends of the break before the end of blowdown is assumed. After

receiving an actuation signal, refill from emergency injection tank is initiated when the reactor inlet plenum pressure drops below 240 psia. However, in accordance with the AEC interim criteria, all coolant injected prior to the end of blowdown is assumed lost out of the break. After the end of blowdown the coolant is assumed to be delivered to the reactor vessel inlet plenum. The water remaining in the downcomer region below the inlet nozzle and in the lower plenum region after blowdown is conservatively neglected. Refill is continued until the coolant reaches the bottom of the core and steam is generated by the hot fuel rods causing a pressure buildup in the core and retarding the inlet flooding rate. Heat transfer is evaluated for the hot fuel rods during the steam cooling period after blowdown when the core is uncovered. After core reflooding is initiated heat transfer coefficients from the FLECHT data (Reference 12) can be used.

2. Vessel Refill. Driving head for the refill injection is provided by the difference between the nitrogen pressure in the tank and the reactor vessel back pressure. The rate of coolant injection depends on the magnitude of the driving head and pressure losses in the piping between the injection tank and reactor vessel downcomer. The gas pressure in the tank is supplied by a series of gas bottles and is regulated such that the pressure remains constant during the period of injection. The nominal design injection rate is 100 gpm based on an assumed containment back pressure of 155 psia. The lower containment pressure calculated by RELAP-3 after a LOCA should result in a higher coolant injection rate. Figure 2 shows the refill times in terms of the emergency injection flow rate. This curve is based on the reactor vessel volumes and a constant coolant injection rate. Boil off due to heat transfer from the reactor vessel walls and hot internals is not included in the calculations.

An estimate of the maximum temperature rise of the coolant during refill was made based on the stored energy in the metal below the core region and the coolant volume. Assuming complete mixing of the coolant, the equilibrium temperature between the coolant and the reactor vessel metal was determined to be 185°F with an initial metal temperature of 500°F and an initial water temperature of 85°F. Therefore, although local steam generation would occur as the result of quenching of the hot metal surfaces of the reactor vessel, the bulk coolant temperature would remain below the saturation temperature (approximately 340°F) while the coolant level is below the active core region. For rapid refilling rates, a relatively small temperature rise in the bulk coolant would be expected. This is desirable because increased subcooling of the water improves the flooding heat transfer.

3. Core Reflooding. Until the water reaches the bottom of the core, the water levels in the downcomer region and lower plenum beneath the core are equal. After the coolant level reaches the bottom of the core heat is transferred from the hot fuel rods to the coolant. Initially, the heat transferred serves to remove the subcooling of the water entering core and the core flooding rate is the same as the vessel flooding rate. However, in a short period of time the hot fuel rods begin to generate

steam in the core region which must be vented to the containment. For the hot leg breaks this steam is vented directly out the break from the upper plenum region, having negligible effect on the core flooding rate. However, for the cold leg break the steam generated in the core region must pass through the entire loop before being vented to containment out the break. The flooding rate is thus limited by the resistance of the loop to steam flow.

The pressure drop along the flow path relieving steam after the cold leg break is calculated based on an equivalent loss coefficient for the loop corrected for existing fluid conditions. The reactor coolant pump rotors are assumed to be locked and effects of superheating in the steam generator are considered. The effect of steam binding tends to reduce the core flooding rate, resulting in increased cladding temperatures. The flooding rate during the steam binding period is a function of the elevation head between the water levels in the downcomer and core regions, the loop resistance, and the fraction of the inlet flow rate which is vaporized and must be relieved.

For the purpose of calculating the relievable steam flow rate, the water level in the downcomer is assumed to have reached the bottom of the inlet nozzle and the driving force for the steam venting is assumed to be the elevation head in the downcomer region above the coolant level in the core. Table 4 shows the loss coefficients used in determining the loop equivalent loss coefficient. The relievable steam flow rate defined in terms of the equivalent loss coefficient is expressed as follows:

$$W_s^2 = \frac{2g\,\rho_s(\rho_\ell\,H_D)}{K/A^2}$$

where: W_s = relievable steam flow, lb/sec

H_D = downcomer elevation head, ft

ρ_ℓ = downcomer coolant density, lb/ft^3

ρ_s = saturated steam density, lb/ft^3

g = gravitational constant, ft/sec^2

A = primary pipe flow area, ft^2

K = equivalent loss coefficient

TABLE 4

LOSS COEFFICIENTS FOR MH-1A COLD LEG STEAM VENTING CALCULATION

	Normal Operation	Saturated Steam	Superheated Steam
Upper Plenum to steam generator inlet	1.62	1.62	1.62
Steam generator inlet to break	3.68	4.67	5.79
Pumps (locked)	----	6.10	7.56
Expansion loss to containment	----	.98	1.20
TOTAL equivalent K	5.30	13.37	16.17

The following assumptions are made in calculating the system loss coefficient and relievable steam flow rate:

a. The reactor coolant pump rotors are locked.

b. Steam passing through the steam generator is superheated to 500°F.

c. The coolant leaving the core is saturated steam.

d. The containment back pressure is equal to the initial pre-break pressure plus 80 percent of the increase in pressure calculated for the accident.

e. The emergency injection flow does not affect the relievable steam flow or pressure drop because the injection does not occur in the steam venting flow path and therefore, no flow blockage is assumed.

f. The additional driving pressure for core reflooding caused by nitrogen discharge into the inlet plenum after the injection tanks are empty is conservatively neglected.

Figure 3 shows the relievable steam flow rate for the cold leg breaks at the pump discharge. The actual core flooding rate would depend upon the fraction of coolant entering the core which is vaporized and must be relieved. This effect should be calculated based on the nominal flooding heat transfer data from Reference 12. For the purpose of estimating steam limited core flooding rates it was assumed that 60 percent of the coolant entering the core was vaporized or entrained. Based on this assumption, the

steam limited flooding rate would be approximately 0.75 in/sec. It should be pointed out that a significant portion of the core may be recovered before steam generation causes a reduced flooding rate. In the MH-1A the hot spot at BOL occurs at approximately 8 inches above the bottom of the core. This would probably be effectively cooled before steam limiting could occur. Therefore, the most important factor during the refill phase appears to be the extent of core cooling during the period of time from the end of blowdown to the time the injection water reaches the bottom of the core. Heat transfer during this period is discussed in Section VI-A with respect to the required Emergency Core Cooling System performance.

D. FUEL TEMPERATURE TRANSIENT

1. General. The fuel and cladding temperature calculations are performed with the THETA1-B computer program (Reference 8). This program solves the two dimensional transient heat conduction equations in the fuel rod and one dimensional conservation of energy equations for the associated coolant channel. The surface heat transfer model in THETA1-B provides the boundary conditions required during the solution of the fuel rod and coolant equations. The required input includes coolant channel flow, primary system pressure, core power generation and coolant enthalpy versus time as obtained from RELAP-3. Following blowdown, the heat transfer coefficient versus time during reflooding is input. Heat generation in the clad due to metal water reaction is also included in the model. This section discusses the basic assumptions and methods adopted in using THETA1-B for the analysis of the fuel and clad temperature transient.

2. Fuel Rod Representation The fuel rod in THETA1-B is represented by six equal thickness radial regions in the fuel, two regions in the cladding and eleven axial regions in the coolant. Heat transfer in the axial direction is assumed in the cladding, but is conservatively neglected in the fuel. The gas gap between the fuel and cladding is treated as a heat conducting path with negligible heat capacity. The gap conductance is calculated based upon differential expansion of the fuel and cladding and the thermal conductivity of the gas. The initial steady-state fuel temperature distribution in THETA1-B is consistent with the MH-1A Core 4 calculated temperature distribution at the hot spot (Reference 13).

3. Heat Transfer Coefficients During Blowdown. During the blowdown portion of a LOCA the fuel rod surface experiences rapidly changing conditions of flow, pressure, quality, and temperature. The heat transfer regime and surface heat flux are determined in THETA1-B on the basis of local fluid conditions and cladding surface temperature. The heat transfer regimes which could be encountered during a LOCA, and the corresponding correlations used in THETA1-B, are listed in Table 5. Except for the stable film boiling regime, these are the correlations recommended in the THETA1-B report. For film boiling heat transfer the Groeneveld correlation (equation 5.7 of AECL-3281, December 1969, Reference 14) was used. The time to

departure from nucleate boiling was calculated using the recommended critical heat flux option in the code and heat transfer after departure from nucleate boiling was calculated with the programmed transition boiling correlation. Further details of the heat transfer model in THETA1-B are discussed in Reference 8.

TABLE 5

HEAT TRANSFER CORRELATIONS DURING BLOWDOWN IN THETA1-B

Heat Transfer Regime	Correlation	Reference
1. Forced convection in subcooled liquid	Dittus-Boelter	15
2. Nucleate boiling	Thom	16
3. Forced convection vaporization	Schrock-Grossman	17
4. Transition boiling	McDonough, Milich and King	18
5. Stable film boiling	Groeneveld (equation 5.7)	14
6. Pool film boiling	Berenson	29
7. Forced convection in superheated steam	Dittus-Boelter	15
8. Critical heat flux correlations	Combination of B&W-2 Barnett and Modified Barnett	19,20,21

4. Hot Channel Input Data. The boundary conditions used in solving the fluid energy equations in THETA1-B are the system pressure, flow rate, and enthalpy of the coolant entering the core and the fuel rod surface heat flux. The first three of these boundary conditions are obtained directly from RELAP-3. If the core flow at the upper and lower core junctions in RELAP-3 is in the same direction then 0.8 of the RELAP-3 smoothed flow at the junction entering the core is used. If the flows are opposed, a stagnation point in the core is assumed and zero flow is used. The pressure and enthalpy used in THETA1-B are the entering plenum conditions obtained from RELAP-3. The heat flux at the fuel rod surface is computed by the heat transfer routines.

5. Reactor Power. The reactor power in the form of internal heat generation as a function of time is input to THETA1-B. The normalized power calculated in RELAP-3 from the kinetics equations considering the various reactivity feedback effects is used until shutdown to the residual level occurs. Then the decay heat curve described in the proposed ANS Standard (Reference 22) is used. This curve is increased by 20 percent to account for uncertainties and includes an additional allowance for heat generation due to heavy element decay. The fraction of decay heat generated in the hot fuel rod is considered to be 100 percent of this value.

6. Core Power Distribution. The MH-1A Core 4 axial power distribution having a maximum axial peak of 1.98 was assumed in THETA1-B. The Core 4 radial peaking factor of 1.95 was assumed resulting in a maximum three dimensional nuclear peaking factor of 3.86. An additional 10 percent uncertainty in the nuclear power distribution was assumed and a 3 percent uncertainty due to fabrication and engineering tolerances was added. This results in a peak linear heat rate of 19.1 kw/ft rated power and 21.1 kw/ft at 110 percent power.

7. Fuel Rod Properties. The variation of conditions in the core during a loss coolant accident requires a knowledge of the high temperature physical properties of the core materials. Property data including heat capacity, thermal conductivity, density and mean thermal expansion over the range of temperatures encountered during a LOCA are incorporated into THETA1-B consistent with the information reported in Reference 23. The thermal conductivity for the cladding was taken as the recommended value for stainless steel with a 5 percent uncertainty. The cladding heat capacity was determined from the weighted contributions of the principal constituents of the stainless steel alloy. The property data for the UO_2 fuel used in the analysis is consistent with the irradiated UO_2 data reported in Reference 23. Further details of the materials property data in THETA1-B are presented in Appendix F.

8. Metal Water Reaction. Transient clad surface temperature and amount of stainless steel reaction is determined for a spectrum of peaking factors from the THETA1-B code. The stainless steel-steam reaction rate was conservatively taken as 100 percent of the value determined from the parabolic rate law (assuming no steam limiting). The rate equation incorporated into THETA1-B is discussed in Appendix G. The fraction of the core associated with a given 3 dimensional peaking factor is determined by combining the output of the two dimensional radial peaking factor with the design axial power distribution to give the core wide power peaking distribution. The fraction of the core associated with a given peaking factor is then combined with the fraction of metal water reaction for a given peaking factor to establish the percent metal water reaction in the core.

V. RESULTS

Analyses were performed for the full range of break sizes shown in Table 1 using the conservative assumptions and procedures described in Section IV. The blowdown portion of the analysis was carried out to the time when zero break flow was first computed. Information regarding the performance of the ECCS and the variation of significant parameters during blowdown was obtained. Results for each of the cases are summarized in the form of curves of significant parameters as a function of time. The fuel temperature transient during blowdown and during the initial phase of core heat up was calculated for the hot fuel rod using THETA1-B. Several representative cases are discussed in detail and the effect of continued core heat up with no emergency cooling is evaluated. Results of this analysis are used to identify the most severe break condition and determine the minimum time for core cooling to become effective.

A. BLOWDOWN

The sequence of events occurring during the subcooled and saturated phases of blowdown of the primary system were calculated using RELAP-3. The results of these analyses for the spectrum of break sizes and locations are summarized in Figures 4 through 12. These curves plot the variation of important parameters during the depressurization including the break flow rate, the system pressure, reactor power, core flow rate, and inlet enthalpy as a function of time. For the cold leg breaks in which the flow rate through the core reverses, the upper plenum conditions are presented.

As shown in the figures, the system is rapidly depressurized immediately after the break until the vapor pressure of the coolant is reached. During this subcooled phase pressure waves are propagated through the system at the speed of sound resulting in significant pressure differentials across system components. Figure 13 and 14 show the calculated core pressure drop as a function of time for the breaks at the inlet and outlet of the reactor vessel indicating that pressure differentials between 80 and 90 psi can occur momentarily across the core. However, the pressure oscillations are quickly damped due to the formation of voids in the system. Within approximately 0.02 seconds the initial subcooled depressurization is complete and saturated blowdown commences with choked flow occurring at the break location. The core power level is rapidly reduced due to formation of voids in the core region and the flow rate stabilizes and decreases. Reactor scram due to low pressure occurs after approximately two seconds, being delayed by the blowdown of the pressurizer liquid volume through the surge line. Heat transfer in the core during blowdown continues at a high rate until the critical heat flux is reached at which time a significant reduction in heat transfer at the clad surface occurs. For large breaks in the MH-1A the period of effective core cooling is from three to five seconds and the blowdown is essentially complete after approximately six seconds.

Table 6 shows the times at which significant events occur during the blowdown as calculated by RELAP-3. The table includes the time at which zero break flow is first computed, the times at which low pressurizer pressure and high containment pressure actuation signals are initiated, and the time at which the pressure in the inlet plenum drops below the pressure in the safety injection tank permitting the flow of emergency coolant into the vessel. As shown in Table 6, the delay in the receipt of the safety injection actuation signal from the pressurizer is the controlling signal for safety injection for large breaks. The high containment pressure setpoint is reached shortly after the breaks occurs. Actuation of the valves in the nitrogen pressurizing and safety injection lines and flow of coolant in the piping from the check valve to the injection point would be a source of additional delay.

The values of various calculated parameters at the time when zero break flow first occurs are shown in Table 7. The results of the calculation with RELAP-3 as shown indicate that from 96 to 98 percent of the initial primary system coolant is lost out of the break by the end of blowdown and the liquid mass remaining in the reactor inlet plenum below recirculation nozzles is a small percentage of the initial inlet plenum volume. These results are consistent with experimental observations of coolant remaining in the system after rupture and decompression of the semiscale test loop (Reference 30). The calculated containment pressure after blowdown varies from approximately 118 to 128 psia considerably below the design pressure of 155 psia. Smaller break sizes resulting in a larger amount of energy transferred from the core to the containment could result in higher containment back pressure after blowdown. However, for the break sizes analyzed the lower containment back pressure would indicate an improvement in safety injection flow rate of approximately 10 percent over the nominal design value. Also shown is the core average fuel temperature in the high heat flux axial region at the end of blowdown. These temperatures indicate the relative heat generation and removal rates for the average core during blowdown and depend primarily upon the length of time of blowdown and the effective heat transfer coefficient calculated in RELAP-3. These results appear to confirm that the double-ended guillotine break of the primary pipe is the most severe break with respect to the clad temperature transient because of lower amount of energy removed during blowdown.

The effect of the reactor coolant pump characteristics during blowdown was evaluated for the 0.6 DE slot break in the cold leg. Two cases were examined; the first considered a break at the pump discharge with assumptions resulting in minimum pump resistance and the second case considered a break at the pump inlet. For the break at the pump discharge it was assumed that the pumps remained running during the blowdown, following the pump head curve until cavitation occurred. For the break at the pump inlet it was assumed that the pumps tripped at the time the break occurred due to a loss of power and that a resistance due to a free spinning rotor existed after

TABLE 6

TIME FOR SIGNIFICANT EVENTS CALCULATED DURING BLOWDOWN (RELAP-3)

Break Type	Break Flow = 0 sec	High Containment Pressure (10 ± 3 psig) sec	Low Pressurizer Pressure (500 ± 80 psig) sec	Downcomer Pressure (230 psia) sec
DE Hot Leg Break (G)	6.04	0.17	3.14	3.42
DE Hot Leg Break (S)	6.30	0.19	3.19	3.44
SE Hot Leg Break (S)	6.98	0.32	4.13	5.75
DE Break at Pump Discharge (G)	6.20	0.22	3.28	3.44
DE Break at Pump Discharge (S)	6.50	0.23	3.23	3.28
.6 DE Break at Pump Discharge (S)	6.00	0.31	3.69	4.42
.6 DE Break at Pump Inlet (S)	8.90	0.38	4.98	6.39
0.5 ft^2 Break at Pump Discharge (S)	8.70	0.41	5.18	6.35
.18 ft^2 Surge Line Break	19.18	0.52	3.13	16.13

TABLE 7

CALCULATED PARAMETERS AT THE END OF BLOWDOWN (BREAK FLOW = 0)

Break Type	Total Mass Lost to Containment %	Liquid Mass in Downcomer +Inlet Plenum %	Containment Pressure psia	Core Ave. Fuel Temperature Region 2 °F
DE Hot Leg Break (G)	96	3.6	122.1	1258
DE Hot Leg Break (S)	96	3.0	122.0	1240
SE Hot Leg Break (S)	96	2.8	122.7	1214
DE Break at Pump Discharge (G)	98	1.6	118.5	1229
DE Break at Pump Discharge (S)	98	1.4	118.5	1210
.6 DE Break at Pump Discharge (S)	97	1.6	118.1	1226
.6 DE Break at Pump Inlet (S)	96	2.5	127.6	1205
0.5 ft^2 Break at Pump Discharge (S)	97	1.4	118.2	1217
.18 ft^2 Surge Line Break	96	3.3	124.6	632

the pumps shutdown. Table 8 summarizes the assumptions used in the two cases. Figures 15 and 16 show the effects of the assumptions on the resistance across the pump and the flow rate through the break. The more rapid blowdown for the case with the minimum pump resistance (case 1) resulted in reduced heat removal from the core and consequently the more severe temperature transient. These assumptions were used for the remainder of the cold leg breaks.

TABLE 8

REACTOR COOLANT PUMP ASSUMPTIONS

Case	Break Location	Pump Trip	Pump Head after Cavitation	Shutdown Pump Resistance
1	Pump Discharge	No	None	None
2	Pump Inlet	Yes	None	Free Rotor

B. CORE HEAT UP WITH PRESENT INJECTION SYSTEM

The thermal response of the fuel and the cladding at the hot spot is calculated during blowdown and initial core heat up using THETA1-B. Initially after the break occurs, high convective and nucleate boiling heat transfer rates continue to prevail in the core. However, as the blowdown proceeds conditions resulting in departure from nucleate boiling occur and the surface heat flux is drastically reduced. After the blowdown is complete, the majority of the coolant inventory is lost and primary mechanism for removing heat from the core is through radiation and convection to steam generated from coolant in contact with vessel walls beneath the core.

The present MH-1A ECCS is designed to deliver coolant at the rate of 100 gpm, resulting in a time of approximately 6 minutes to refill the reactor vessel to the bottom of the core. Thus, with the present system there exists an extended period of time in which steam cooling is relied upon. For the purpose of estimating the minimum time required before emergency cooling must become effective and of assessing the relative severity of the various cases, the assumption of no heat transfer at the cladding surface was applied at the end of blowdown. It is clear that this assumption is conservative and results in continued core heat up at a rate depending primarily on the stored energy in the fuel at the end of blowdown and the residual heat generation rate. At temperatures above approximately 2100°F, additional heat is added due to the reaction of cladding with steam.

Figures 17 through 19 show the results of the hot spot temperature transient during blowdown and the initial core heat up for the hot and cold leg double ended guillotine breaks and the pressurizer surge line break. The boundary conditions from RELAP-3 were used up until the end of blowdown at which time zero heat transfer was assumed at the clad surface. Fuel and clad temperatures, heat transfer coefficient, fluid temperature, and local quality and void fraction at the location of the hot spot are plotted for each case. The plots of fuel and clad temperature variation with time illustrate the redistribution of sensible heat in the fuel and cladding immediately following the rupture. This effect results in the major source of clad heating up to about 20 seconds after the break. Following this time continued core heat up due to decay heat generation and metal water reaction occurs.

The effect of continued cladding heat up following the double-ended hot leg break for specified volume percentages of the core is shown in Figure 20. The times for the cladding to reach 2300°F and the melting temperature of stainless steel (2550°F) are shown in Table 9. The calculation performed for this curve assumed that there was no emergency cooling after blowdown but that sufficient steam was available for metal water reaction. Redistribution of the initially peaked temperature profile occurs in approximately 20 seconds after which continued core heat up occurs at a rate depending on the decay heat level and local power peaking. Figure 21 plots the percent of metal water reaction as a function of time for the hot spot and overall core. From this figure it can be seen that the metal water reaction becomes significant at temperatures above approximately 2100°F and rapidly increases as the temperature rises.

Table 10 presents the results of the clad temperature calculation for each of the break conditions. The values shown are for 30 seconds after rupture at which time redistribution of the clad and fuel temperature is essentially complete. The calculations conservatively assumed no emergency cooling after blowdown. From these results the cold leg break appears to be in general more severe than the hot leg break due to the lower heat transfer during blowdown. The amount of heat removed from the hot spot during blowdown largely determines the period of time remaining before the emergency cooling must become effective. On this basis, the minimum delay for the ECCS to become effective is approximately 30 seconds after the break. This delay results from the conservative assumption that unlimited steam would be available for the metal water reaction but not for cooling the core. In reality the actual delay time would be longer depending upon the amount of heat transfer occuring due to radiation and convection after blowdown. The effect of heat transfer at the hot spot during this period is discussed in Section VI-A.

TABLE 9

TIME REQUIRED FOR CLADDING TO REACH 2300°F AND MELTING TEMPERATURE OF STAINLESS STEEL FOR DE HOT LEG BREAK WITH NO EMERGENCY COOLING

Percent of Clad Volume	Time to Reach 2300°F, sec	Time to Reach Melting Temperature, sec
0 (hot spot)	44	65
2	78	101
10	129	155
25	250	300

TABLE 10

RESULTS OF CLAD TEMPERATURE TRANSIENT AT HOT SPOT 30 SECONDS AFTER BREAK NO EMERGENCY COOLING

Break Type	Hot Spot Clad Temp °F	% Metal Water Reaction (Local)
DE Hot Leg Break (G)	2091	.56
DE Hot Leg Break (S)	2075	.49
SE Hot Leg Break (S)	1796	.02
DE Break at Pump Discharge (G)	2290	2.27
DE Break at Pump Discharge (S)	2163	1.00
.6 DE Break at Pump Discharge (S)	2275	2.08
.6 DE Break at Pump Inlet (S)	2167	.98
0.5 ft^2 Break at Pump Discharge (S)	2284	2.17
0.18 ft^2 Surge Line Break	969	0

VI. REQUIRED EMERGENCY CORE COOLING SYSTEM PERFORMANCE

This section discusses the design and performance of the MH-1A ECCS on the basis of the calculated results of the LOCA and AEC Interim Acceptance Criteria, and estimates the required cooling capability of the system. Consideration of the post blowdown environment in the vessel and heat sources in the core pertaining to the effectiveness of the ECCS are outlined.

The primary requirement for the MH-1A ECCS is to provide reliable and effective core cooling within approximately 30 seconds after a large rupture in the primary piping by rapidly adding coolant into the vessel and core region. For the MH-1A the loss of coolant inventory after a large break occurs within approximately four to six seconds. This rapid blowdown is due primarily to the potentially large break size in a single loop system relative to the vessel size and coolant inventory in the system. However, in a single loop system a large fraction of the coolant is forced to pass through the core region during blowdown and relatively large heat transfer rates exist in the core. After blowdown the ECCS must be capable of controlling the decay heat generation until the cladding is quenched thereby reducing its temperature to that of the coolant. The semi-open lattice design of the MH-1A should promote good distribution of the coolant through the core region before and during core flooding. After the core is quenched long term core cooling would be provided by the decay heat removal system. The primary requirement for this system is reliability due to the extended period of time it would be expected to operate following a LOCA.

A. HEAT REMOVAL CAPABILITY

Following a rupture in the primary system the ECCS must function such that the fuel rod heat energy is removed, and uncontrolled cladding heat up is prevented. The major sources of energy during the LOCA include the initial stored energy in the fuel, the fission energy generated prior to complete shutdown from voids or control rod motion, the residual heat generation due to fission product decay, and possible metal water reaction energy.

The heat transfer during blowdown removes a portion of the stored and fission energy in the fuel, thereby lowering the average fuel temperature at the hot spot. Following a rupture in the primary system, redistribution of sensible heat occurs such that the cladding and fuel temperatures approach a common temperature approximately equal to the fuel average temperature after blowdown. For the MH-1A the blowdown removes approximately 600°F

average temperature from the hot spot. Following blowdown the major source of heat in the fuel is due to fission product decay. The heat flux which must be removed from the hot spot and average core as a function of time after shutdown is shown in Figure 22. This curve is based upon the ANS Standard (Reference 22) for decay heat and the MH-1A power peaking factors. Above temperatures of approximately 2100°F the metal water reaction begins to become significant adding additional heat which must be removed. On this basis the heat transfer coefficient necessary to prevent continued heat up of the fuel and cladding above 2100°F, assuming a sink temperature corresponding to saturated steam (340°F), would be approximately 15 Btu/hr ft^2°F.

Figures 23 and 24 show the hot spot cladding temperature transients for the double ended hot and cold leg guillotine breaks assuming variable heat transfer coefficient at the end of blowdown and a sink temperature of 340°F. The actual heat transfer at the end of blowdown will depend on the calculated local conditions in the core region and can be determined using correlations for forced convection to steam (References 26 and 27) and radiation to steam and adjacent fuel rods (Reference 28). Other considerations would be the amount of steam available in the core region, cladding surface temperatures, and type of fluid flow existing in the coolant channels. Conservative estimates of the radiation to saturated steam result in heat transfer coefficients of approximately 3 to 5 Btu/hr ft^2°F and the minimum convective heat transfer coefficient due to laminar flow is approximately 3.5 Btu/hr ft^2°F. Thus, if sufficient steam were provided in the core region following blowdown, heat transfer coefficients of 6 to 9 or larger could be expected. This would delay the time before effective cooling of the core is required by an additional 20 to 40 seconds or longer.

After core flooding is initiated heat transfer from the FLECHT data can be applied (Reference 12). The major differences between the FLECHT tests and the MH-1A is the heated length of the fuel rods (12 feet as opposed to 3 feet in the MH-1A) and the elevation of the elevation of the peak power density (6 feet in the FLECHT tests as opposed to less than one foot in the MH-1A). As a result of these differences, effective cooling of the hot spot in the MH-1A could be expected shortly after the coolant reached the bottom of the core due to frothing and splashing of the coolant caused by steam generation in the flooded region. Detailed calculations of the refill and reflooding transient considering the improved system design will be required to determine the actual temperature time history of the cladding and the performance of the system relative to the AEC Interim Acceptance Criteria.

B. DESIGN CONSIDERATIONS

In general the design improvements for the MH-1A ECCS should be concerned with improving the response time of the injection system and providing sufficient redundancy and reliability in the system to assure effectiveness. Specifically, the evaluation of the MH-1A ECCS should consider the means of cooling the core over the spectrum of breaks from a small leak to double ended rupture of the primary pipe. The emergency coolant for large breaks should be added in such a way that effective cooling of the core region could be accomplished rapidly after the break occurs. Bottom flooding, as exists with the present system, and flooding from above the core could be considered. Redundant systems would be desirable from the standpoint of the single failure criterion. Testing of the injection system to demonstrate the actual flow rates achievable would aid in the evaluation of the improved system. The effect of loss of power and startup delays of the emergency power equipment should be evaluated and a means of periodically testing the operation of major components to assure reliability and effectiveness of the system should be included.

REFERENCES

1. Atomic Energy Commission, "Interim Acceptance Criteria for Emergency Core Cooling Systems for Light Water Power Reactors", Federal Register June 23, 1971, Vol 36, P. 12247

2. C.G. Lawson, "Emergency Core-Cooling System for Light-Water-Cooled Power Reactors", USAEC Report ORNL-NSIC-24, October 1968

3. MH-1A SAR, "Safety Analysis-Sturgis (MH-1A) Floating Nuclear Power Plant", Nuclear Power Field Office, Revision A, October 1967

4. J. J. Holloway, "Final Design Report, MH-1A Purification and Decay Heat Removal System", Martin Marietta Corporation, Nuclear Division, October 1963

5. J. J. Holloway, "Final Design Report, MH-1A Coolant Charging and Chemical Addition System", Martin Marietta Corporation, Nuclear Division, December 1963

6. J. T. Trushia, "Analysis of MH-1A Loss of Coolant Incident", Martin Marietta Corporation, Nuclear Division, October 18, 1963

7. W. H. Rettig, et al, "RELAP-3 - A Computer Program for Reactor Blowdown Analysis", IN 1321, June 1970

8. Hocevar, C. J. and T. W. Wineinger, "THETA-1B, A Computer Code for Nuclear Reactor Core Thermal Analysis", IN-1445, Feb 1971

9. "The Theoretical Nuclear Analysis of MH-1A Core 4", USAERG ED 7106, 17 Jul 71

10. F. J. Moody, "Maximum Flow Rate of A Single Component, Two-Phase Mixture", J. Heat Trans. - Trans. ASME, 87 n 1 (February 1965) pp. 134-142

11. E. R. Schmidt, et al, "MH-1A Loss of Flow Transient Safety Analysis and Parametric Study", NUS-550, April 1969

12. F.F. Cadek, et al, "PWR FLECHT (Full Length Emergency Cooling Heat Transfer) Final Report", WACP-7665, April 1971

13. "Thermal Hydraulic Analysis of MH-1A Core 4", USAENPG ED 7214, 20 July 1972

14. D. C. Groeneveld, "An Investigation of Heat Transfer in the Liquid Deficient Regime", Atomic Energy of Canada Limited - Chalk River, AECL 3281, December 1968 (Revised December 1969)

15. M. Jakob, Heat Transfer Vol. 1, New York: Wiley & Sons (1957)

16. J. R. S. Thom et al, "Boiling in Subcooled Water During Flow Up Heated Tubes or Annuli", Proc. Instn. Mech. Engrs., Vol. 180, Part 3C (1966) pp. 226-246

17. V. E. Shrock, L. M. Grossman, Forced Convection Boiling Studies. Final Report on Forced Convection Vaporization Project, TID-14632 (1959)

18. J. B. McDonough, W. Milich, E. G. King, Partial Film Boiling with Water at 2000 psig in a Round Vertical Tube, MSA Research Corp, Technical Report 62 (1958) (NP-6976)

19. J. S. Gellerstedt et al, "Correlation of Critical Heat Flux in a Bundle Cooled by Pressurized Water, pp 63-71 of Two-Phase Flow and Heat Transfer in Rod Bundles Symposium, Symposium presented at the Winter Annual Meeting of the Am. Soc. of Mech. Engrs, Los Angeles, California (Nov 1969)

20. E. D. Hughes, A Correlation of Rod Bundle Critical Heat Flux for Water in the Pressure Range 150 to 725 psia, IN-1412 (July 1970)

21. P. G. Barnett, A Correlation of Burnout Data for Uniformly Heated Annuli and Its Use for Predicting Burnout in Uniformly Heated Rod Bundles, AEEW-R 463 (1966)

22. American Nuclear Society, "Proposed ANS Standard - Decay Energy Release Rates Following Shutdown of Uranium - Fueled Thermal Reactors", ANS Standards Committee, October 1971

23. H. C. Brassfield et al, "Recommended Property and Reaction Kinetics Data for Use in Evaluating a Light-Water-Cooled Reactor Loss-of-Coolant Incident..." GEMP-482, April 1968

24. James C. Hesson et al, "Laboratory Simulations of Cladding-Steam Reactions Following Loss-of-Coolant Accidents in Water Cooled Power Reactors", ANL-7609, January 1970

25. H. A. McLain, "Potential Metal-Water Reactions in Light-Water Cooled Power Reactors", USAEC Report ORNL-NSIC-23, August 1968

26. D. M. McEligot et al, "Effect of Large Temperature Gradients on Convective Heat Transfer: Downstream Region", J. of Heat Transfer, Vol. 87, 1965, pp 67-76

27. D. M. McEligot et al, "Internal Low Reynolds Number Turbulent and Transitional Gas Flow with Heat Transfer," J. of Heat Transfer, Vol 88, 1966, pp 239-245

28. W. H. McAdmas, Heat Transmission, Chapter 4, McGraw Hill, New York, 1954

29. P. J. Berenson, "Film-Boiling Heat Transfer from Horizontal Surface," J. of Heat Transmission, Vol. 83, August 1961

30. D. J. Olson et al, "Semiscale Blowdown and Emergency Core Cooling (ECC) Project Test Report: Tests 824 and 825", IN-1481, June 1971

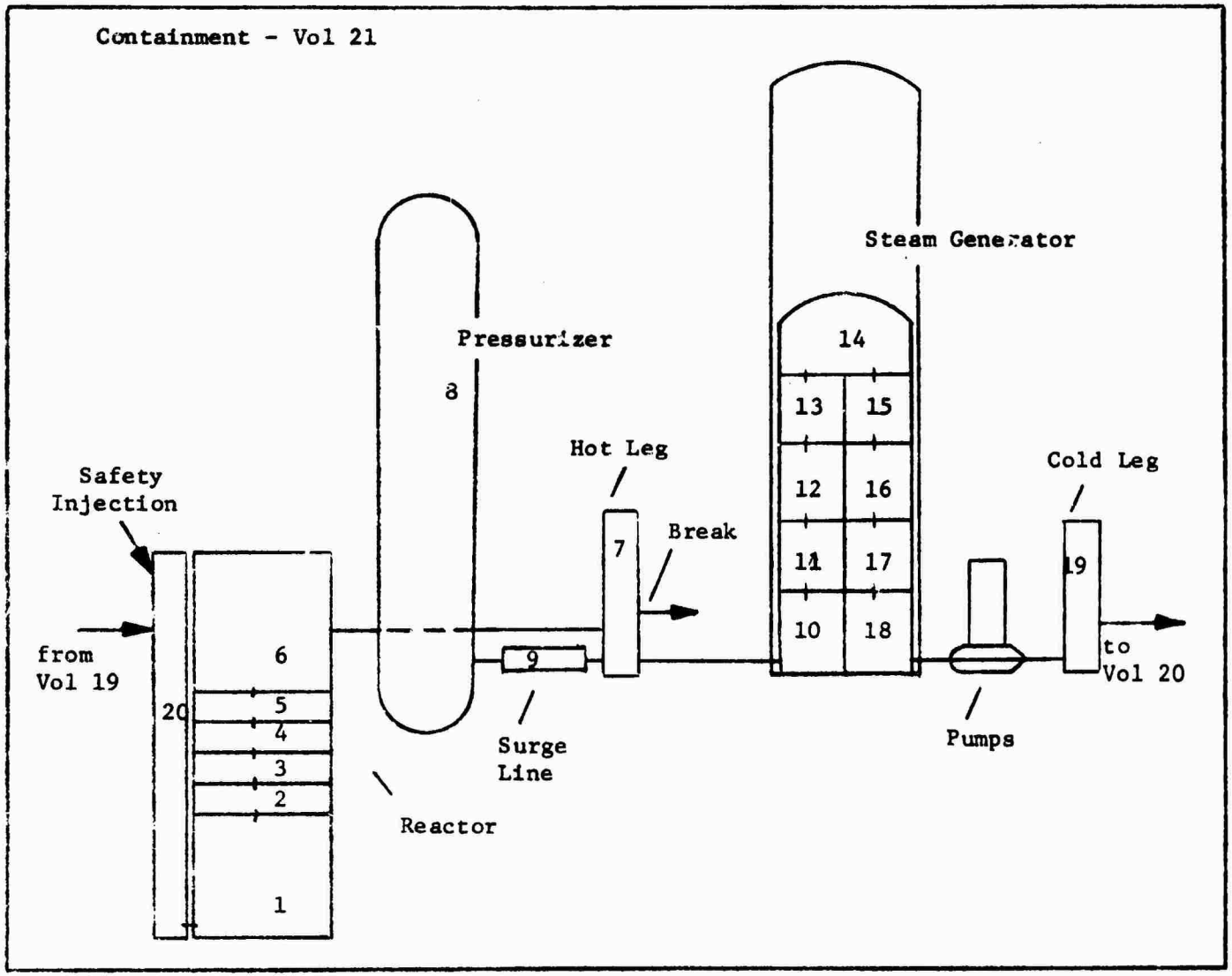

FIGURE 1 . MH-1A MODEL - SINGLE ENDED HOT LEG SLOT BREAK
21 VOLUME-/22 JUNCTIONS

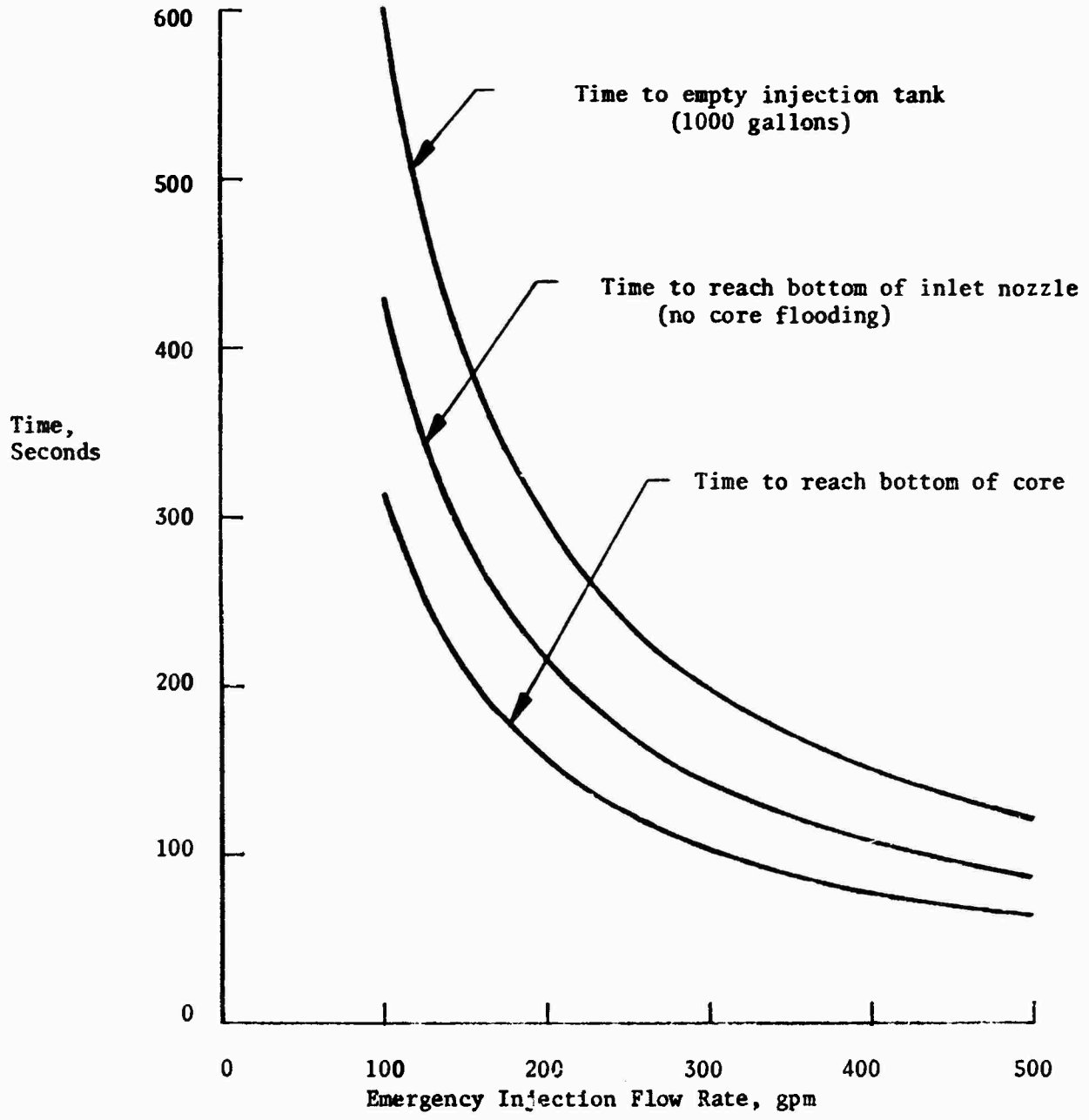

FIGURE 2 REFILL TIMES VERSUS EMERGENCY INJECTION FLOW RATE

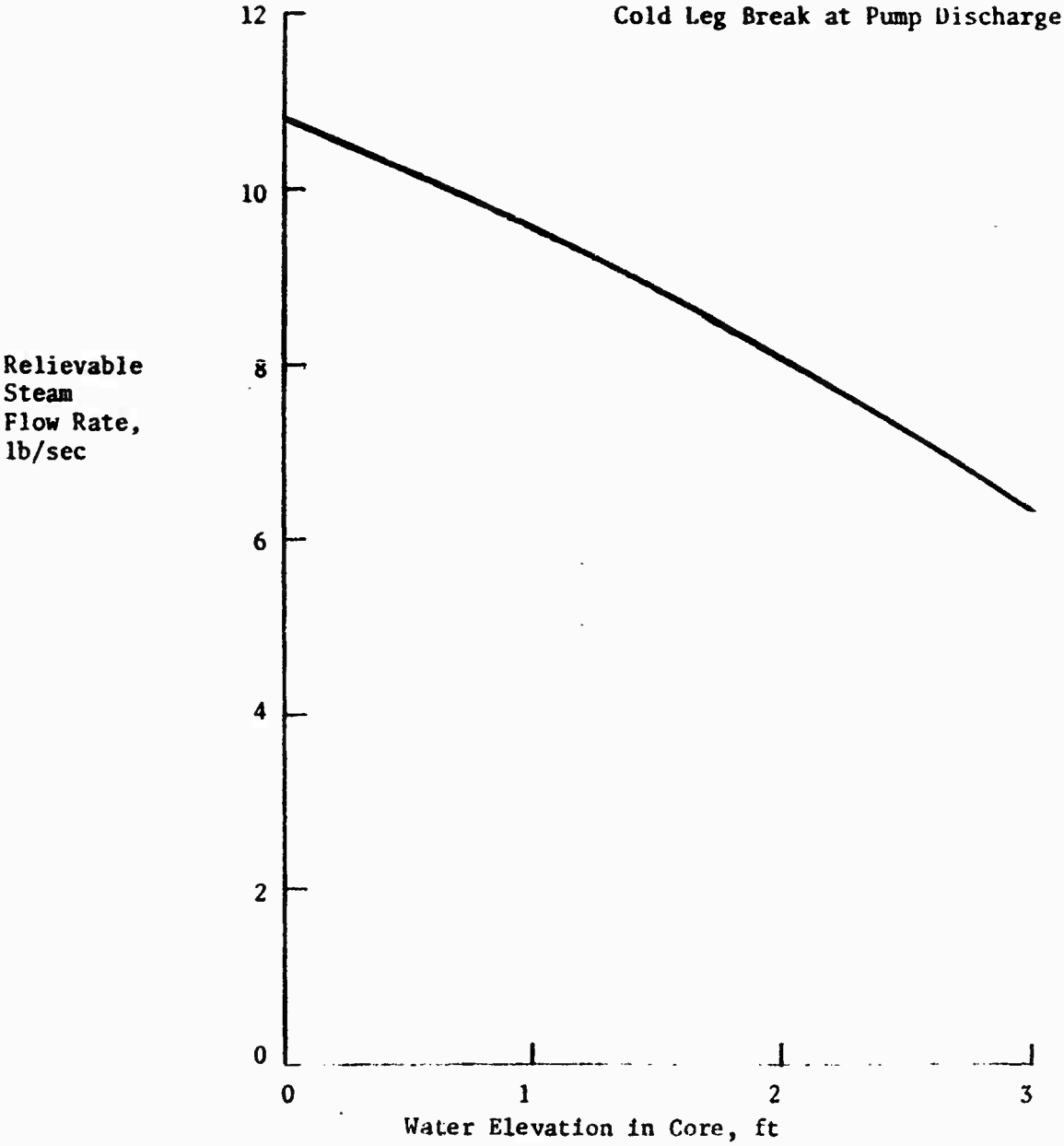

FIGURE 3 RELIEVABLE STEAM FLOW RATE VS. WATER ELEVATION IN THE CORE

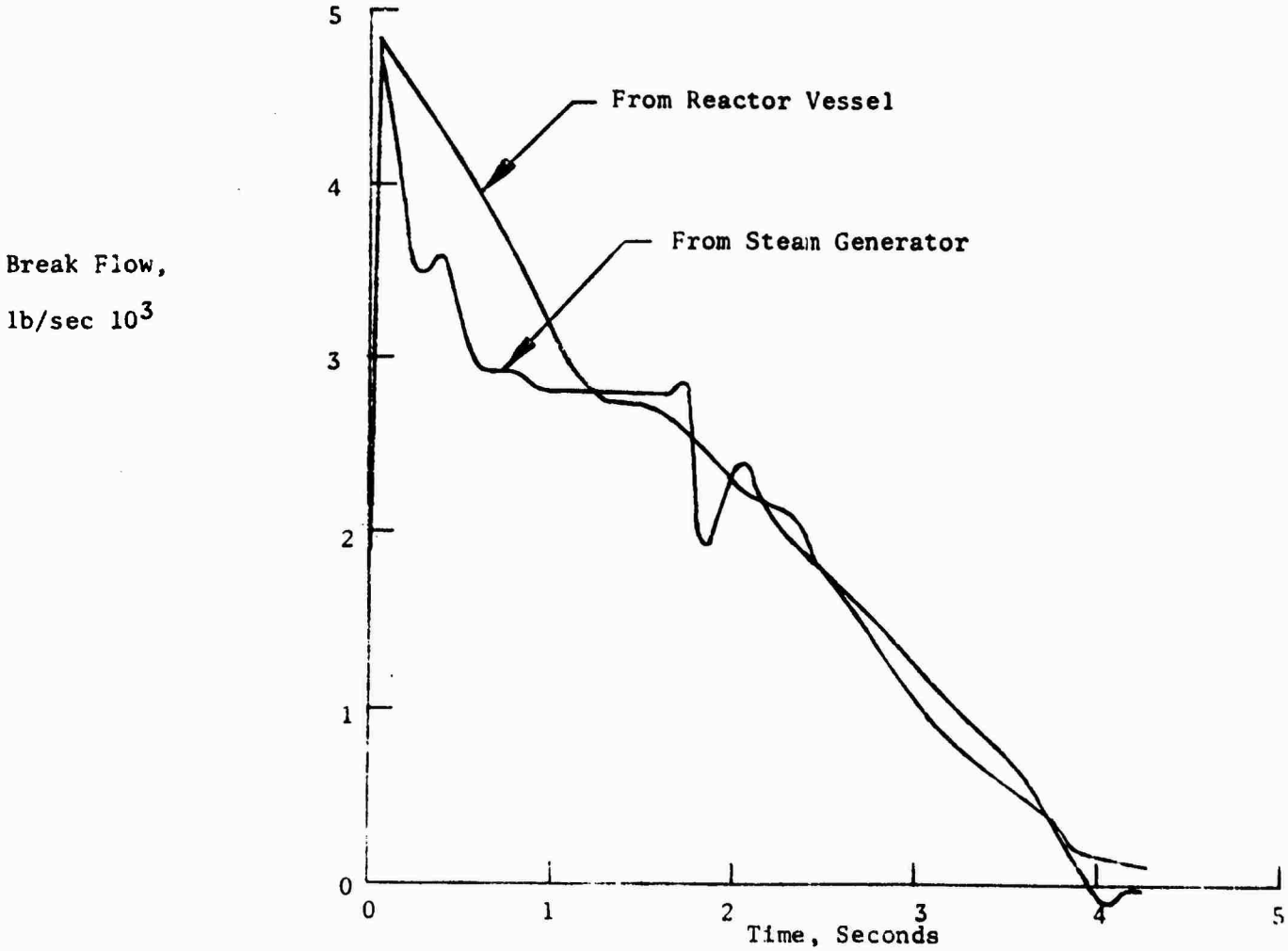

FIGURE 4A DOUBLE ENDED HOT LEG BREAK (GUILLOTINE) BREAK FLOW VS. TIME

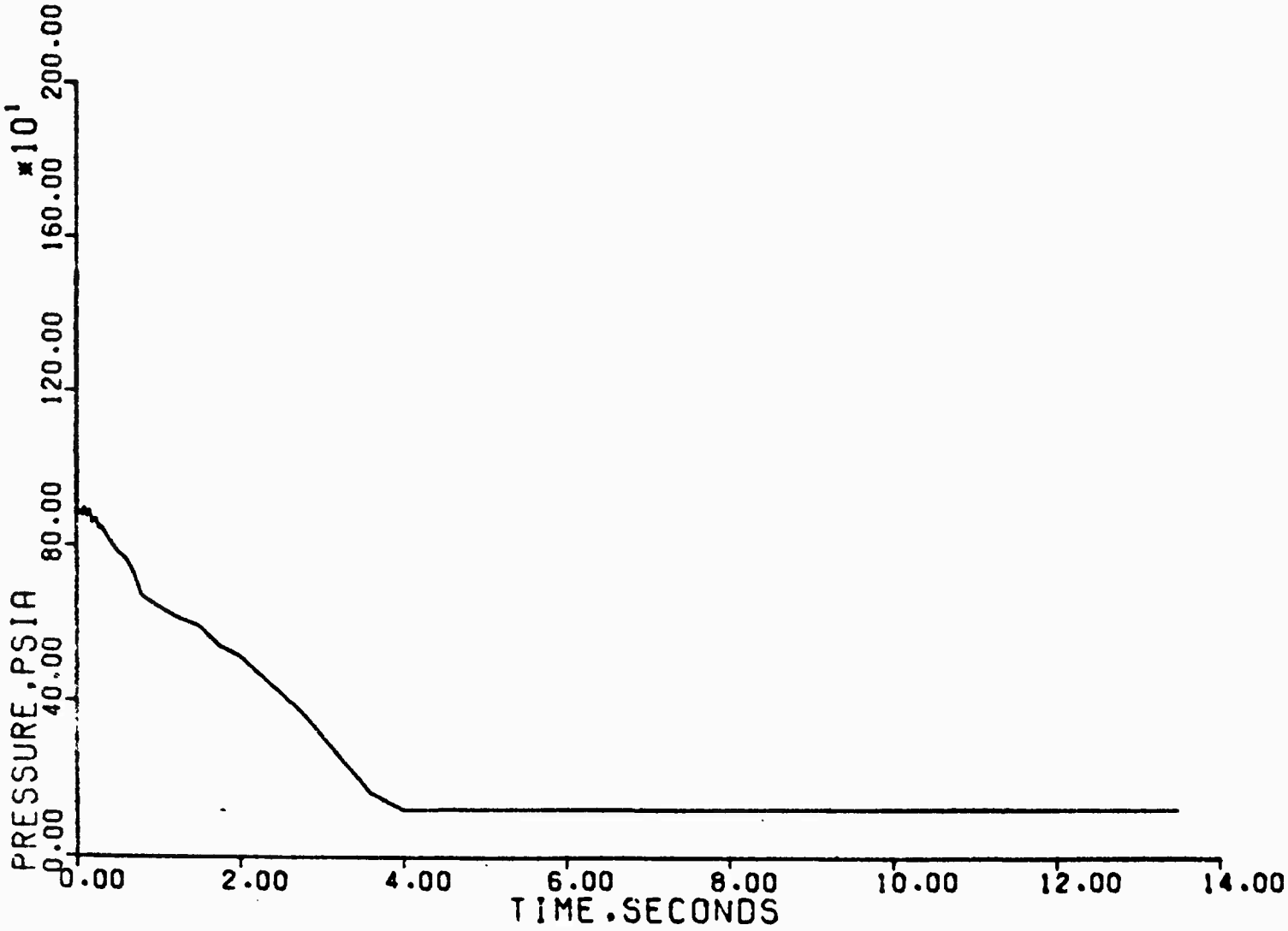

FIGURE 4B DOUBLE ENDED HOT LEG BREAK (GUILLOTINE) PRESSURE VS. TIME

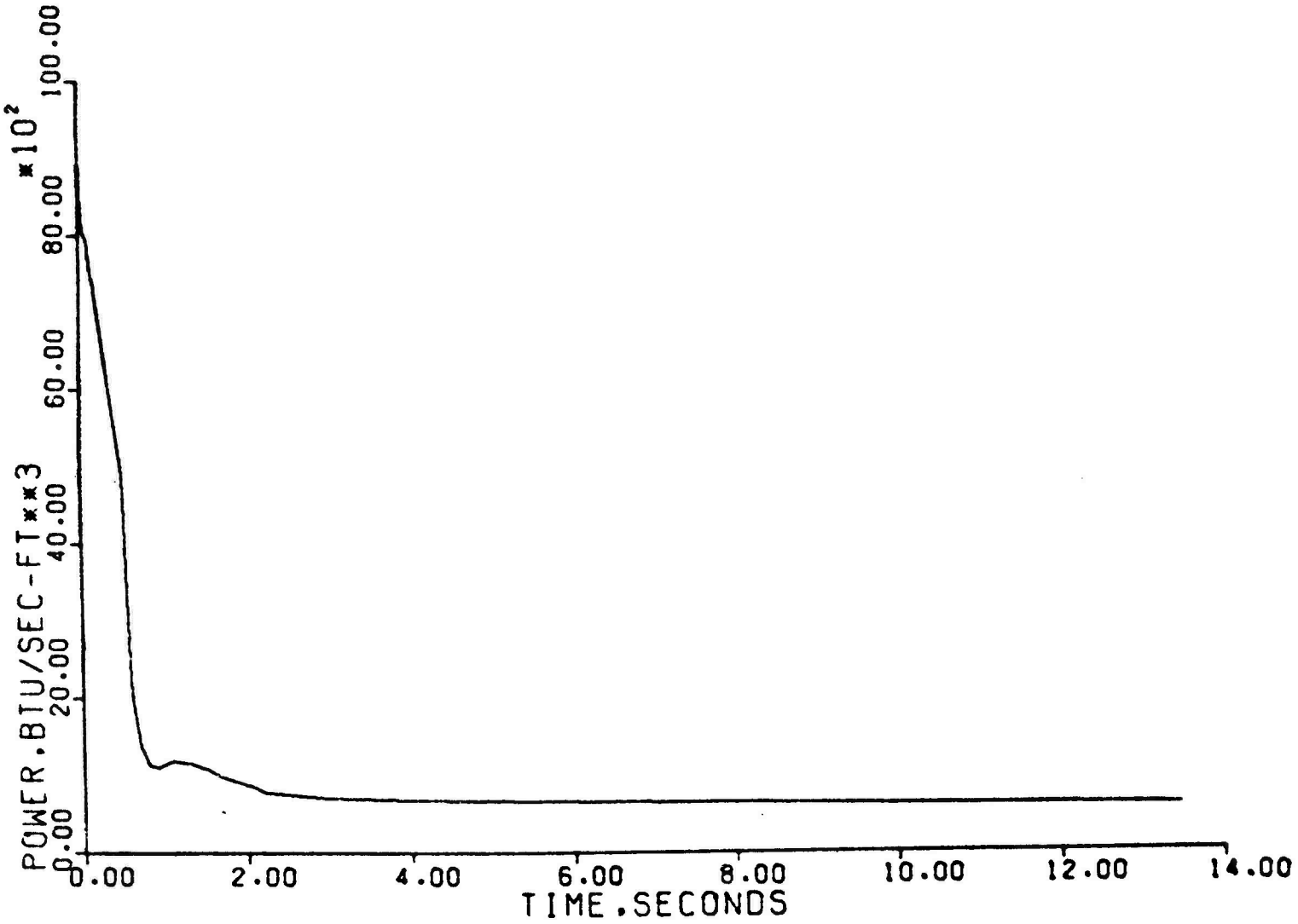

FIGURE 4C DOUBLE ENDED HOT LEG BREAK (GUILLOTINE) POWER LEVEL VS. TIME

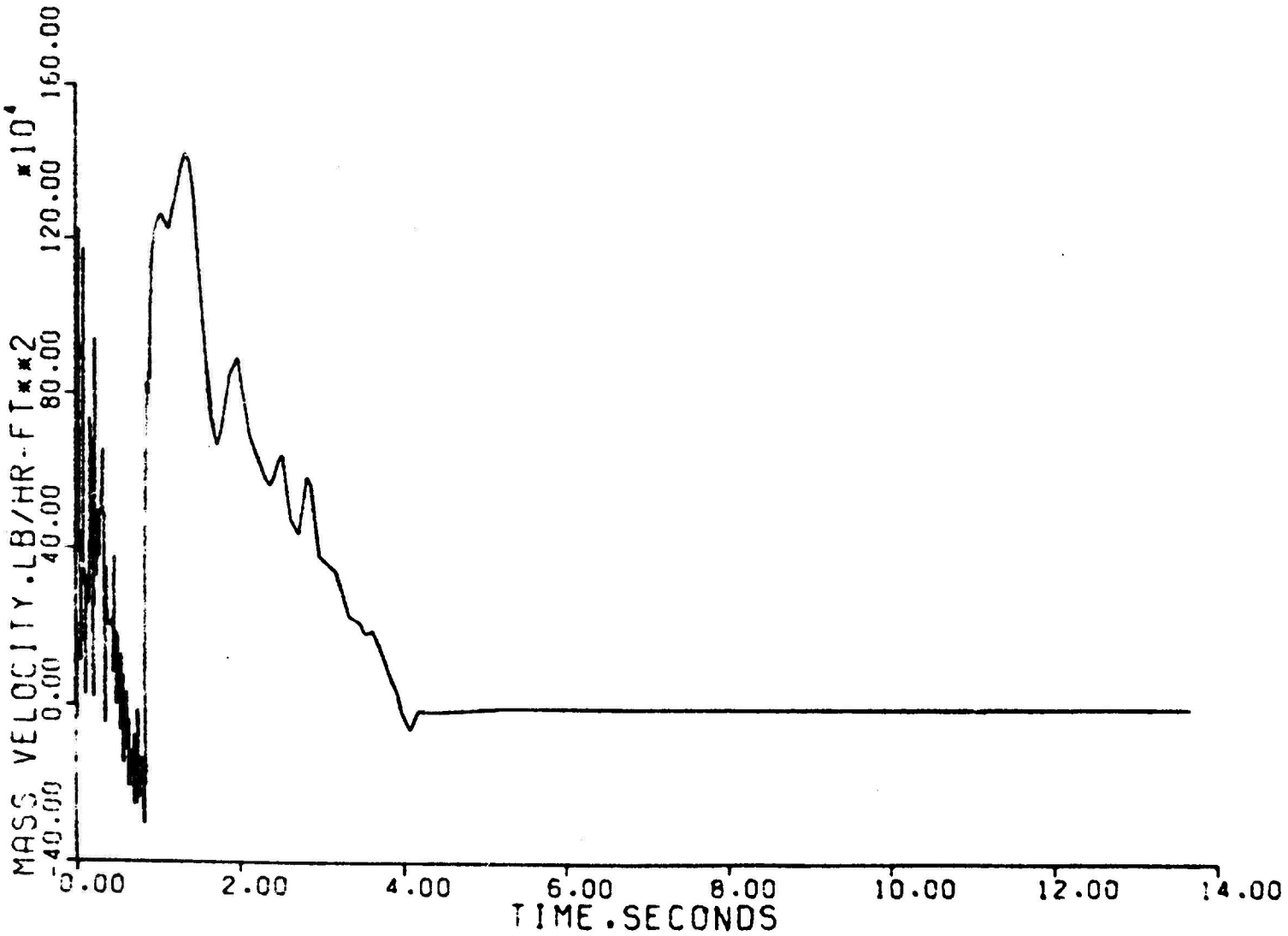

FIGURE 4D DOUBLE ENDED HOT LEG BREAK (GUILLOTINE) CORE FLOW VS. TIME

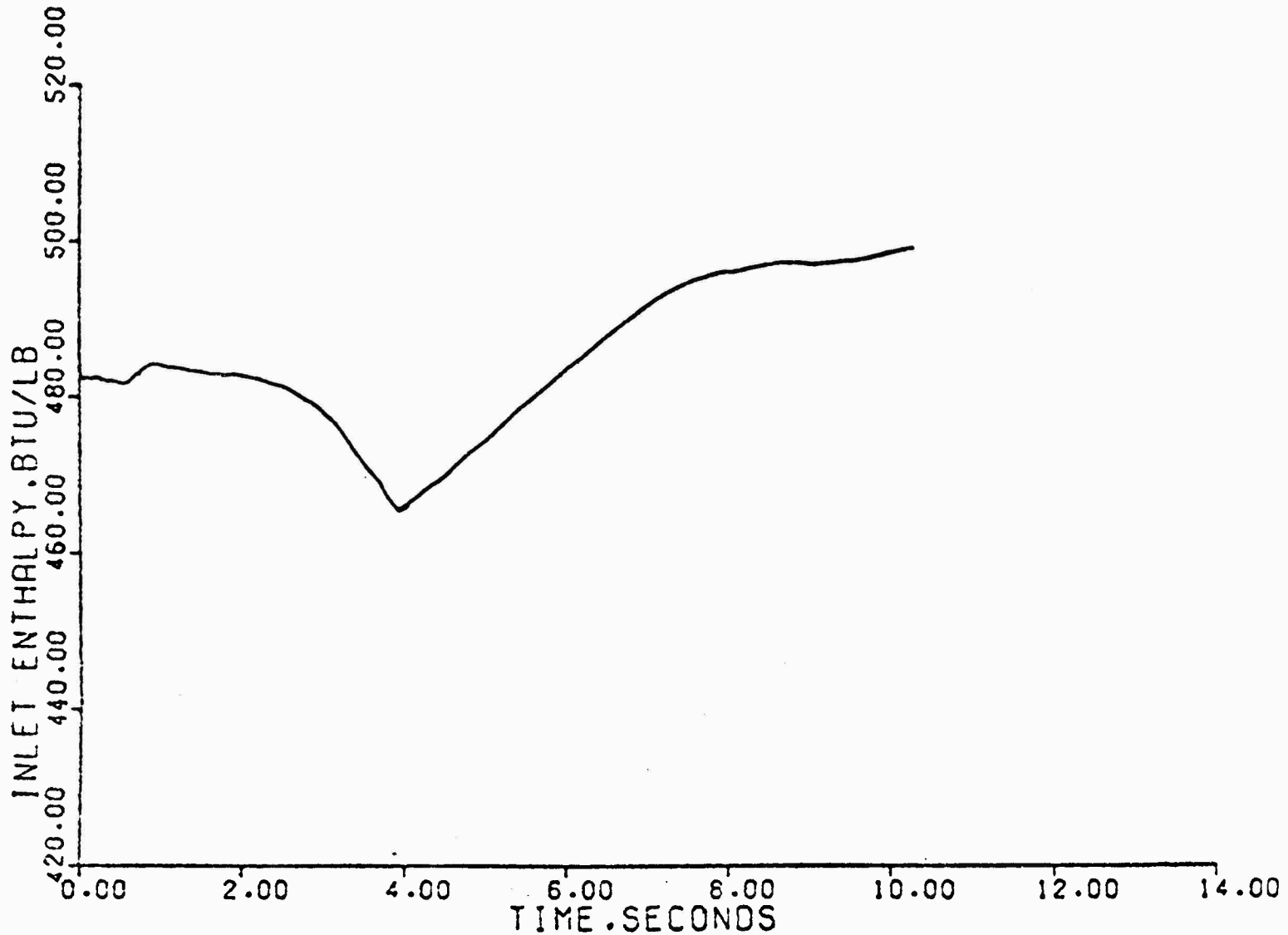

FIGURE 4E DOUBLE ENDED HOT LEG BREAK (GUILLOTINE) INLET ENTHALPY VS. TIME

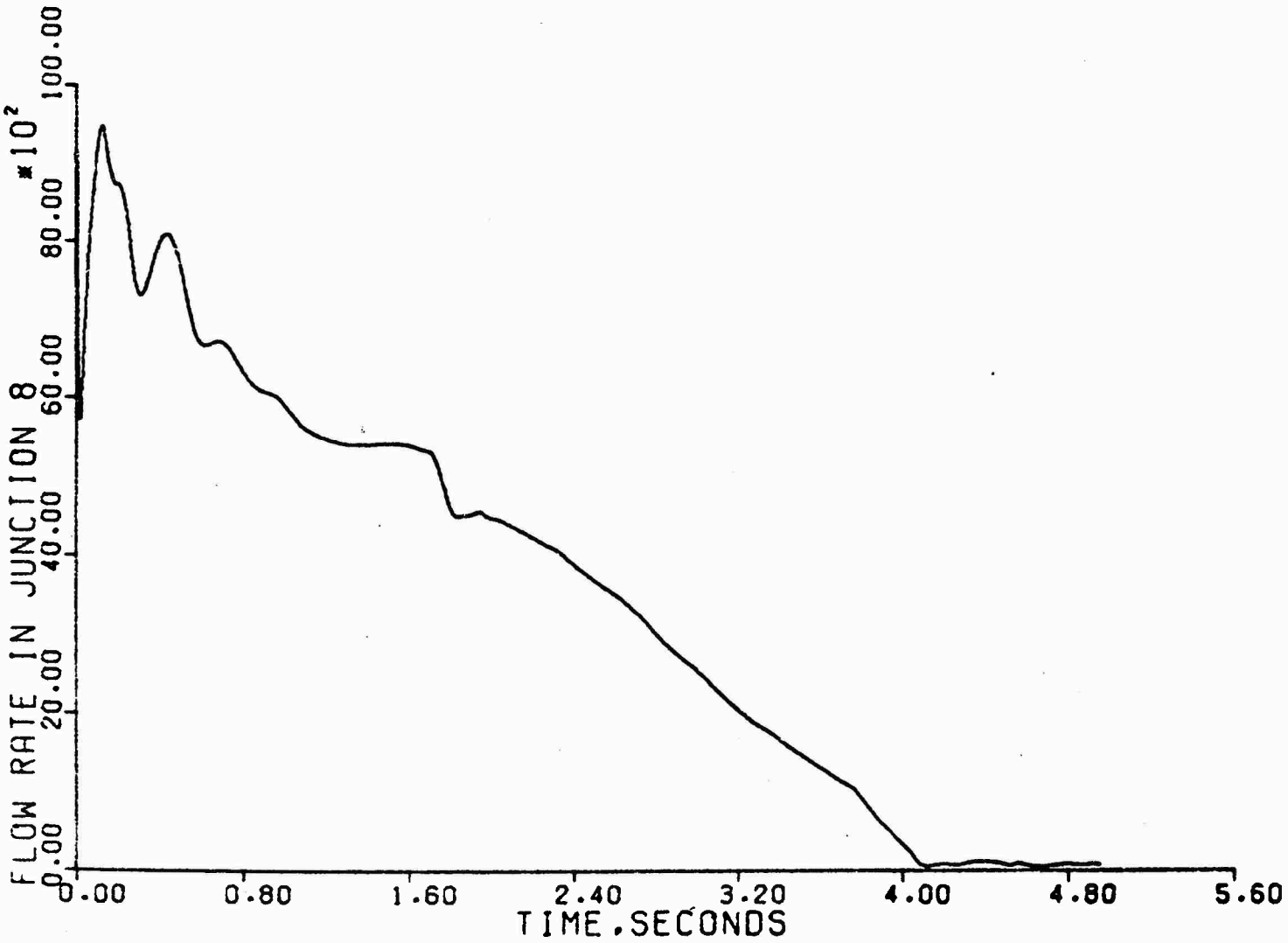

FIGURE 5A. DOUBLE ENDED HOT LEG BREAK (SLOT) BREAK FLOW RATE VS. TIME

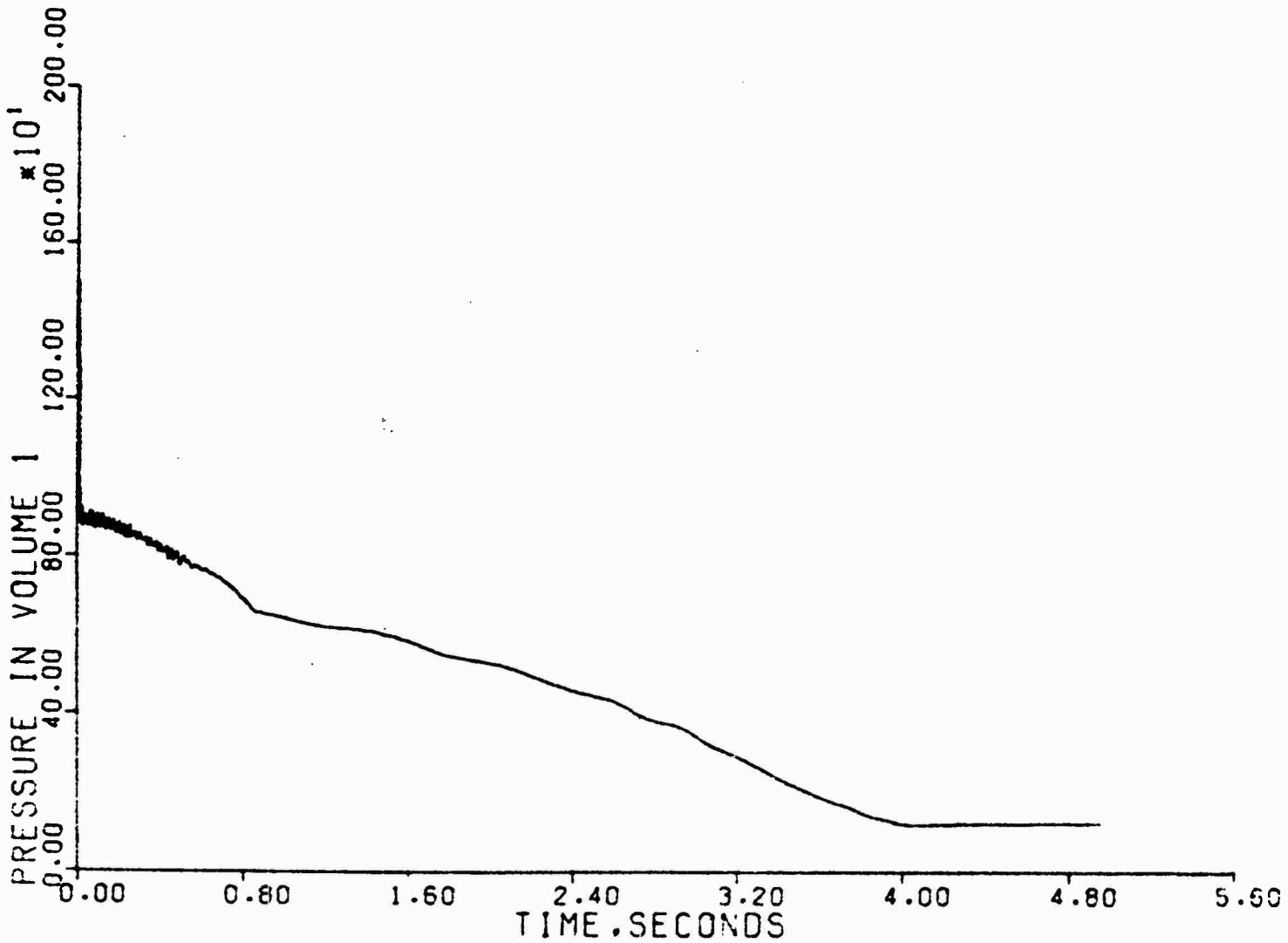

FIGURE 5B. DOUBLE ENDED HOT LEG BREAK (SLOT) PRESSURE VS. TIME

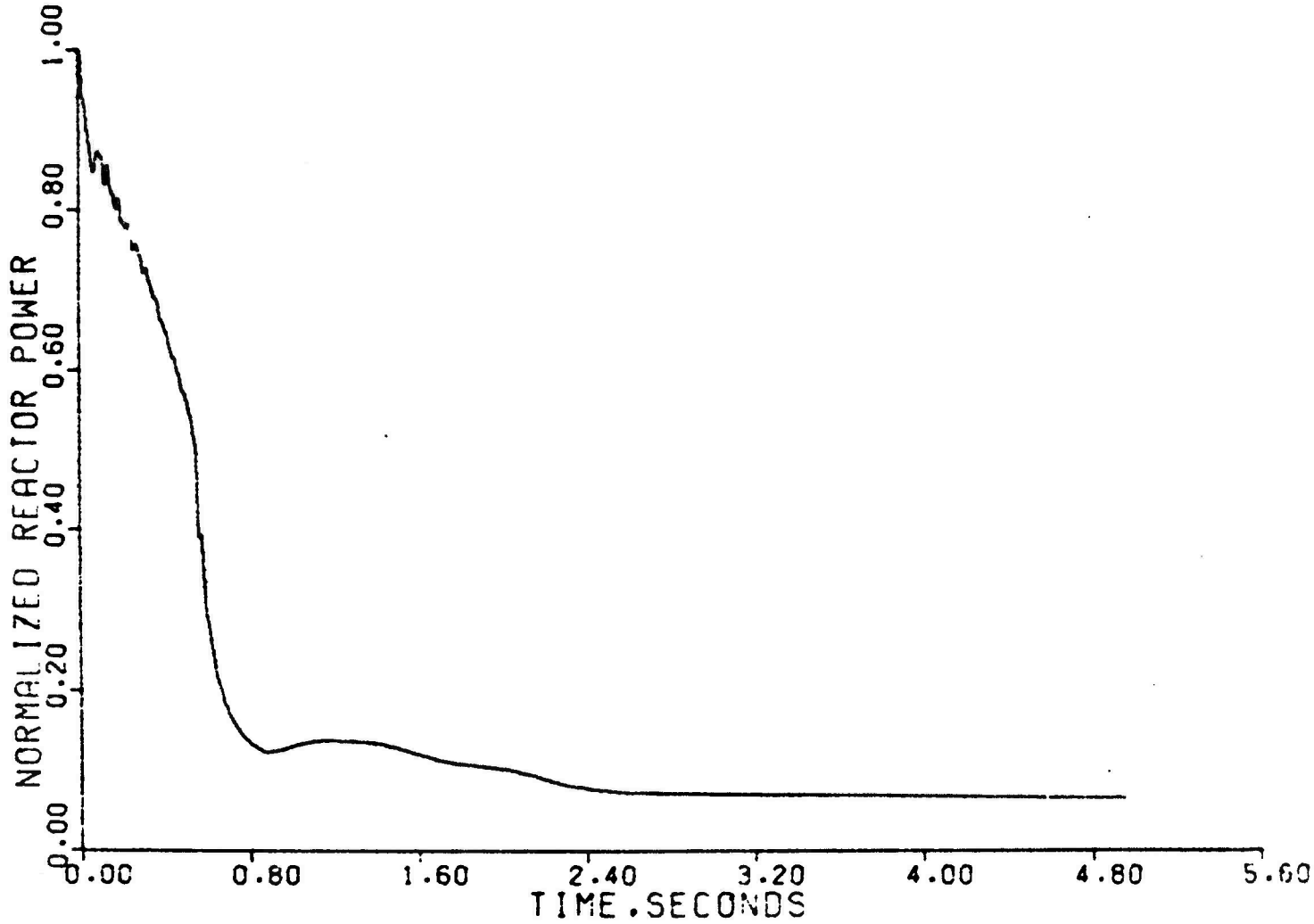

FIGURE 5C. DOUBLE ENDED HOT LEG BREAK (SLOT) POWER LEVEL VS. TIME

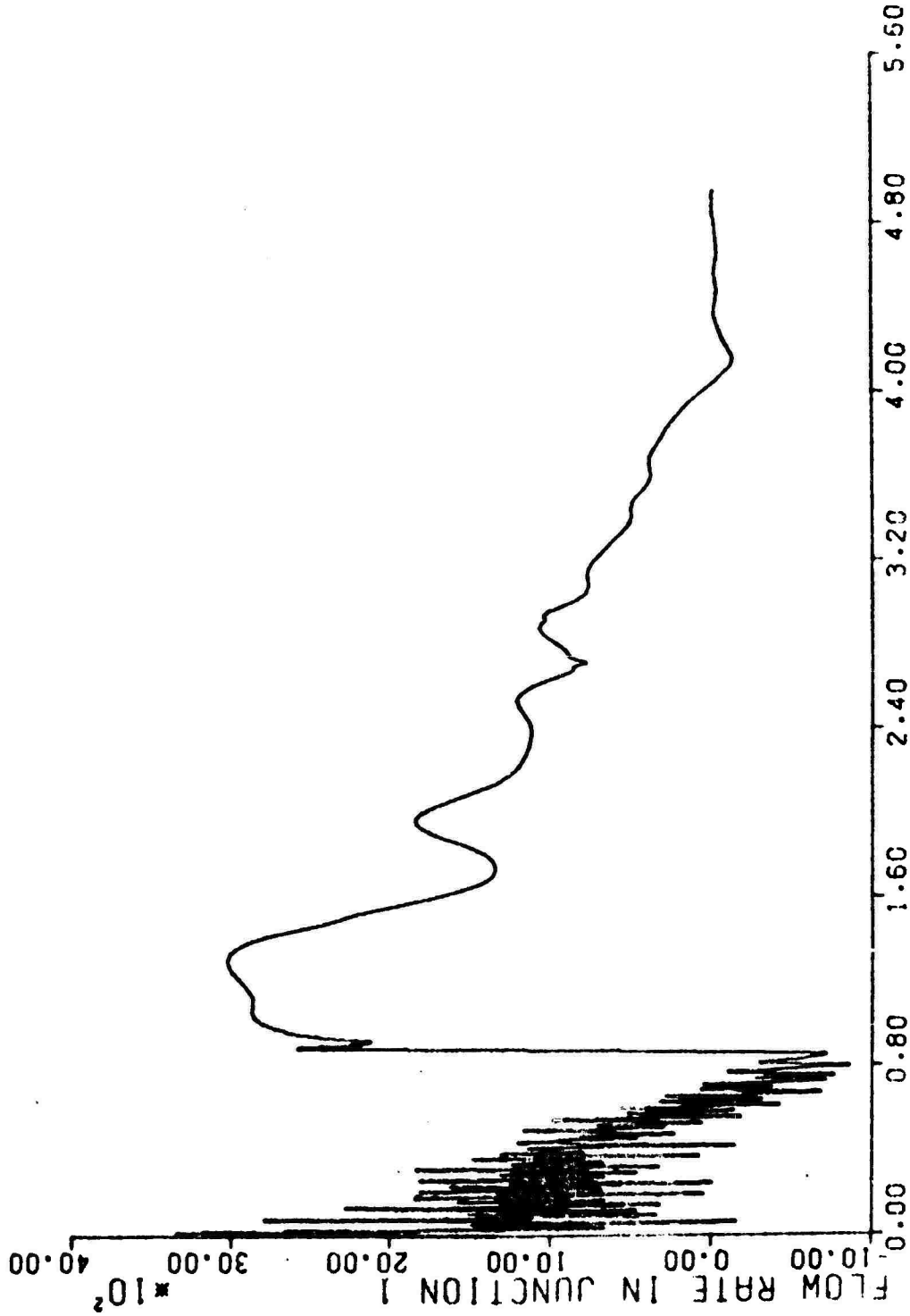

FIGURE 5D. DOUBLE ENDED HOT LEG BREAK (SLOT) CORE FLOW VS. TIME

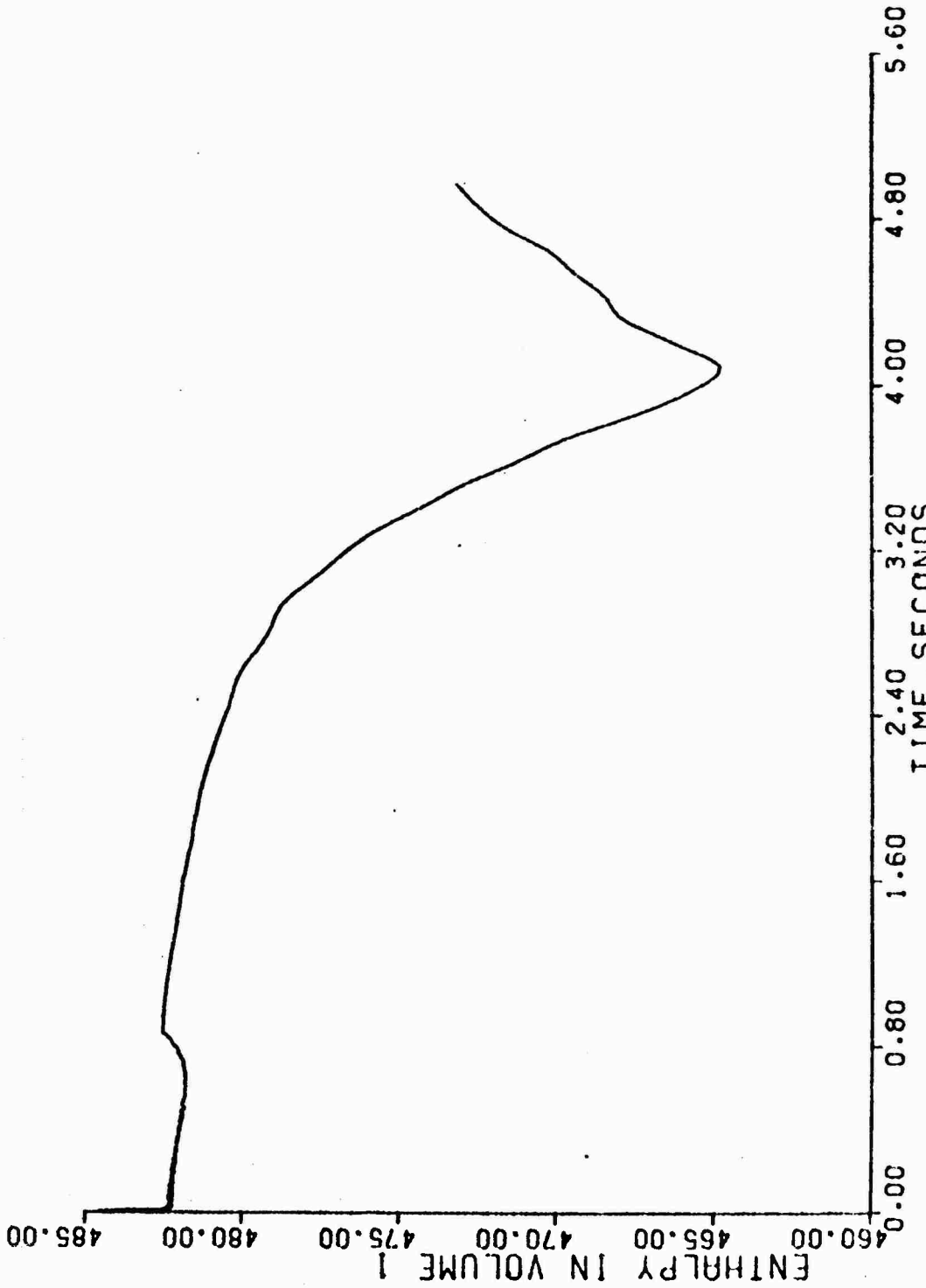

FIGURE 5E. DOUBLE ENDED HOT LEG BREAK (SLOT) INLET ENTHALPY VS. TIME

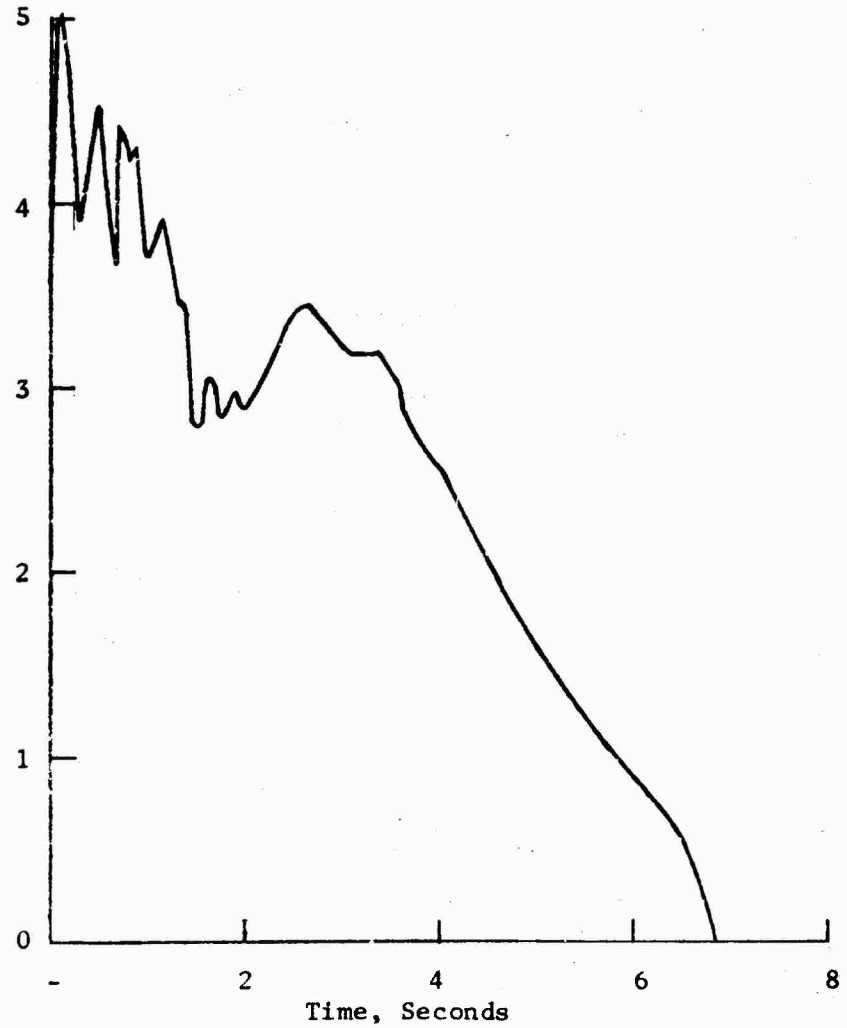

FIGURE 6A. SINGLE ENDED HOT LEG BREAK (SLOT) BREAK FLOW VS. TIME

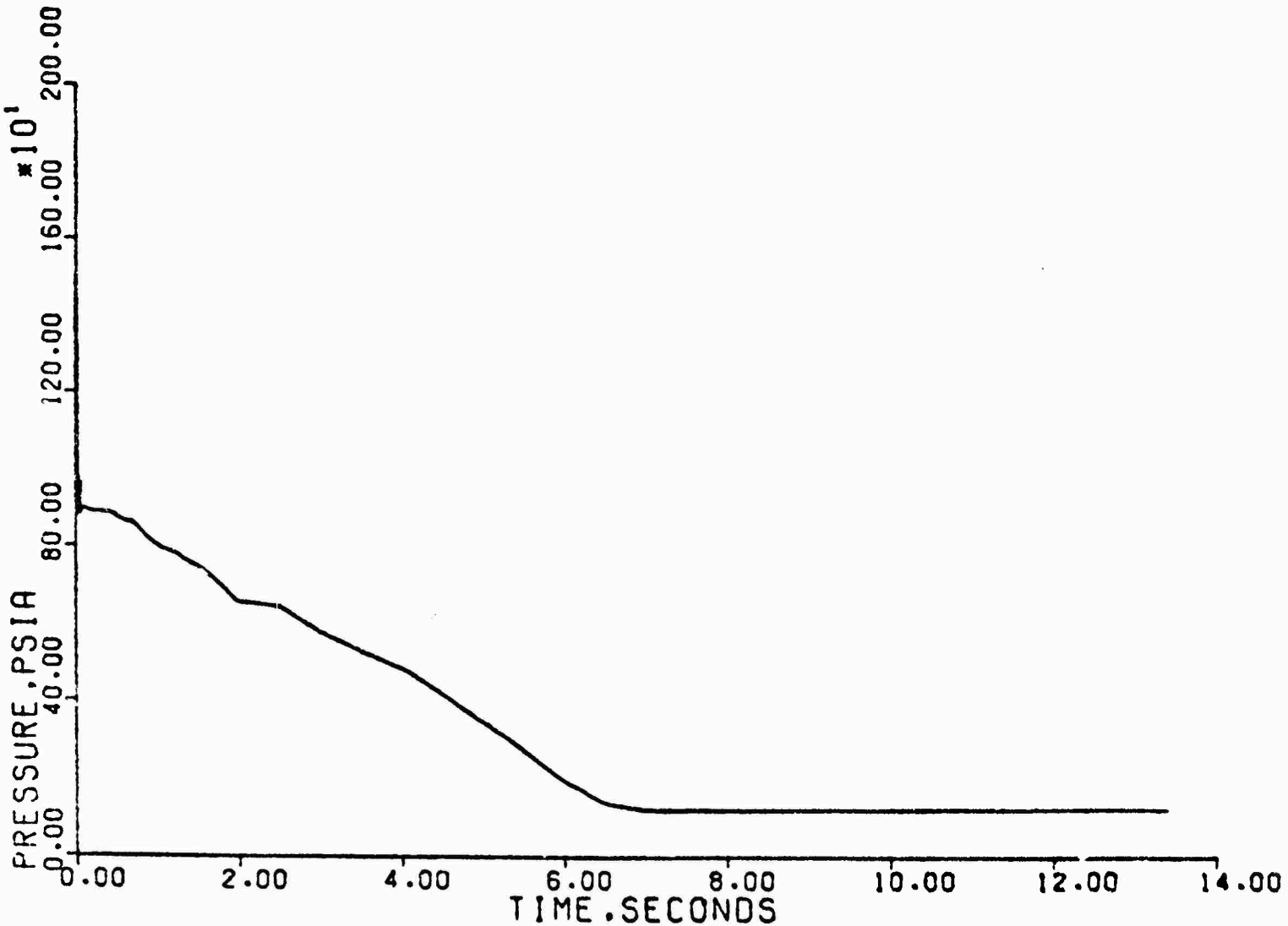

FIGURE 6B. SINGLE ENDED HOT LEG BREAK (SLOT) PRESSURE VS. TIME

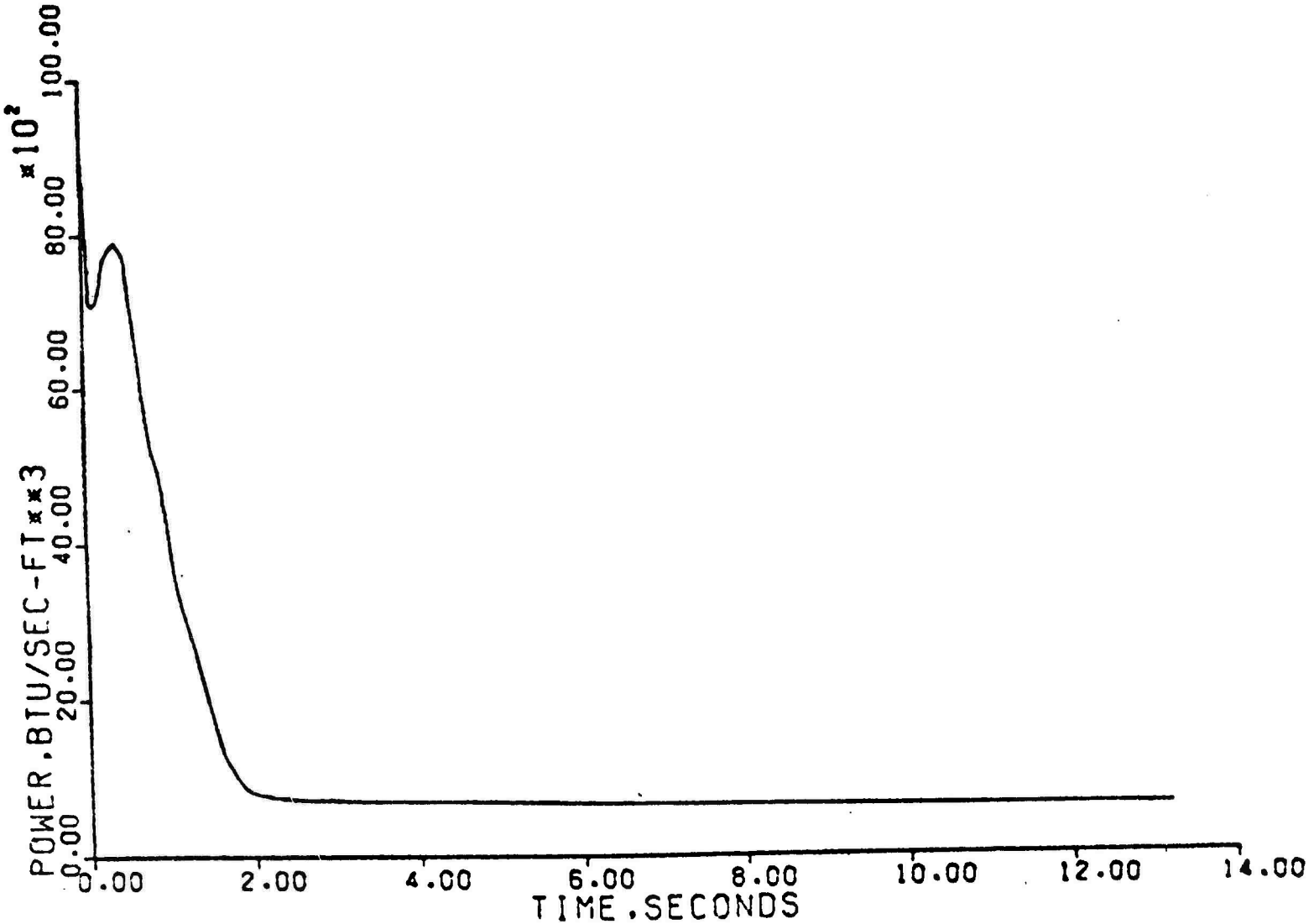

FIGURE 6C. SINGLE ENDED HOT LEG BREAK (SLOT) POWER LEVEL VS. TIME

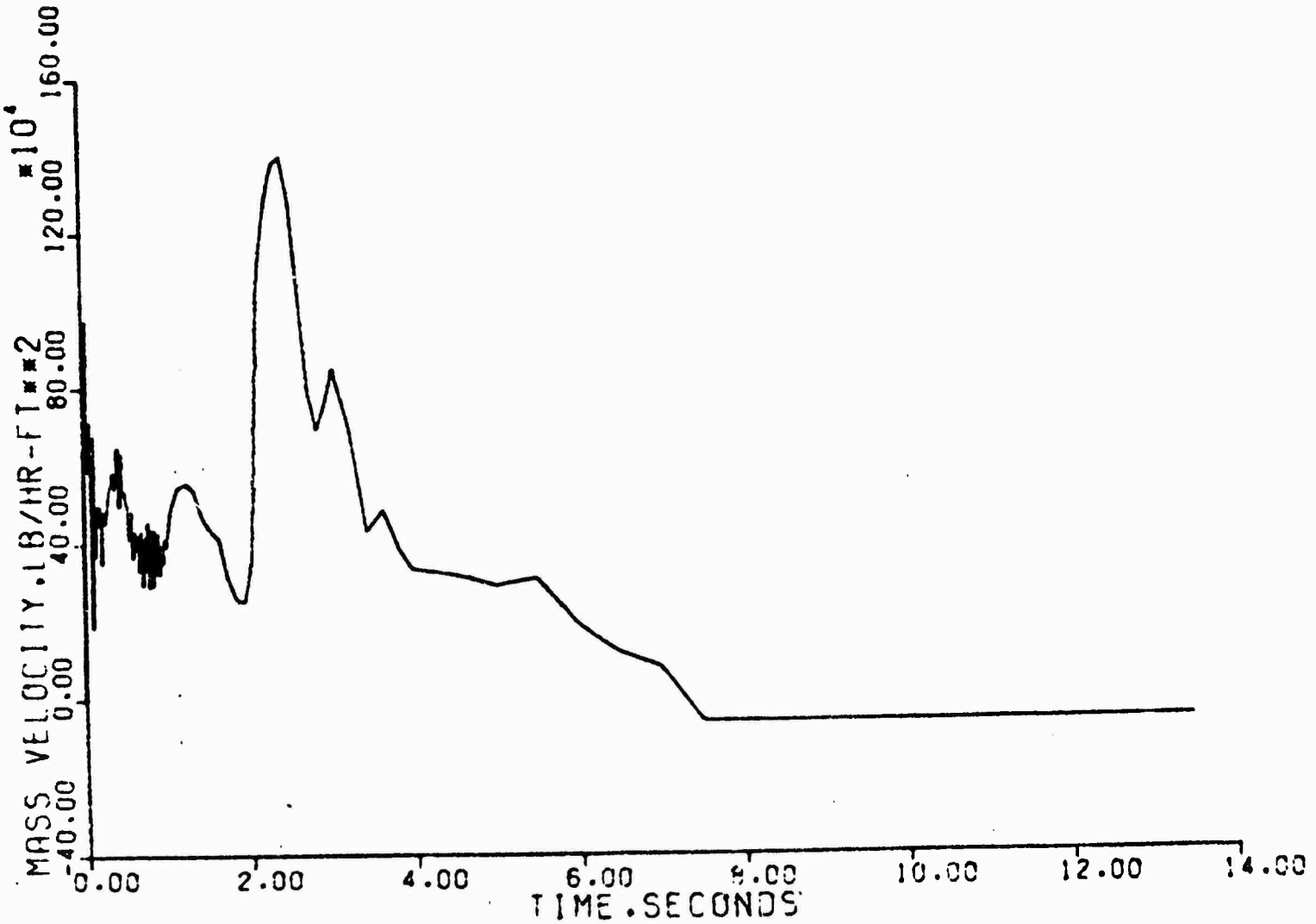

FIGURE 6D. SINGLE ENDED HOT LEG BREAK (SLOT) CORE FLOW VS. TIME

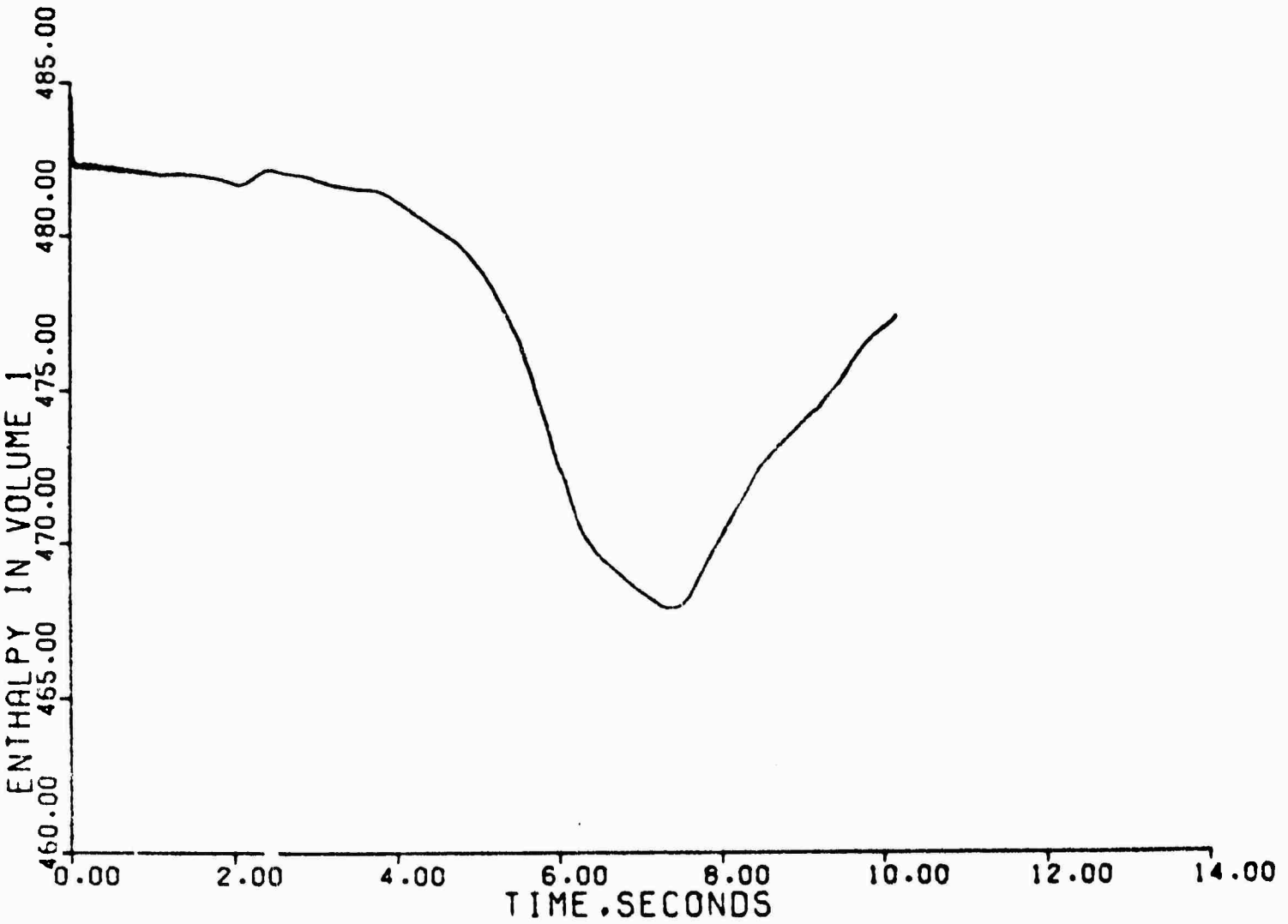

FIGURE 6E. SINGLE ENDED HOT LEG BREAK (SLOT) INLET ENTHALPY VS. TIME

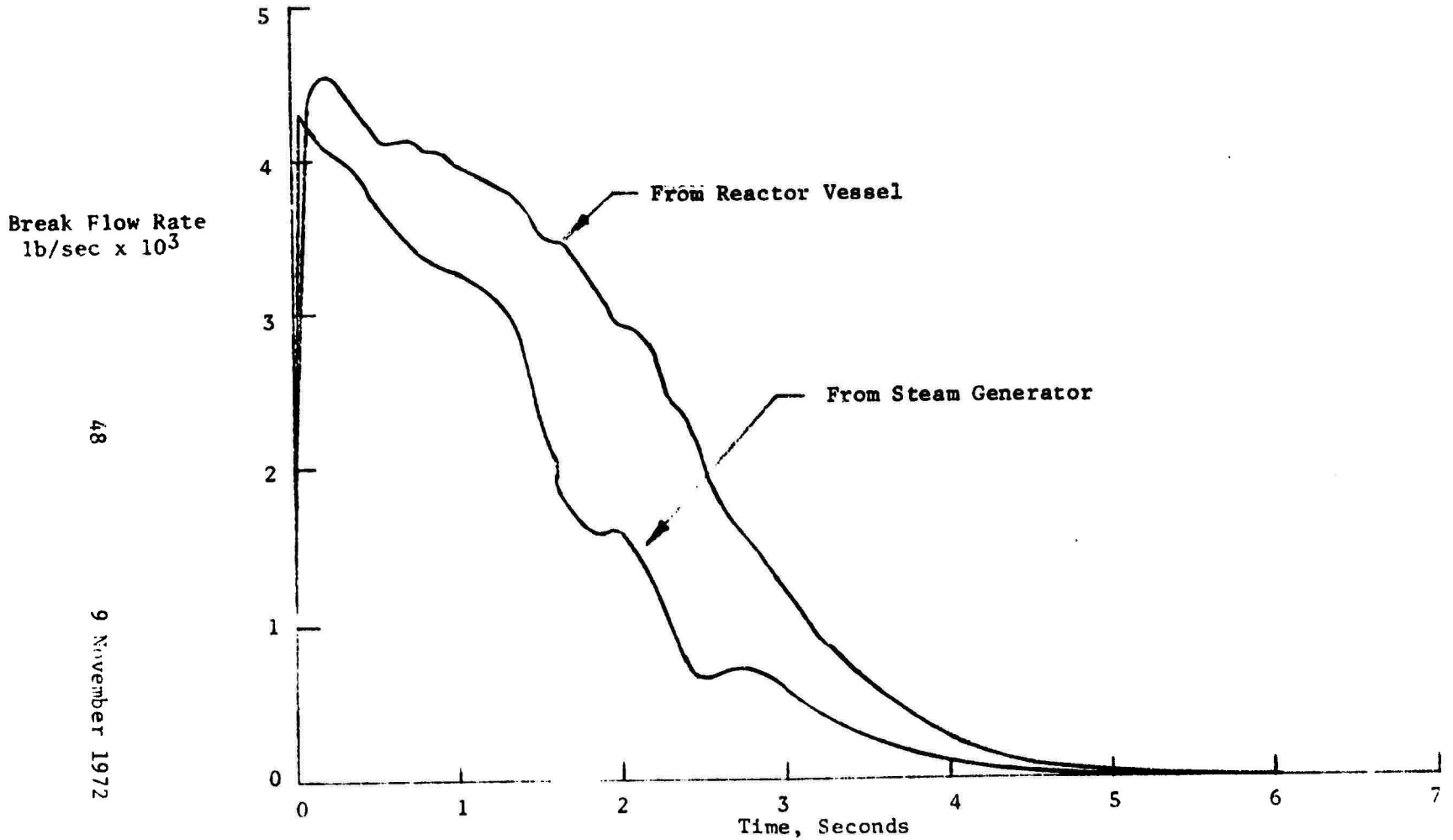

FIGURE 7A. DOUBLE ENDED BREAK AT PUMP DISCHARGE (GUILLOTINE) BREAK FLOW VS. TIME

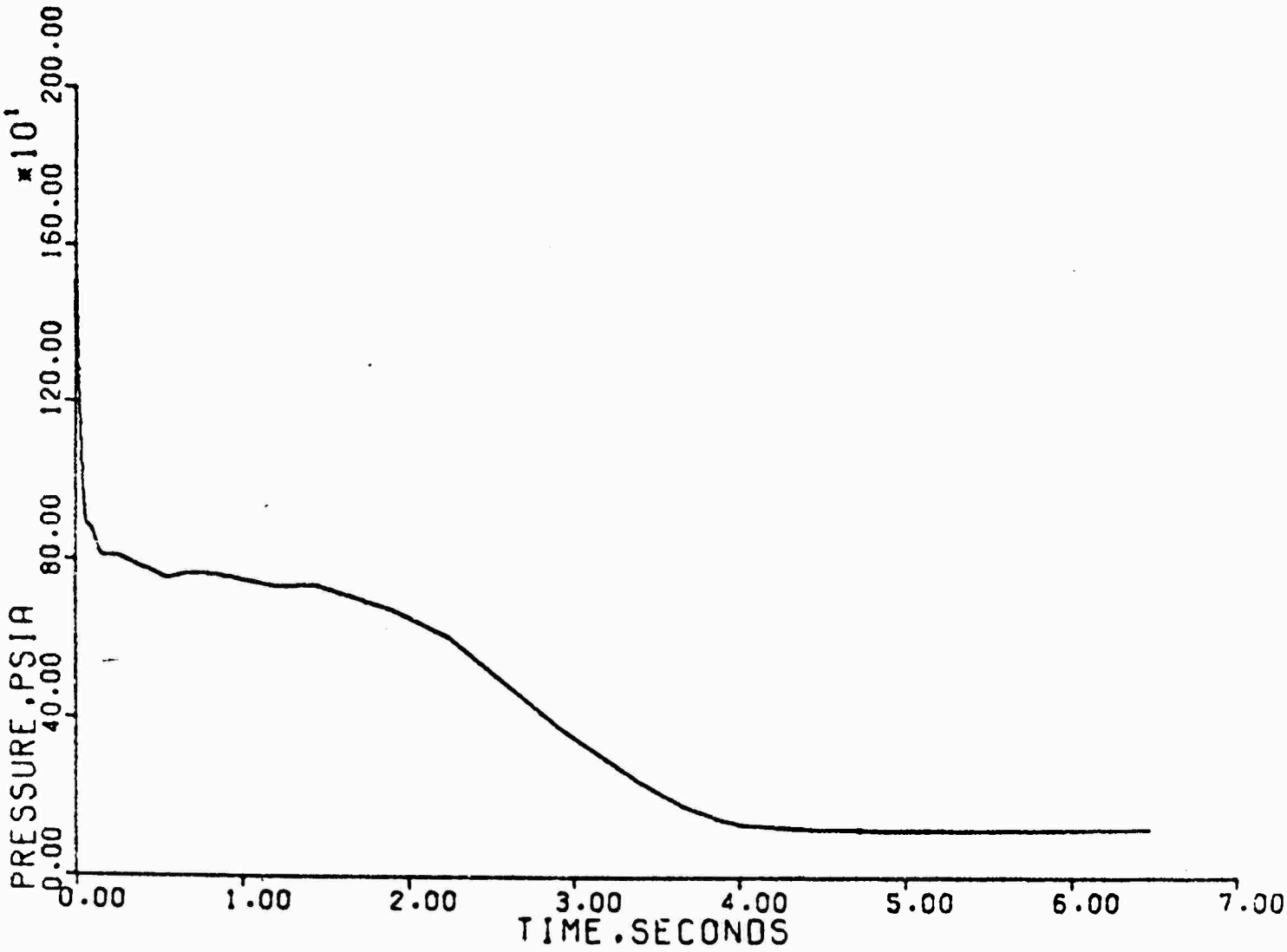

FIGURE 7B. DOUBLE ENDED COLD LEG BREAK AT PUMP DISCHARGE (GUILLOTINE) PRESSURE VS. TIME

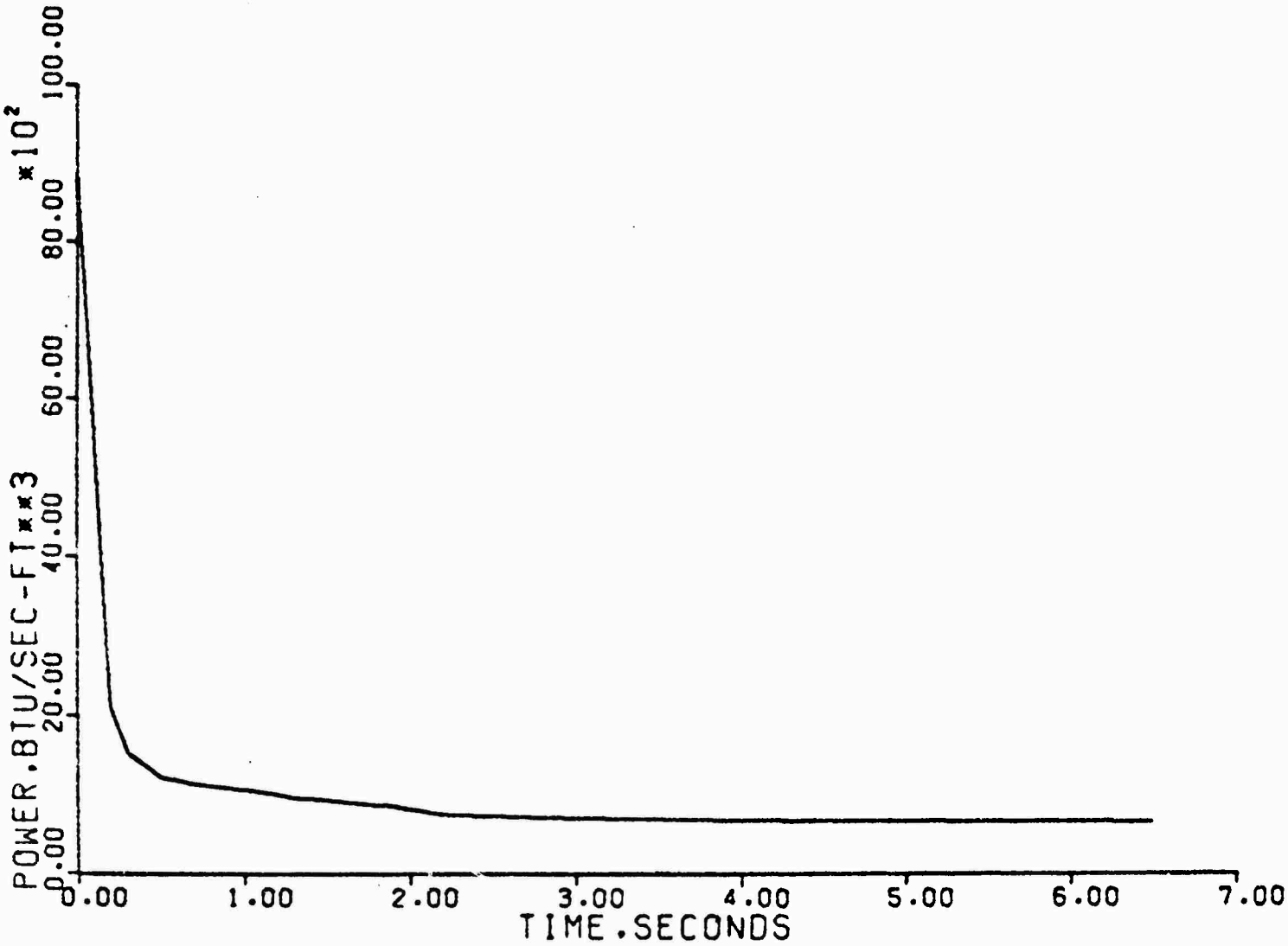

FIGURE 7C. DOUBLE ENDED COLD LEG BREAK AT PUMP DISCHARGE (GUILLOTINE) POWER LEVEL VS. TIME

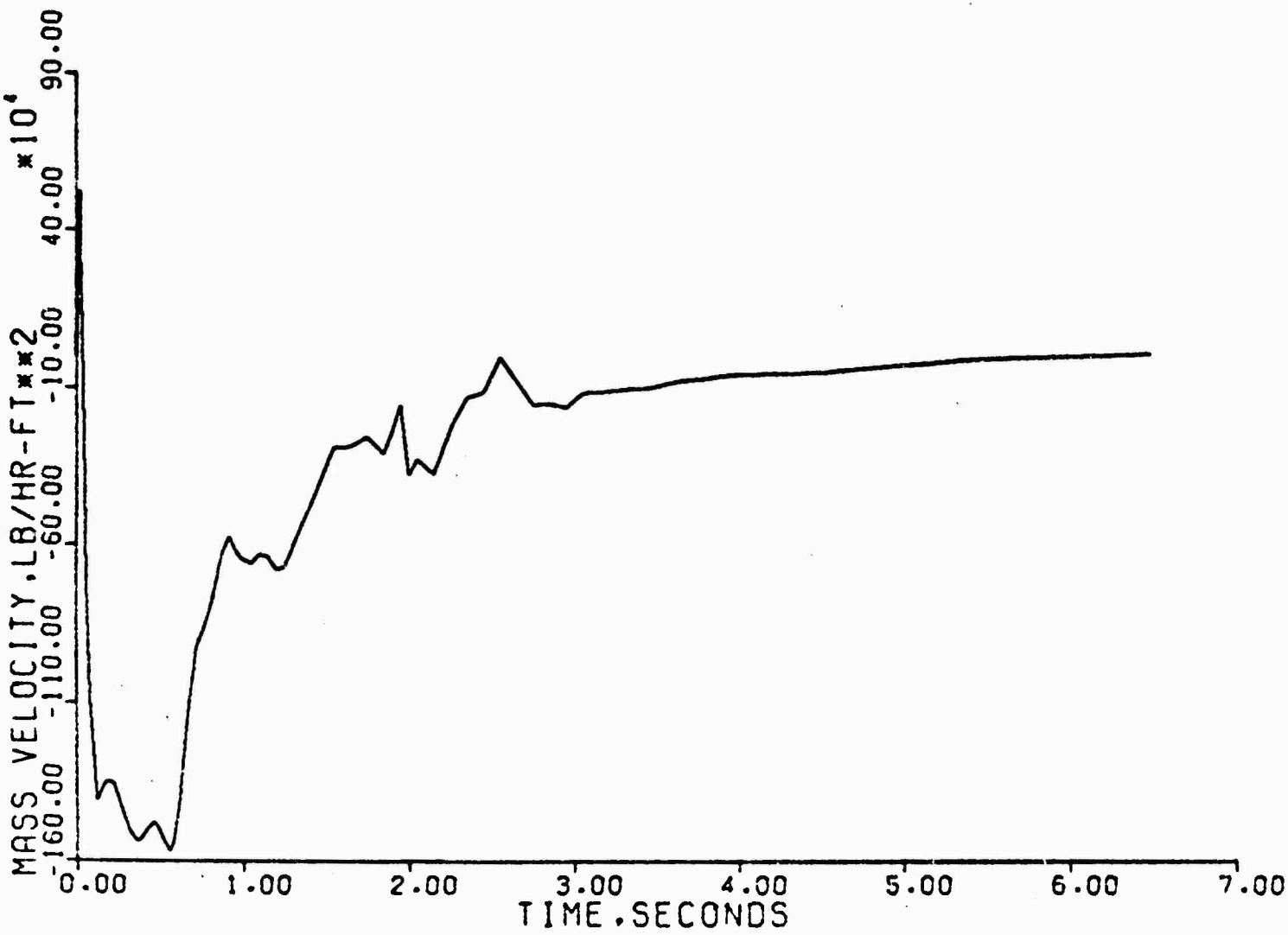

FIGURE 7D. DOUBLE ENDED COLD LEG BREAK AT PUMP DISCHARGE (GUILLOTINE) CORE FLOW VS. TIME

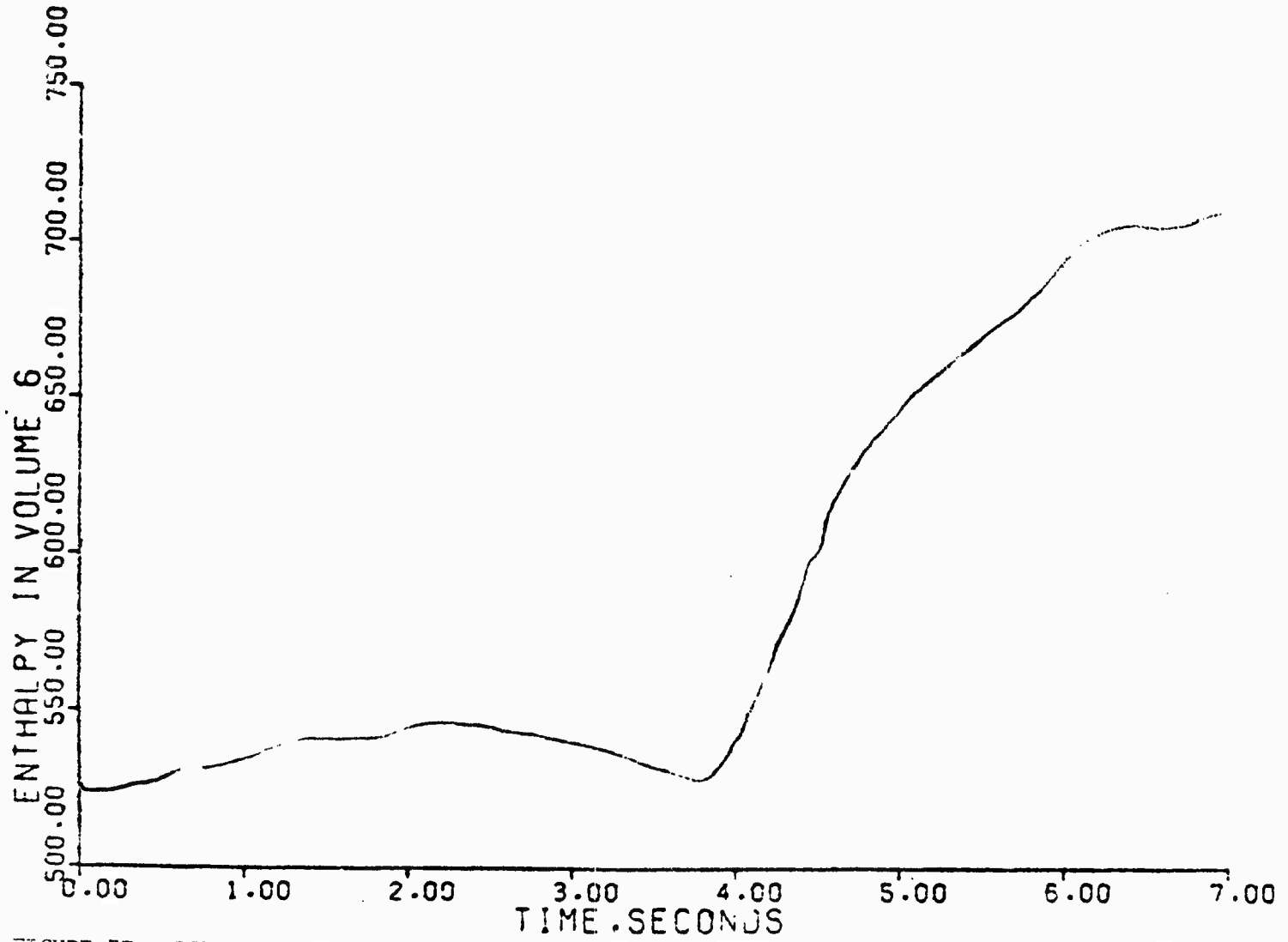

FIGURE 7E. DOUBLE ENDED COLD LEG BREAK AT PUMP DISCHARGE (GUILLOTINE) INLET ENTHALPY VS TIME

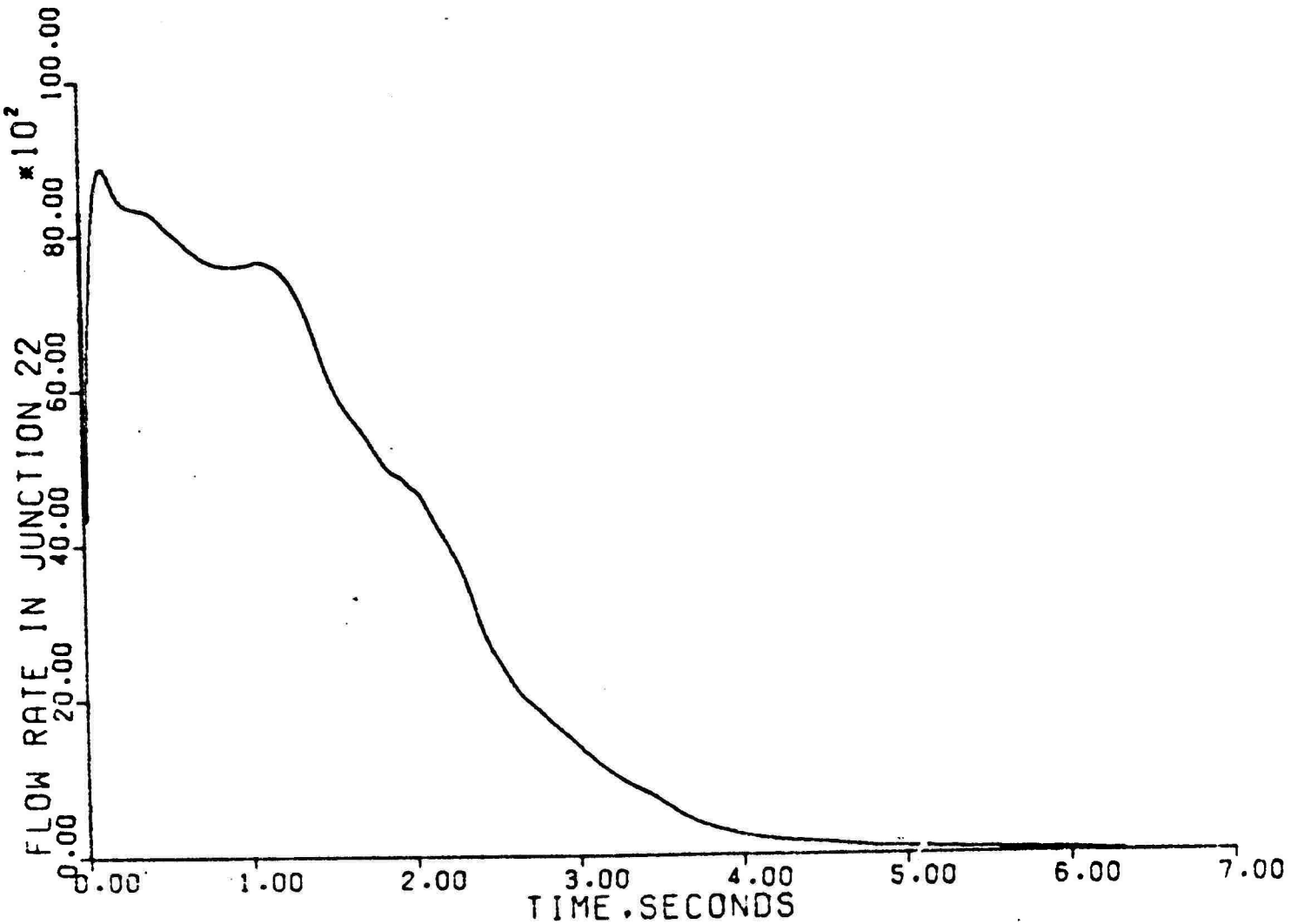

FIGURE 8A. DOUBLE ENDED COLD LEG AT PUMP DISCHARGE (SLOT) BREAK FLOW RATE VS. TIME

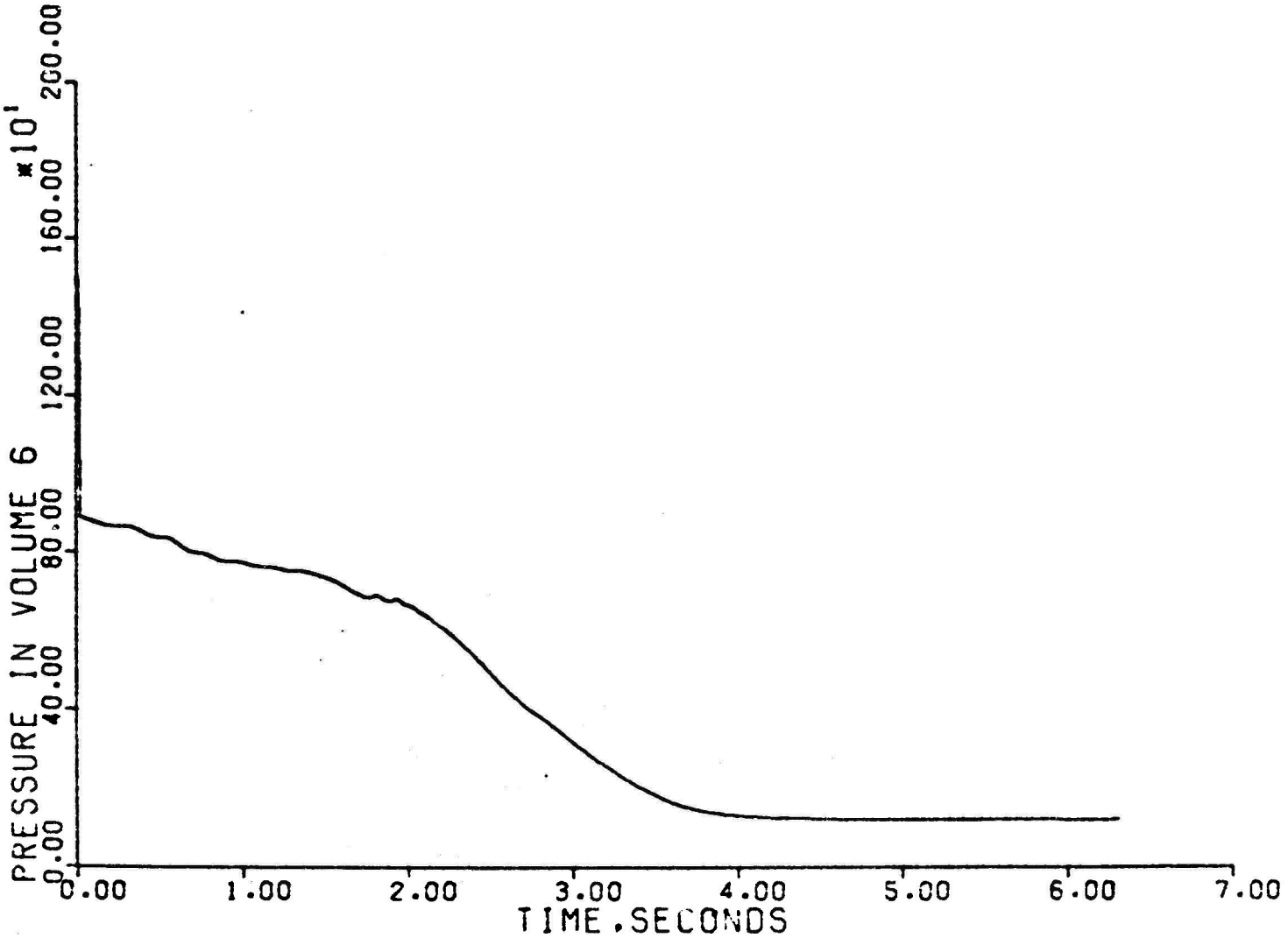

FIGURE 8B. DOUBLE ENDED COLD LEG BREAK AT PUMP DISCHARGE (SLOT) PRESSURE VS. TIME

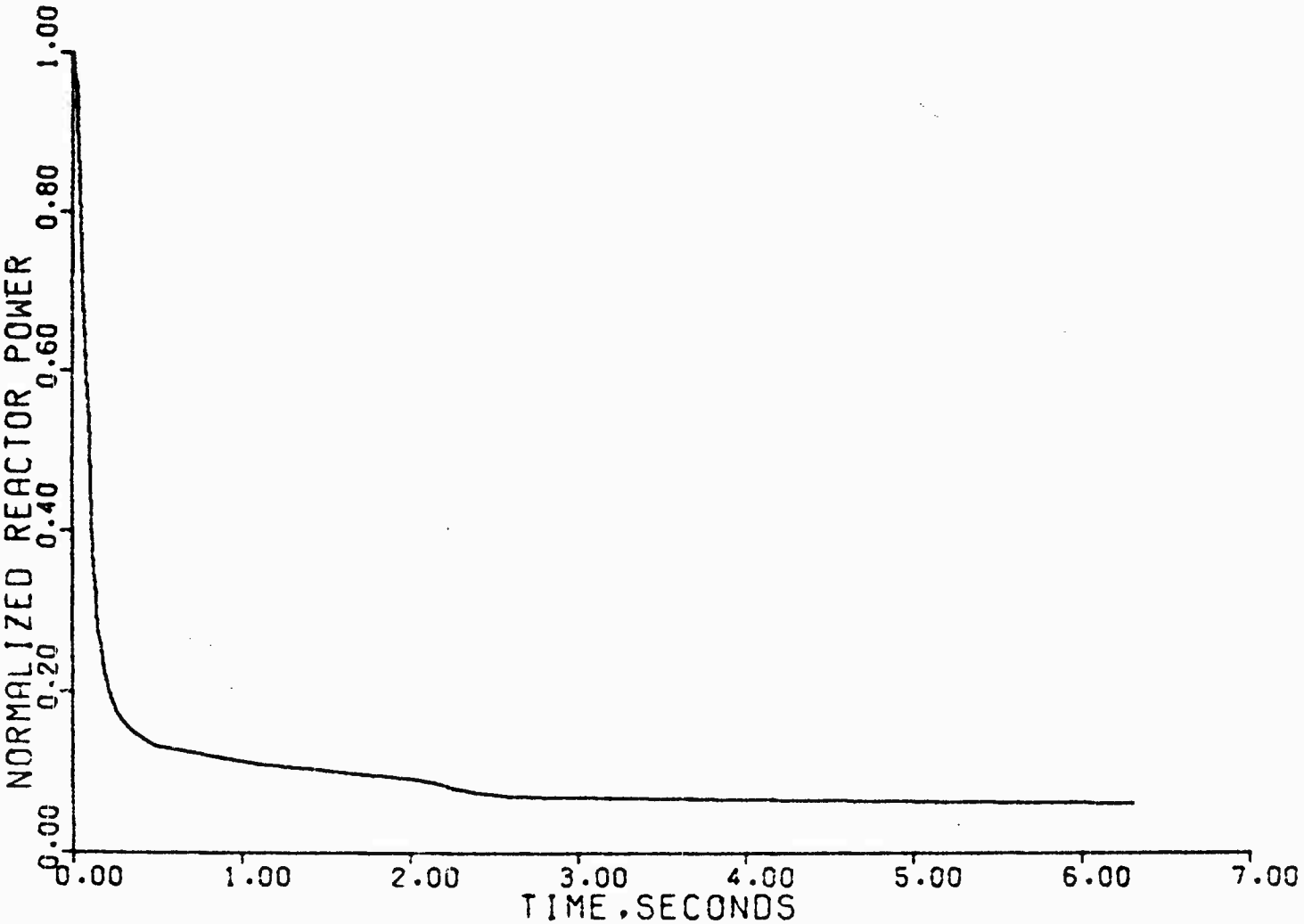

FIGURE 8C. DOUBLE ENDED COLD LEG BREAK AT PUMP DISCHARGE (SLOT) POWER LEVEL VS. TIME

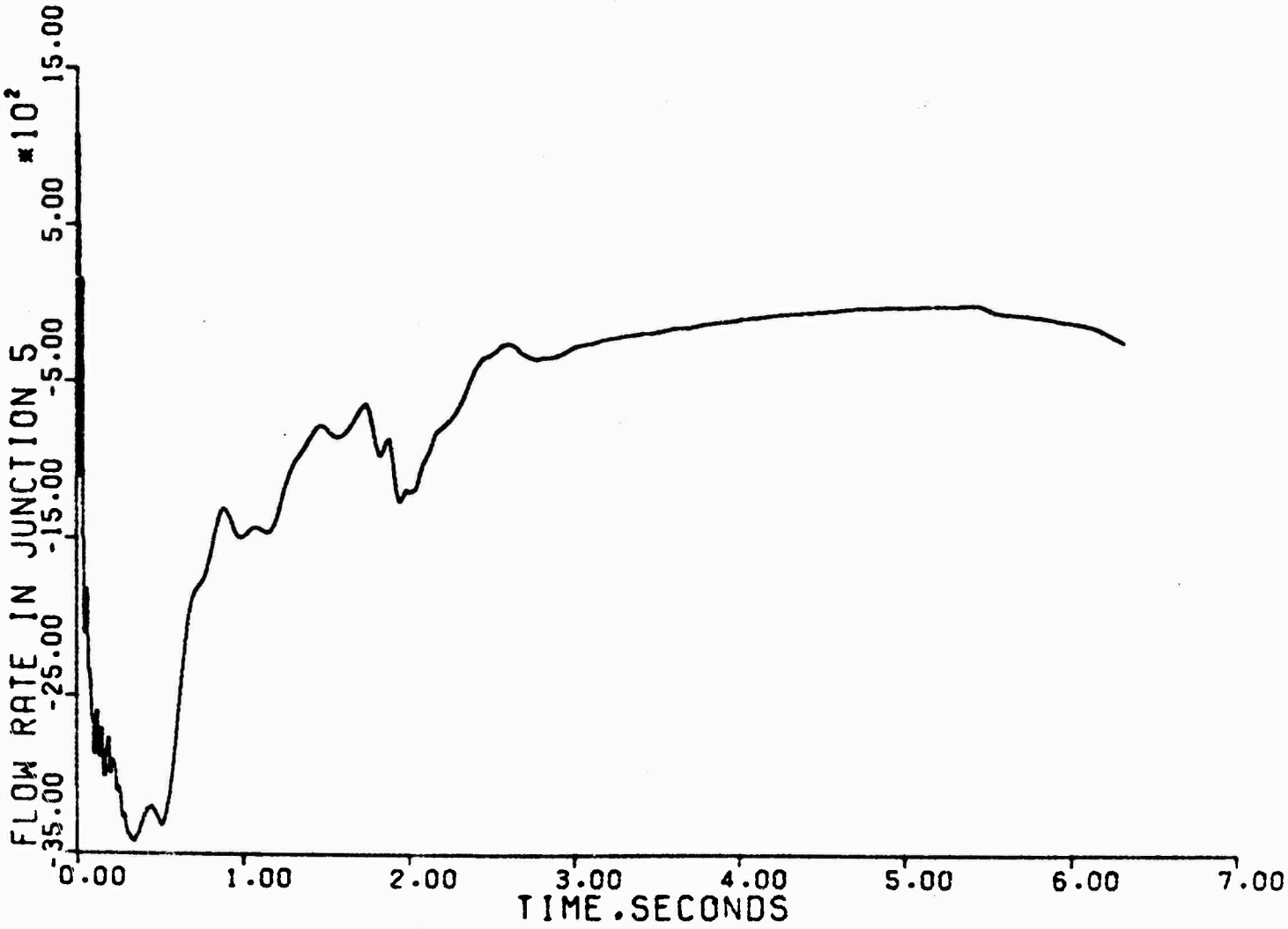

FIGURE 8D. DOUBLE ENDED COLD LEG BREAK AT PUMP DISCHARGE (SLOT) CORE FLOW VS. TIME

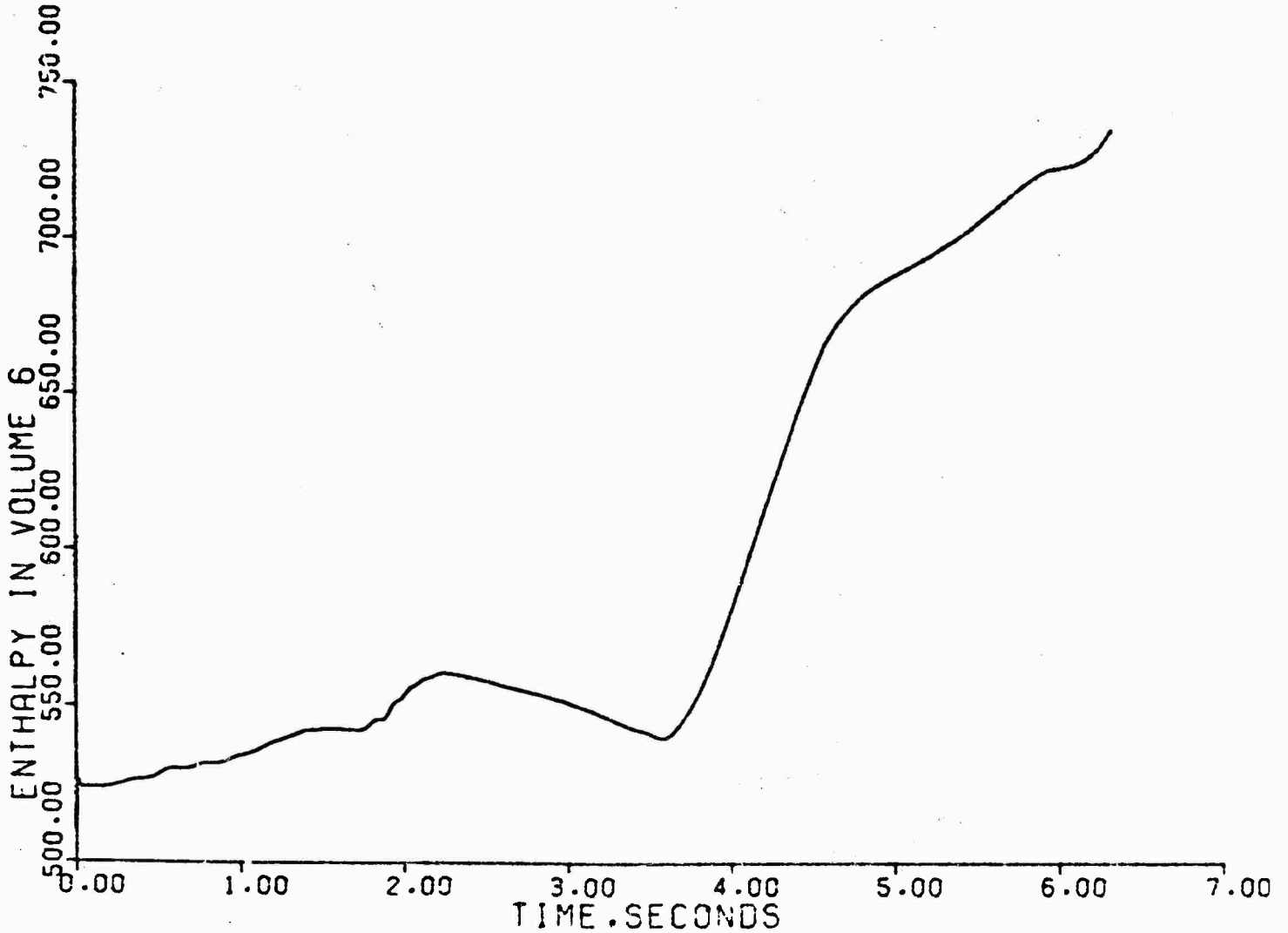

FIGURE 8E. DOUBLE ENDED COLD LEG BREAK AT PUMP DISCHARGE (SLOT) INLET ENTHALPY VS. TIME

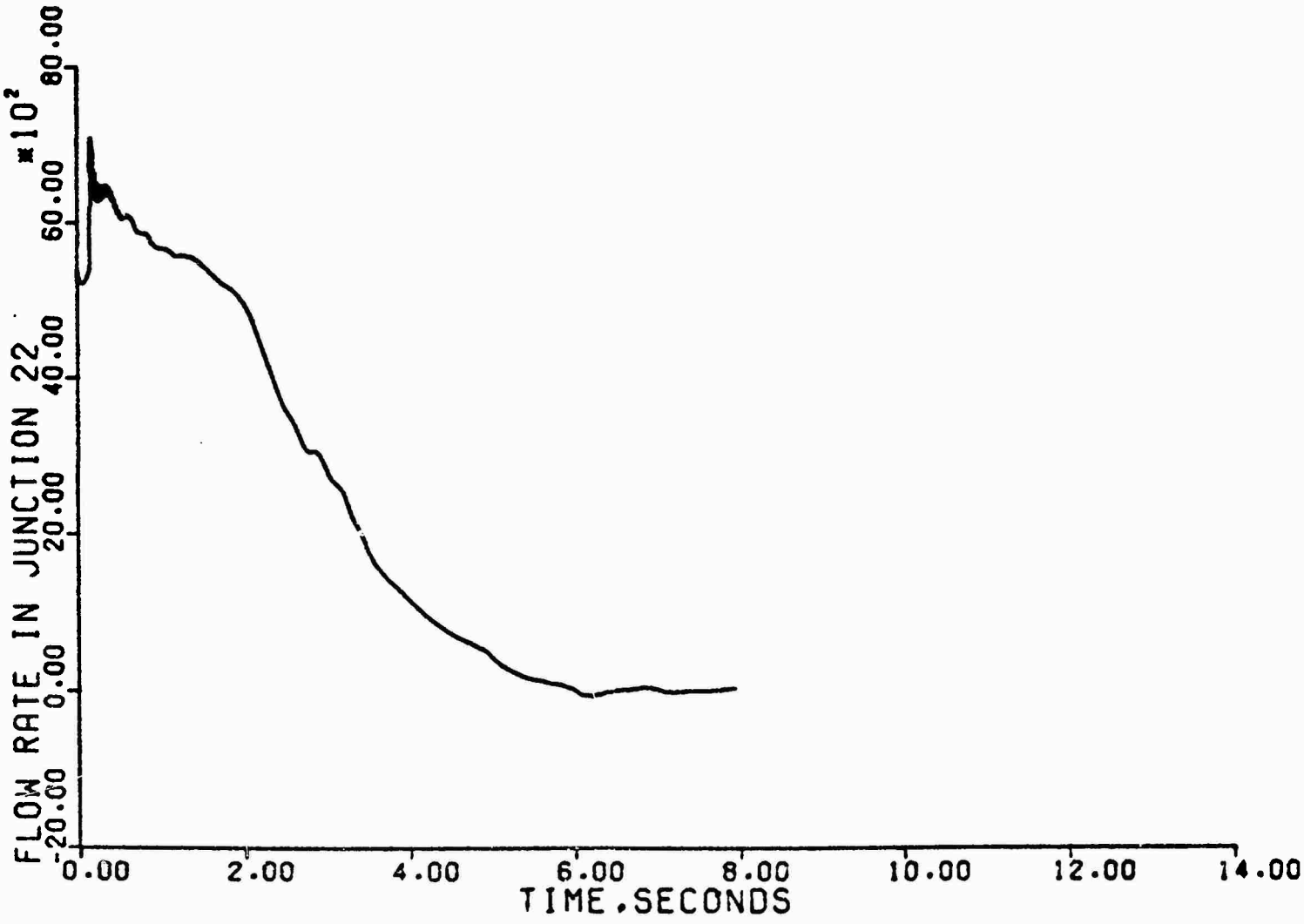

FIGURE 9A. 0.6 DOUBLE ENDED COLD LEG BREAK AT PUMP DISCHARGE (SLOT) BREAK FLOW RATE VS. TIME

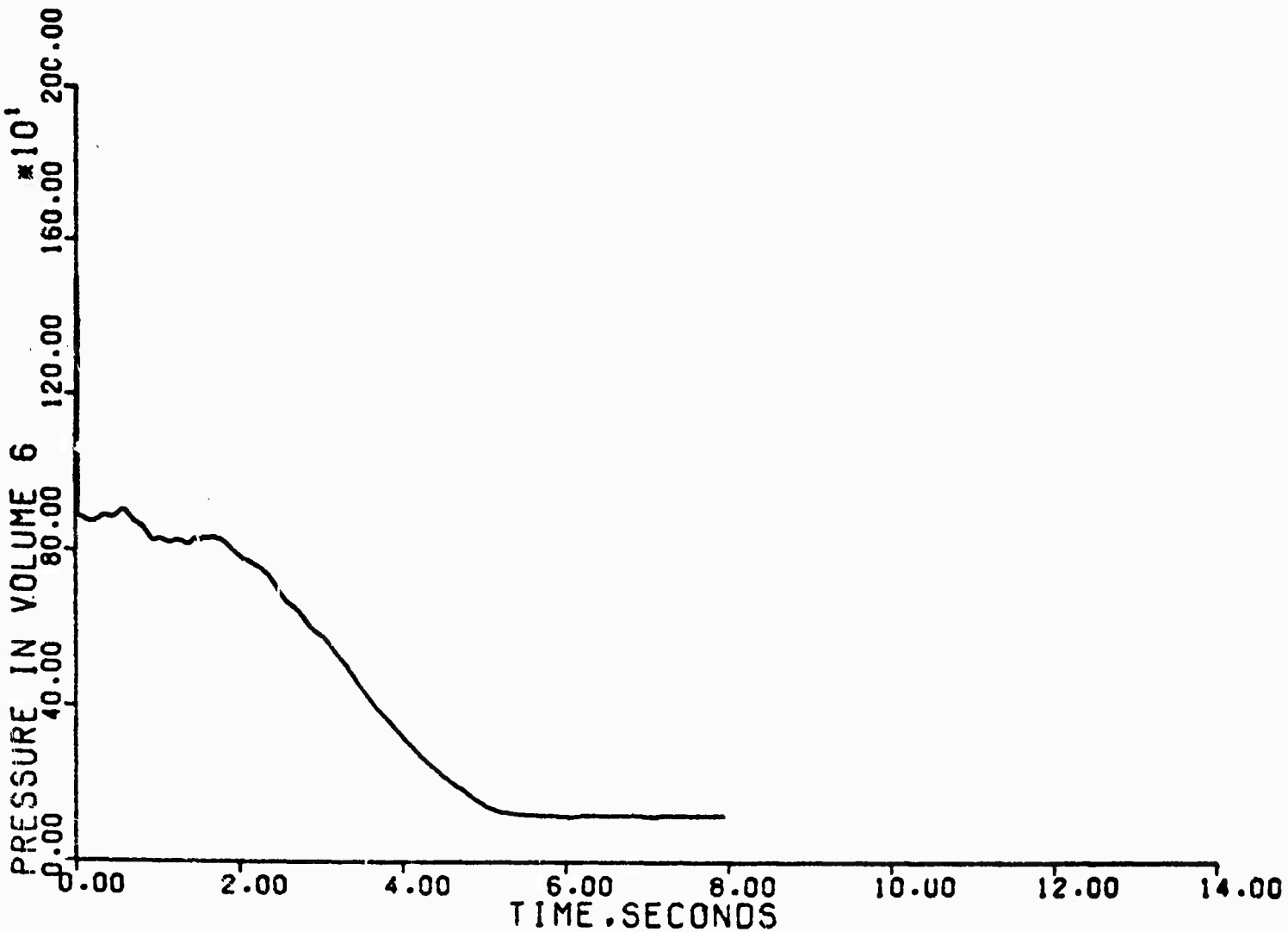

FIGURE 9B. DOUBLE ENDED COLD LEG BREAK AT PUMP DISCHARGE (SLOT) PRESSURE VS. TIME

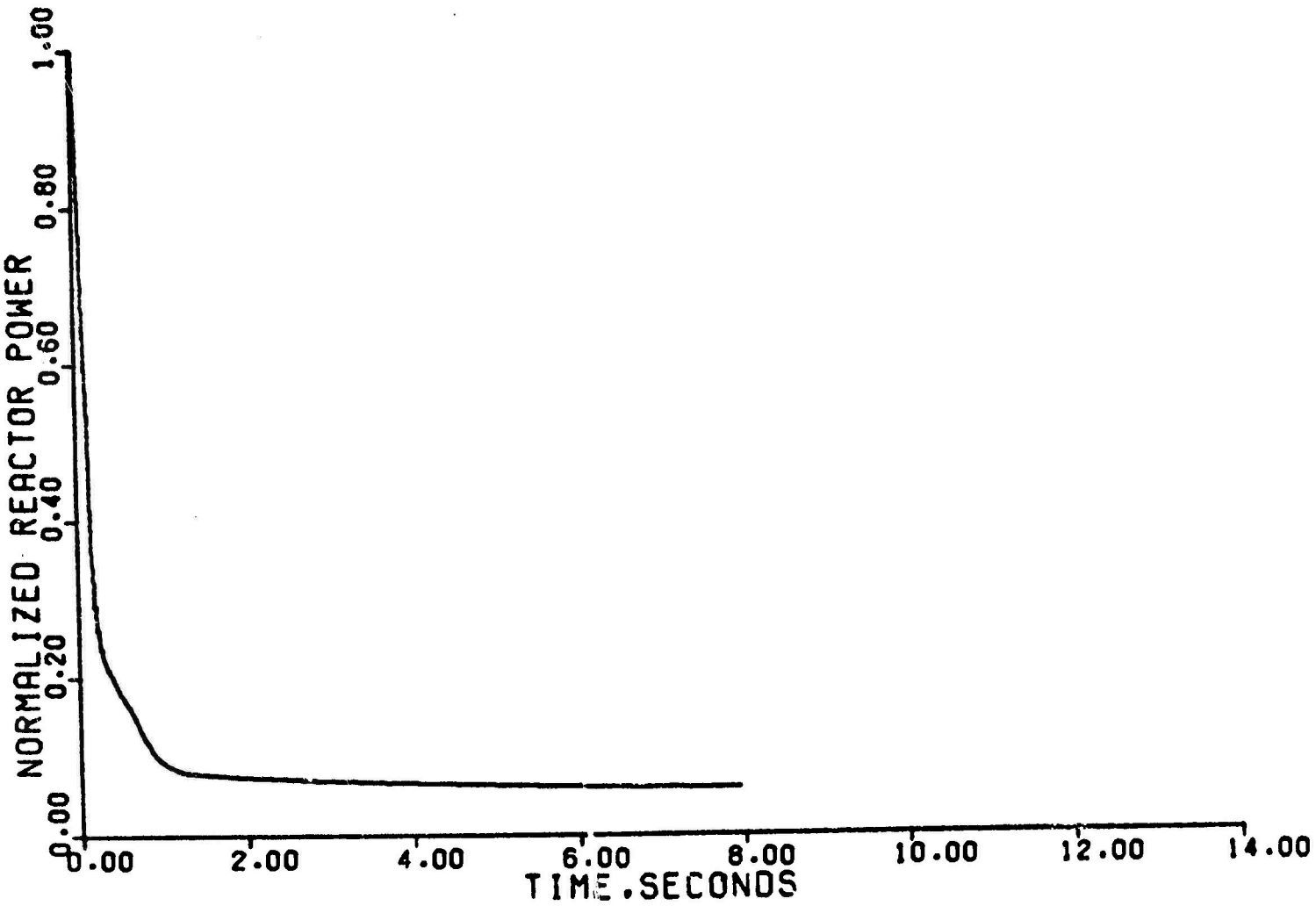

FIGURE 9C. 0.6 DOUBLE ENDED COLD LEG BREAK AT PUMP DISCHARGE (SLOT) POWER LEVEL VS. TIME

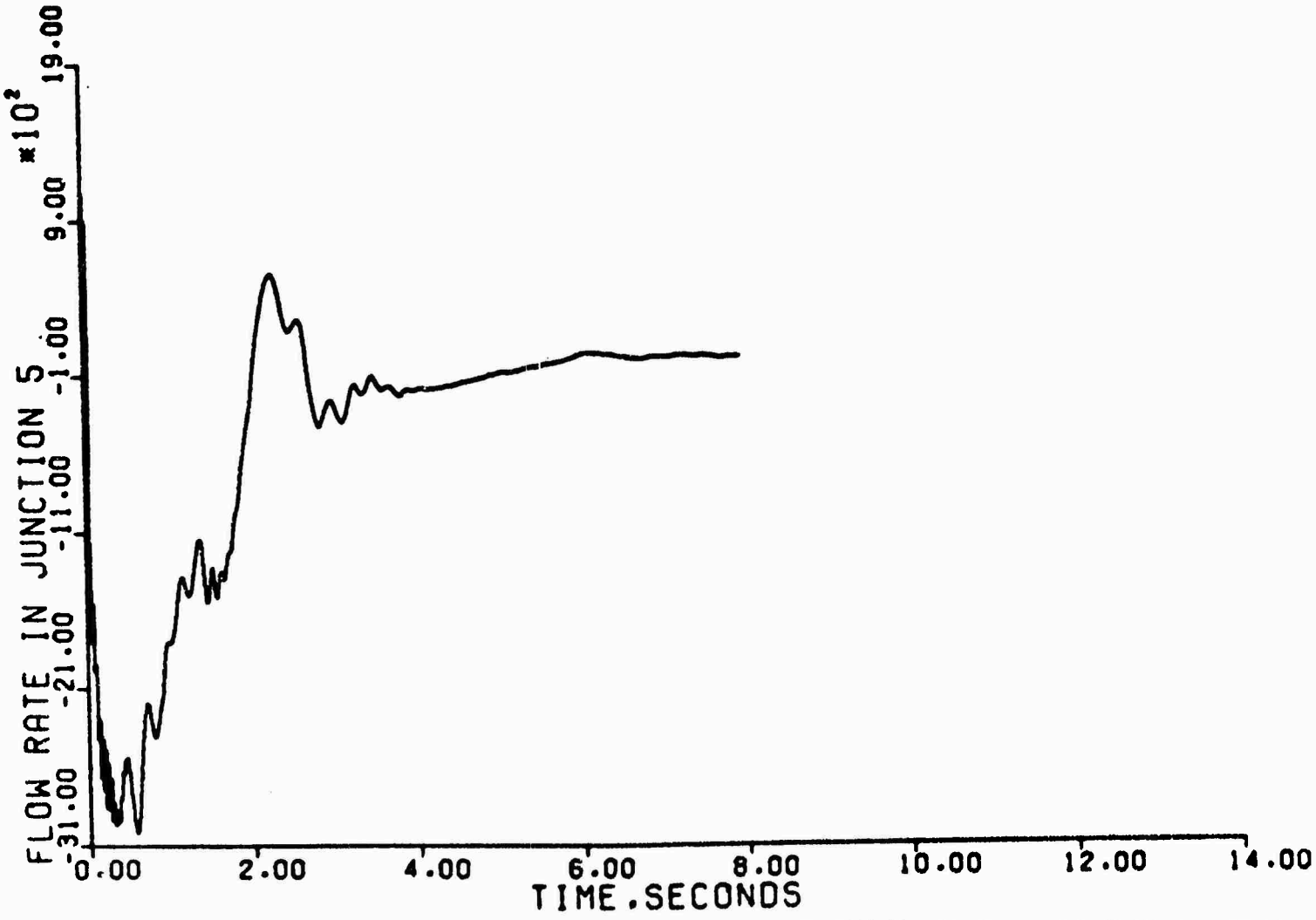

FIGURE 9D. 0.6 DOUBLE ENDED COLD LEG BREAK AT PUMP DISCHARGE (SLOT) CORE FLOW VS. TIME

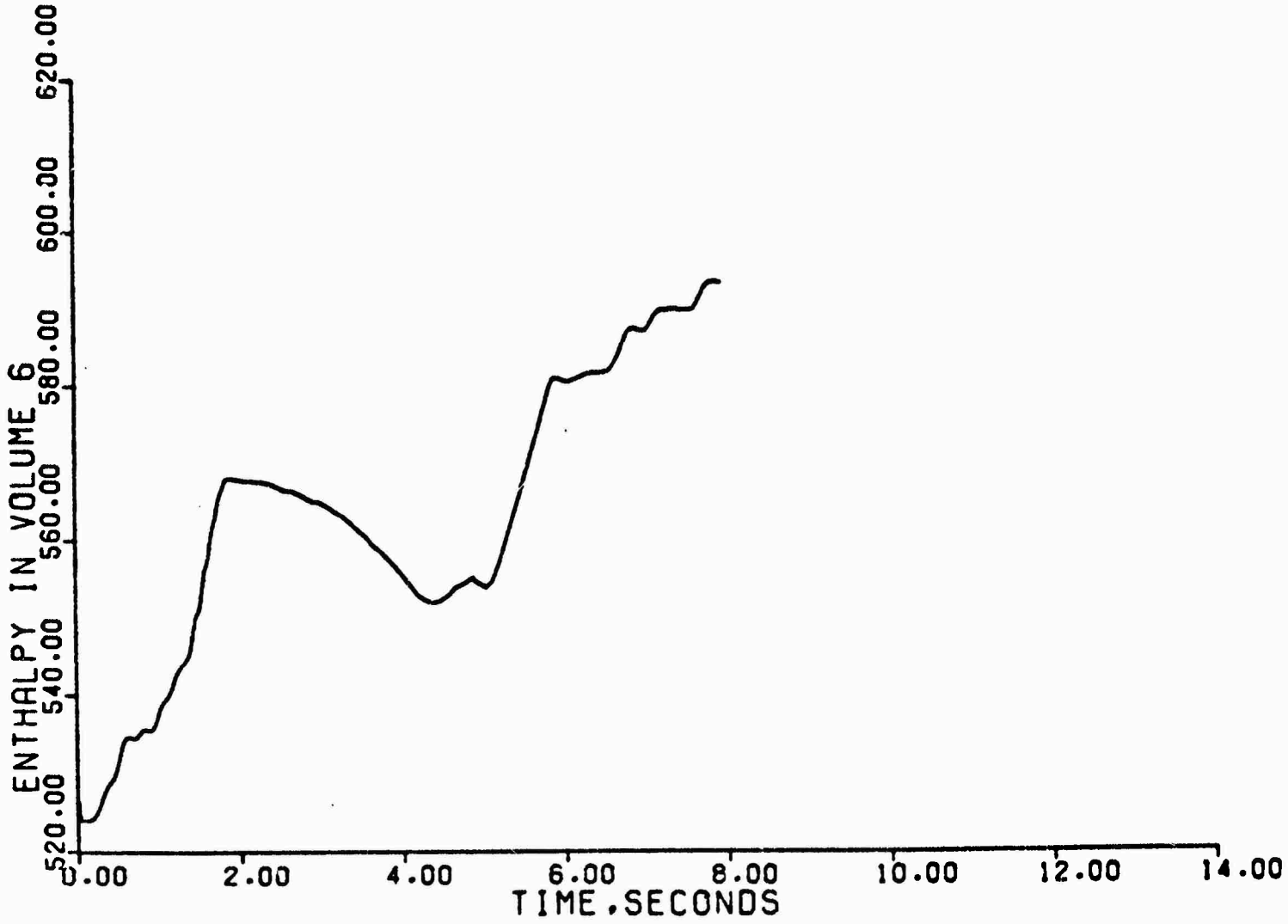

FIGURE 9E. 0.6 DOUBLE ENDED COLD LEG BREAK AT PUMP DISCHARGE (SLOT) INLET ENTHALPY VS. TIME

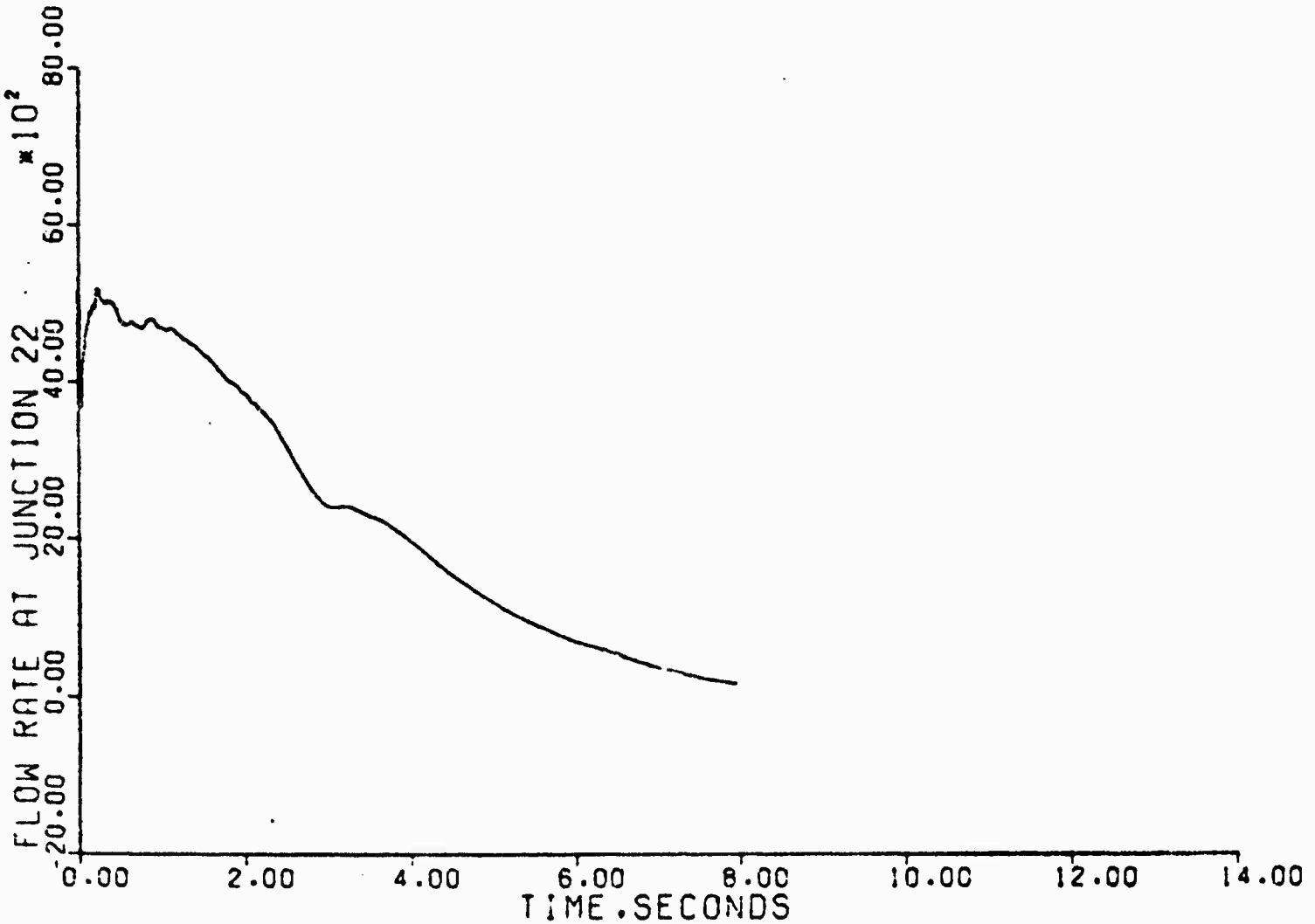

FIGURE 10A. 0.6 DOUBLE ENDED COLD LEG BREAK AT PUMP INLET (SLOT) BREAK FLOW RATE VS. TIME

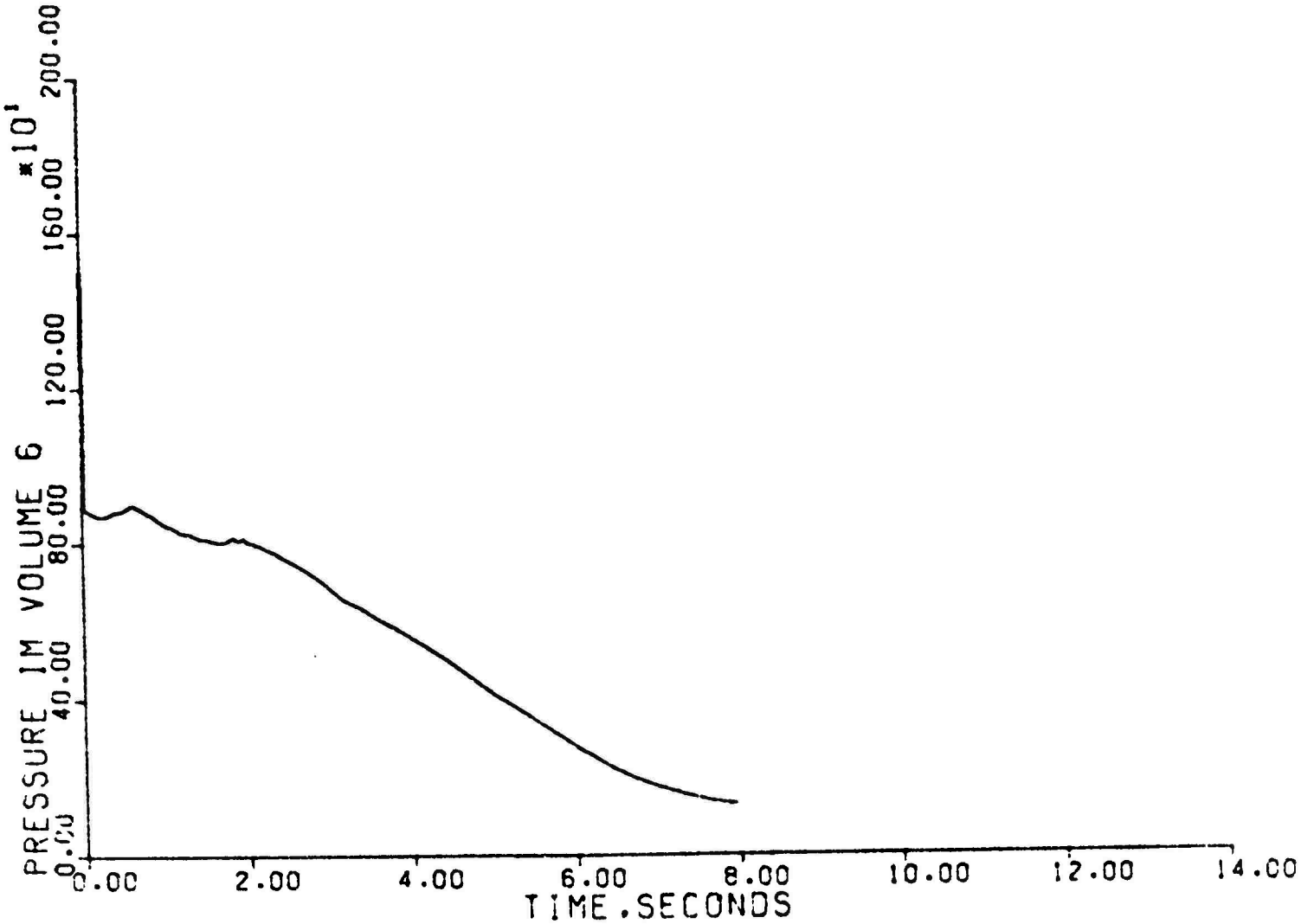

FIGURE 10B. 0.6 DOUBLE ENDED COLD LEG BREAK AT PUMP INLET (SLOT) PRESSURE VS. TIME

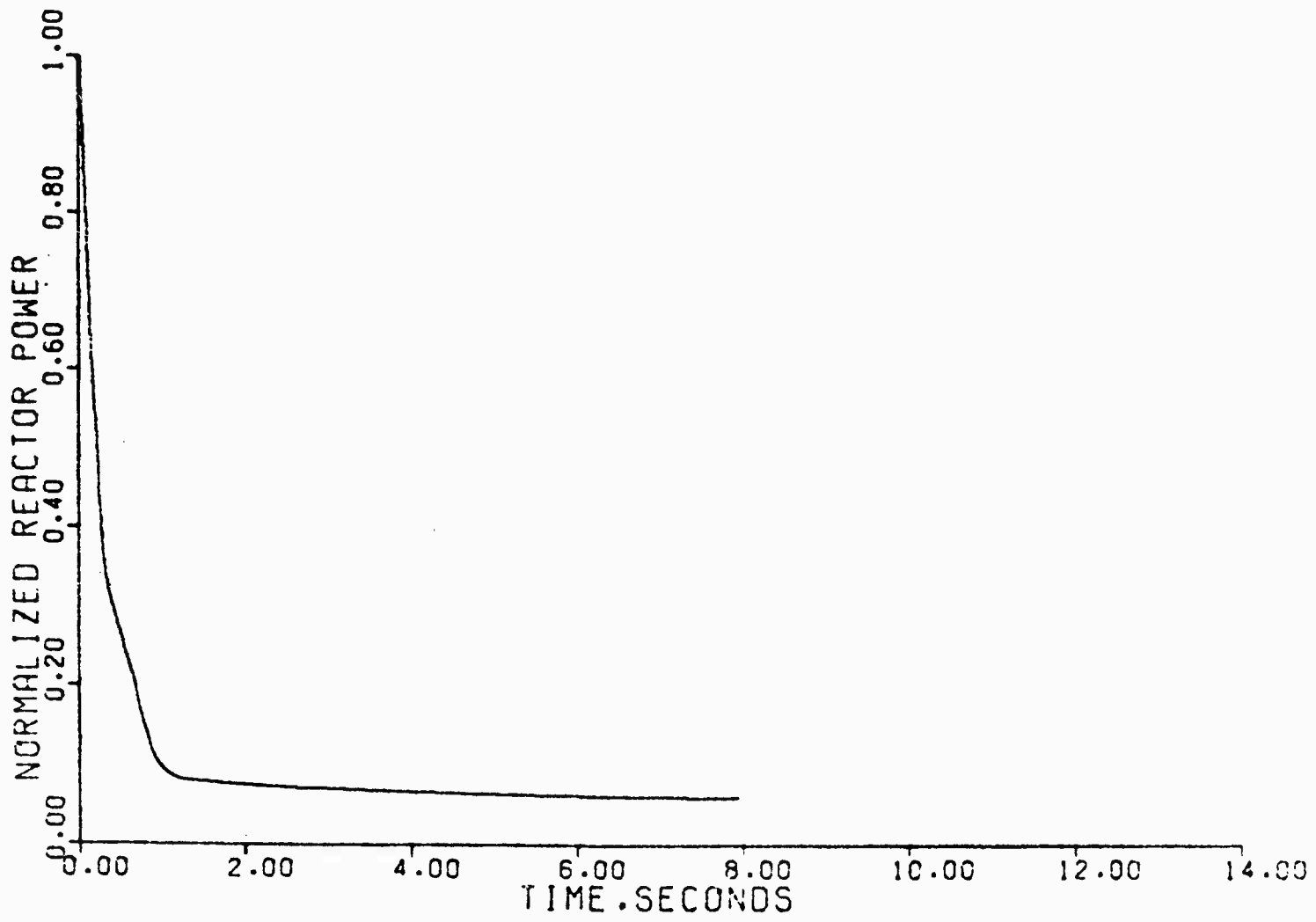

FIGURE 10C. 0.6 DOUBLE ENDED COLD LEG BREAK AT PUMP INLET (SLOT) POWER LEVEL VS. TIME

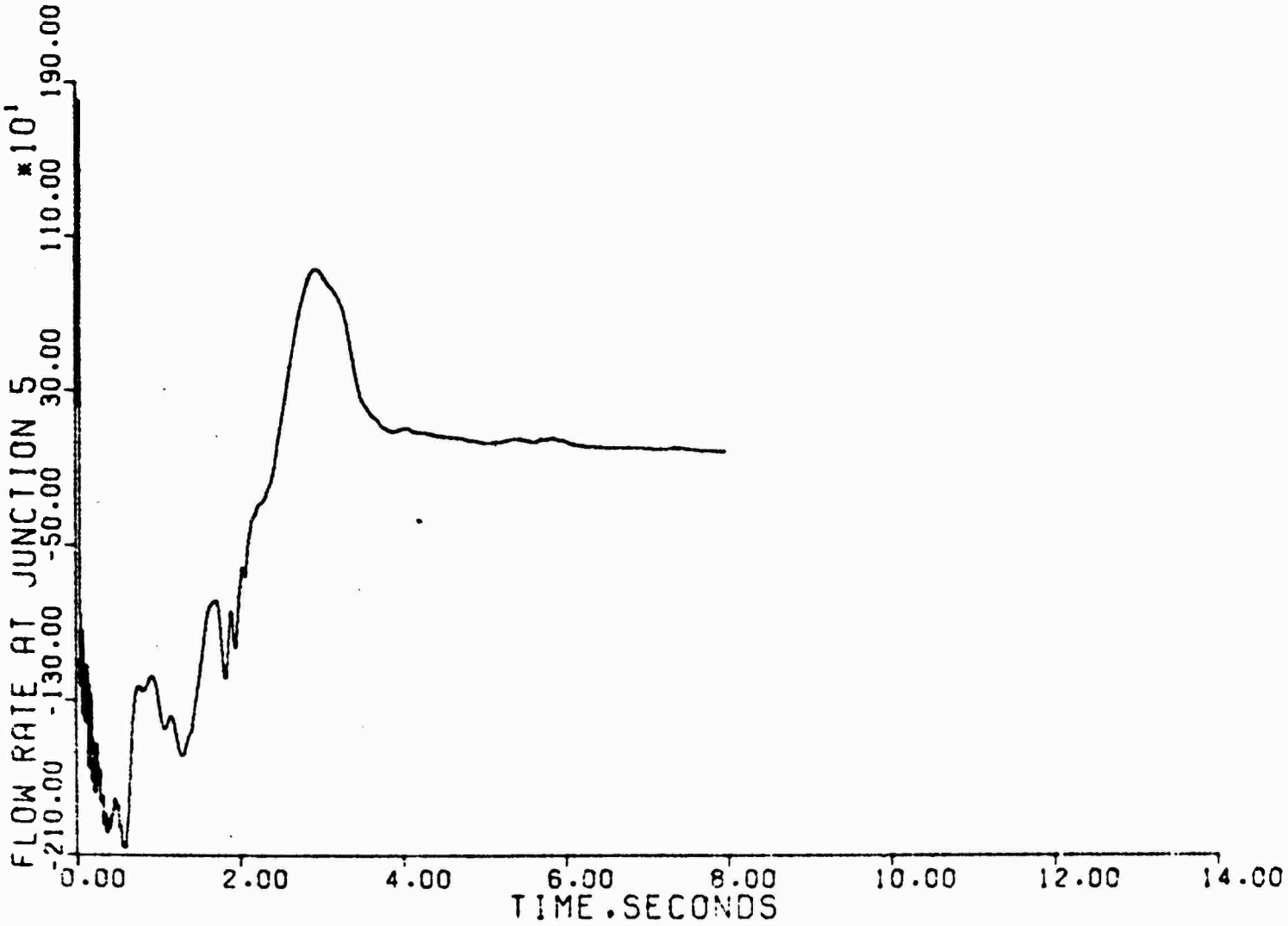

FIGURE 10D. 0.6 DOUBLE ENDED COLD LEG BREAK AT PUMP INLET (SLOT) CORE FLOW VS. TIME

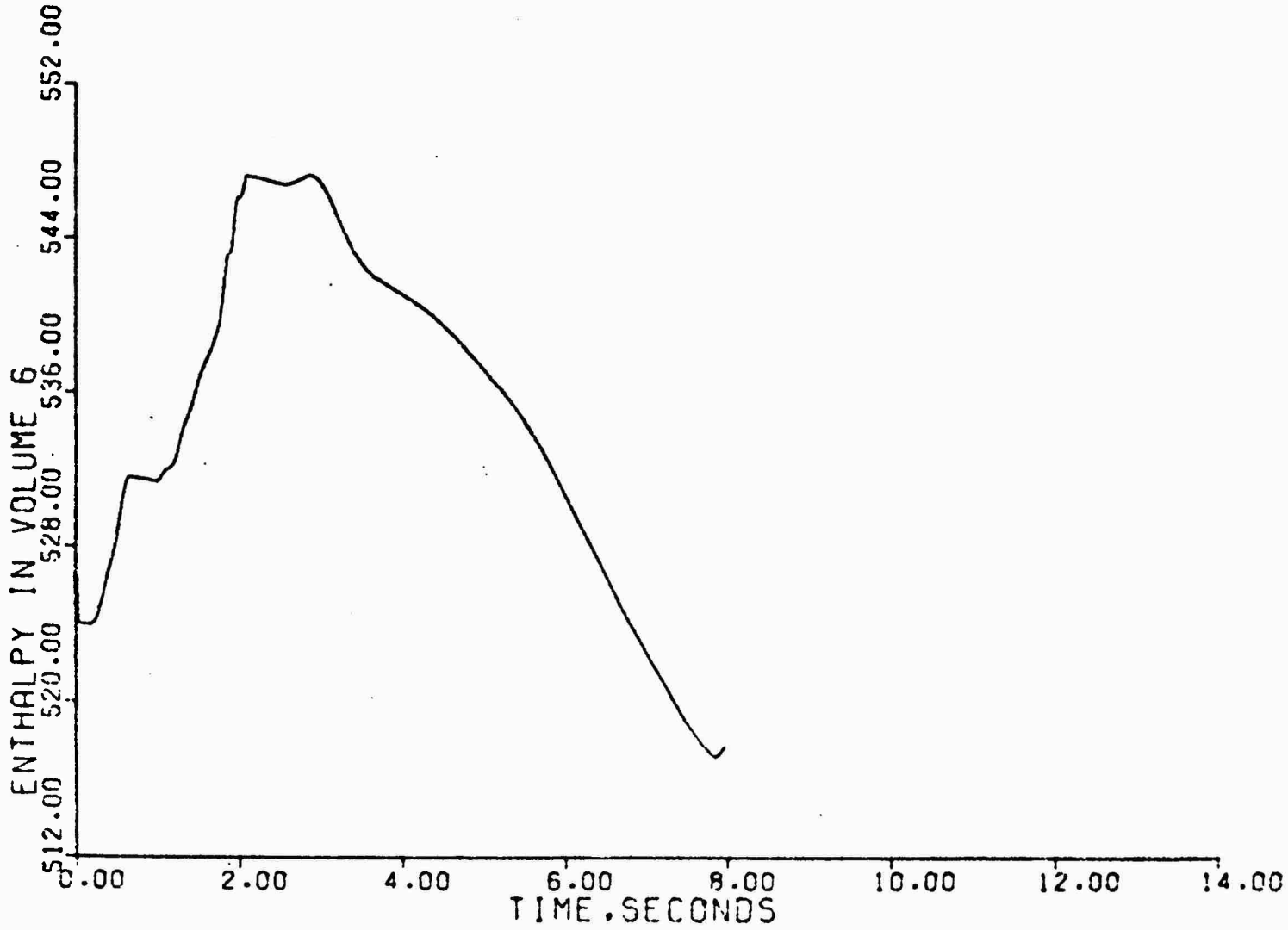

FIGURE 10E. 0.6 DOUBLE ENDED COLD LEG BREAK AT PUMP INLET (SLOT) INLET ENTHALPY VS. TIME

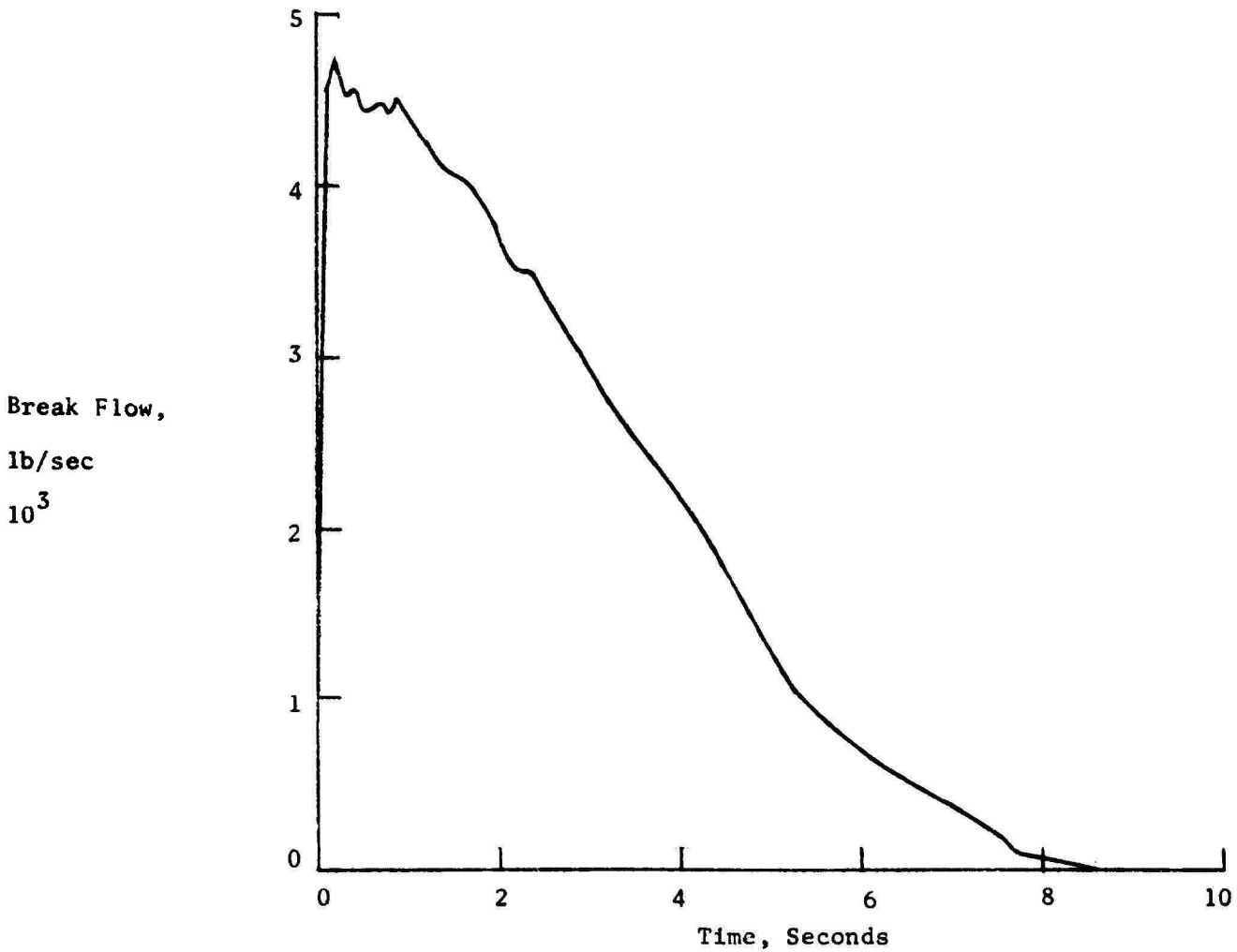

FIGURE 11A. 0.5 ft^2 BREAK AT PUMP DISCHARGE (SLOT) BREAK FLOW VS. TIME

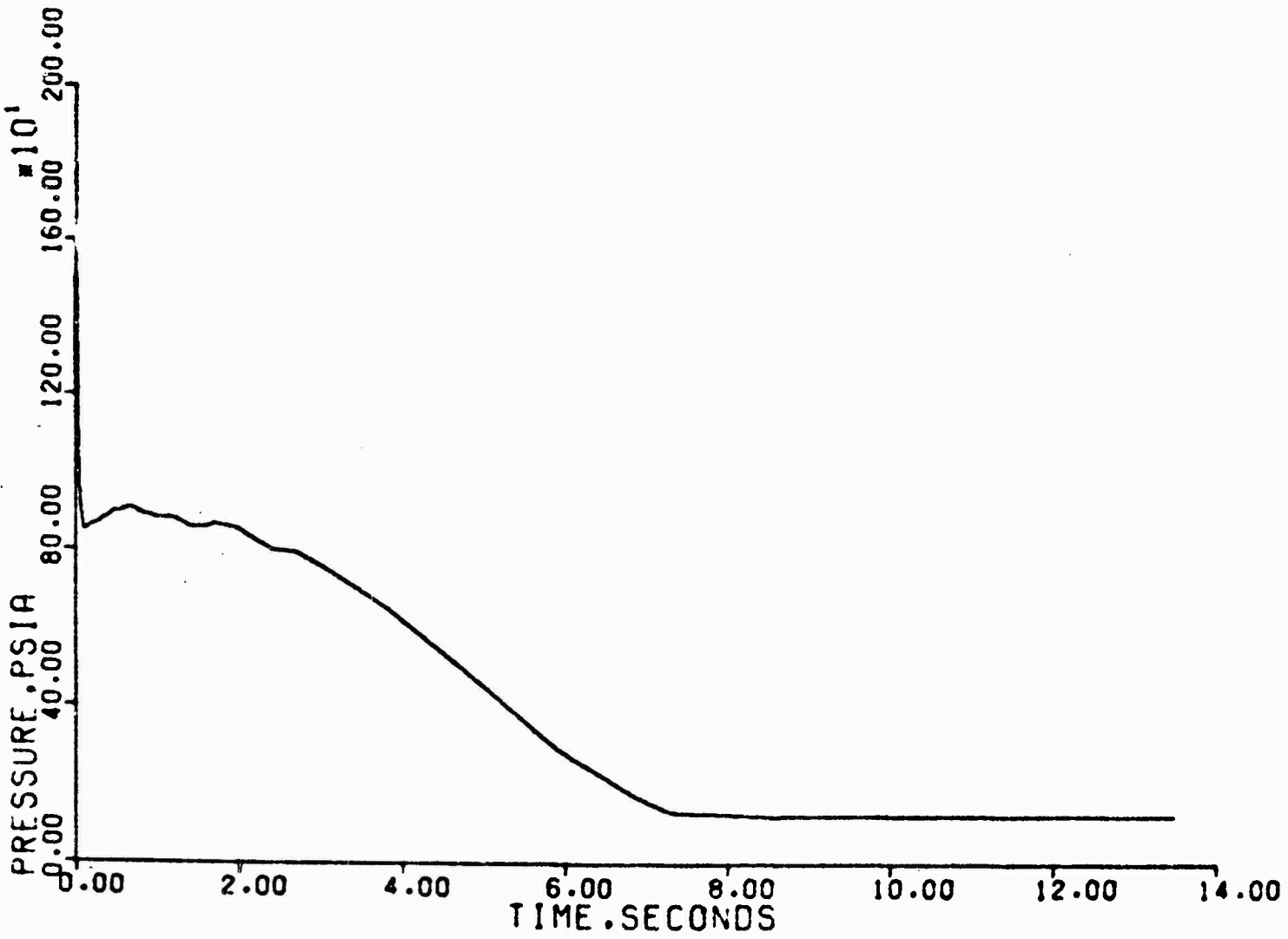

FIGURE 11B. 0.5 ft^2 COLD LEG BREAK AT PUMP DISCHARGE (SLOT) PRESSURE VS. TIME

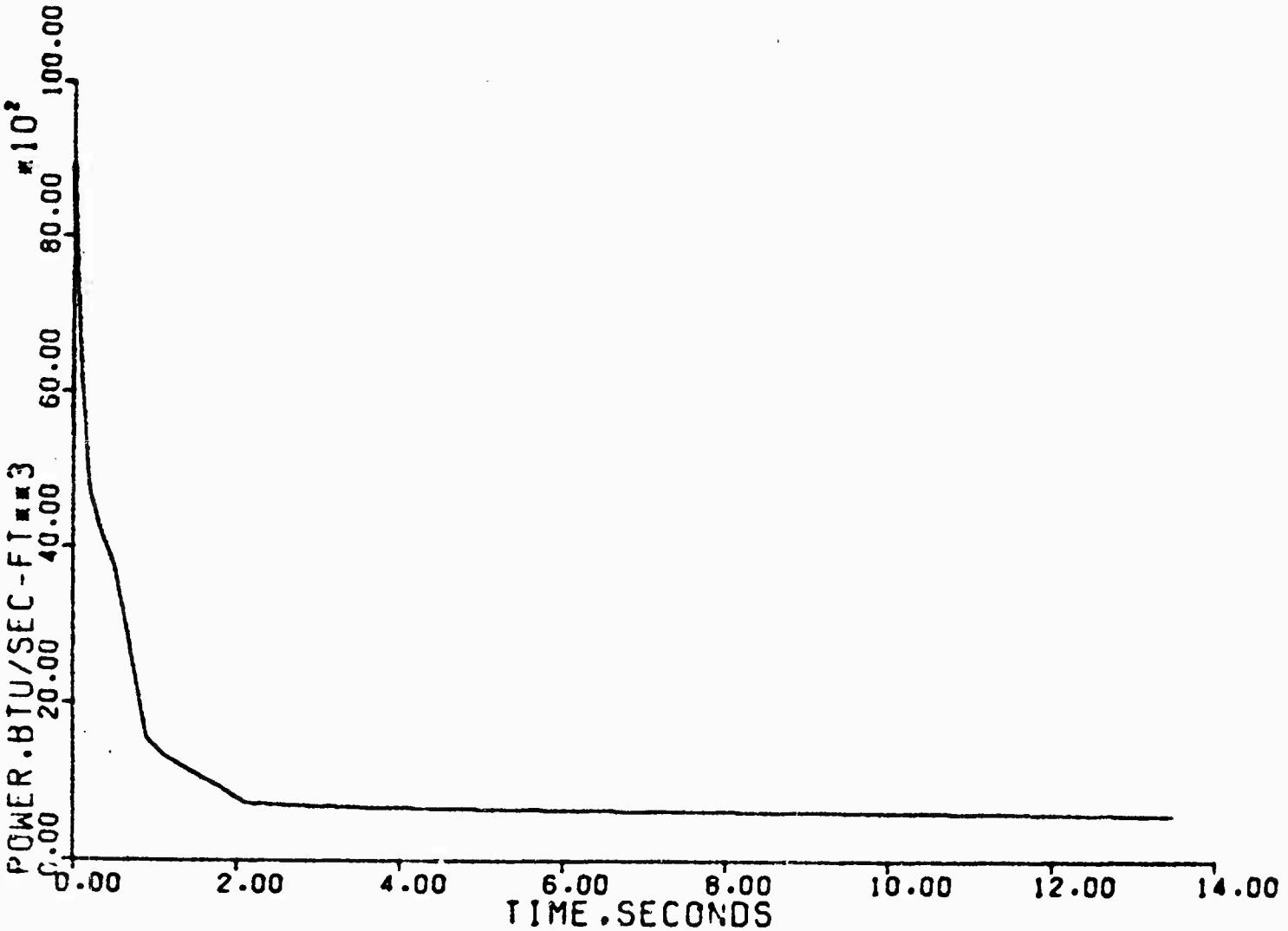

FIGURE 11C. 0.5 ft^2 COLD LEG BREAK AT PUMP DISCHARGE (SLOT) POWER LEVEL VS. TIME

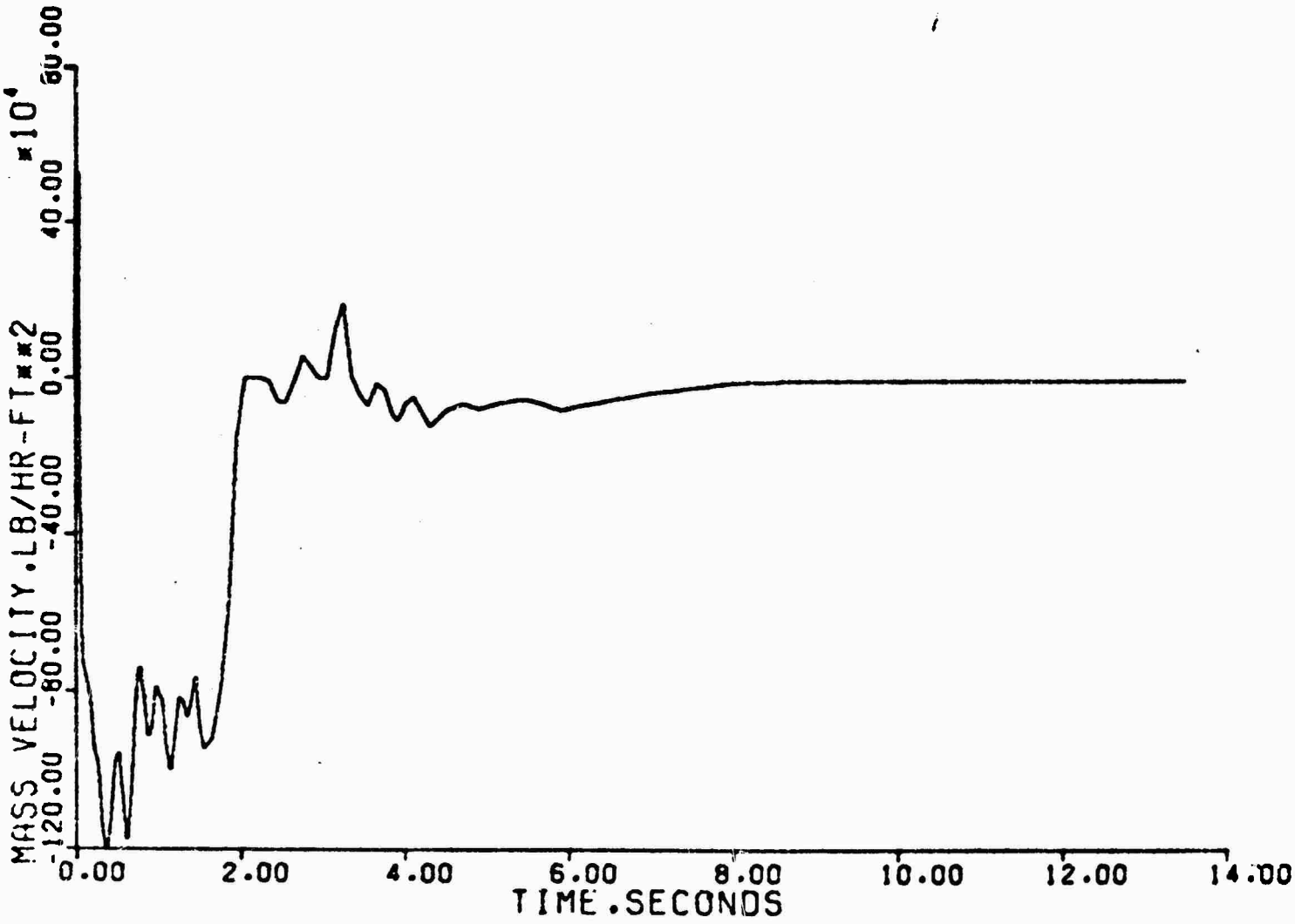

FIGURE 11D. 0.5 ft^2 COLD LEG BREAK AT PUMP DISCHARGE (SLOT) CORE FLOW VS. TIME

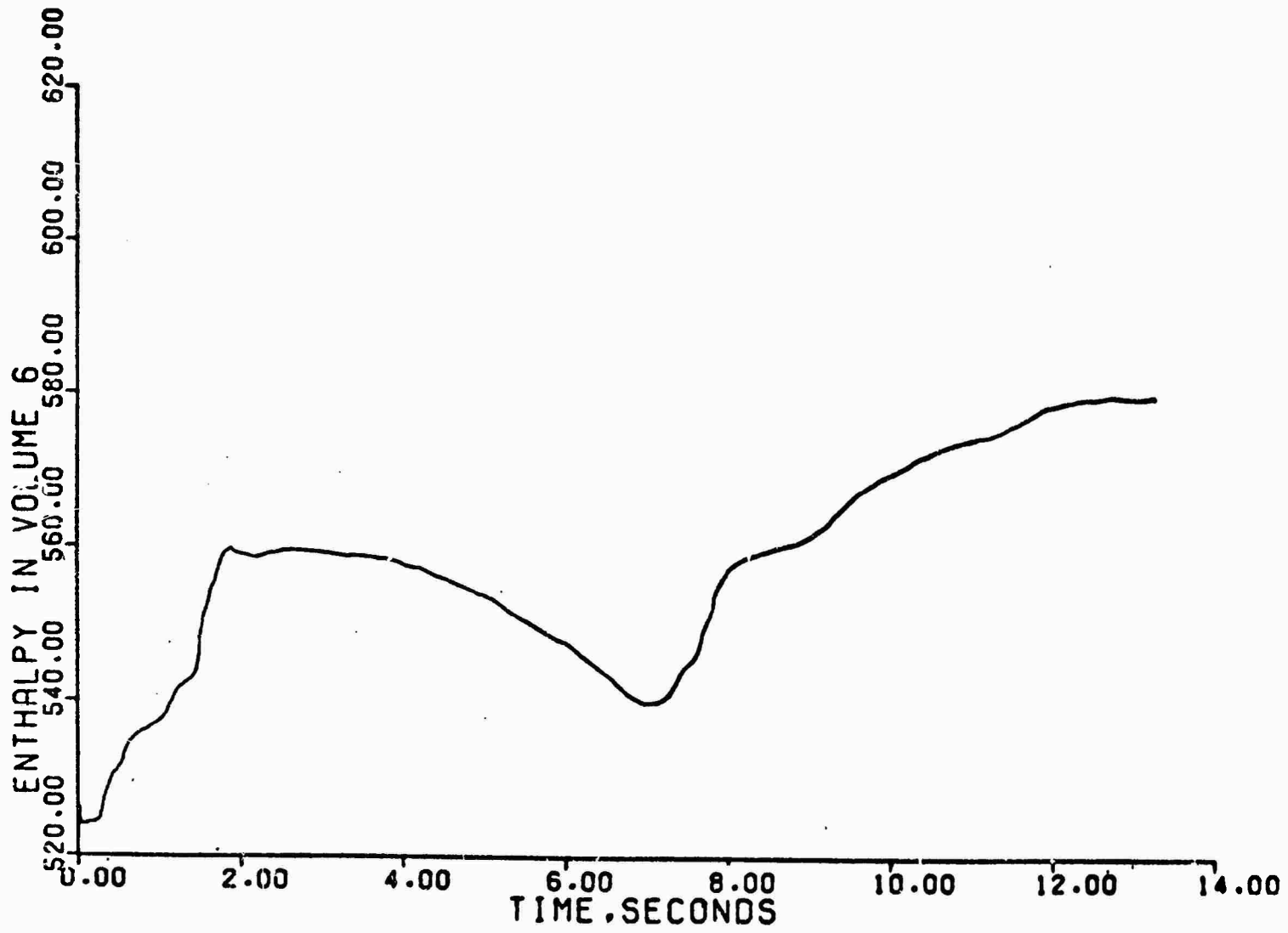

FIGURE 11E. 0.5 ft^2 COLD LEG BREAK AT PUMP DISCHARGE (SLOT) INLET ENTHALPY VS. TIME

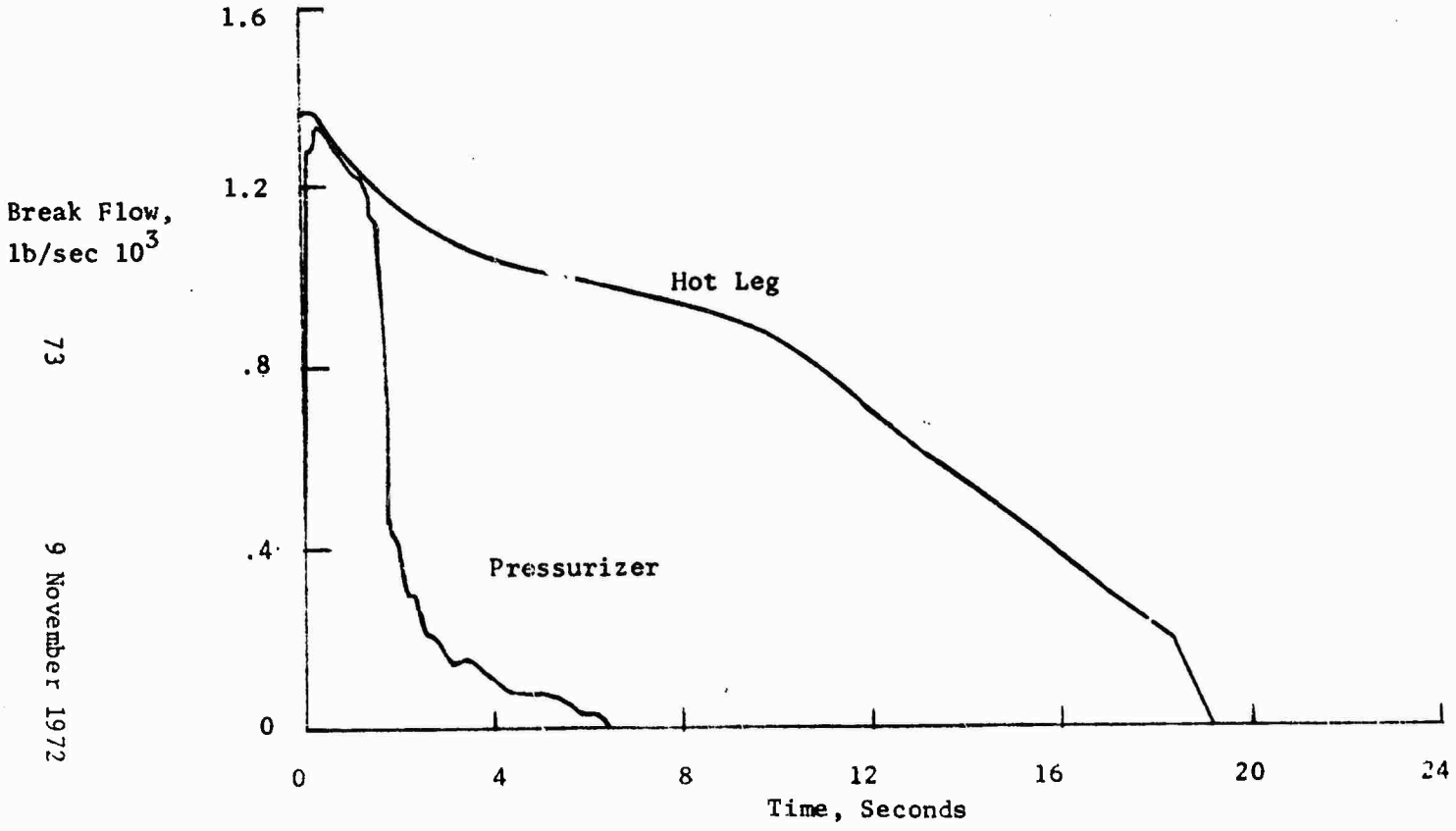

FIGURE 12 A. 0.18 ft^2 PRESSURIZER SURGE LINE BREAK BREAK FLOW RATE VS. TIME

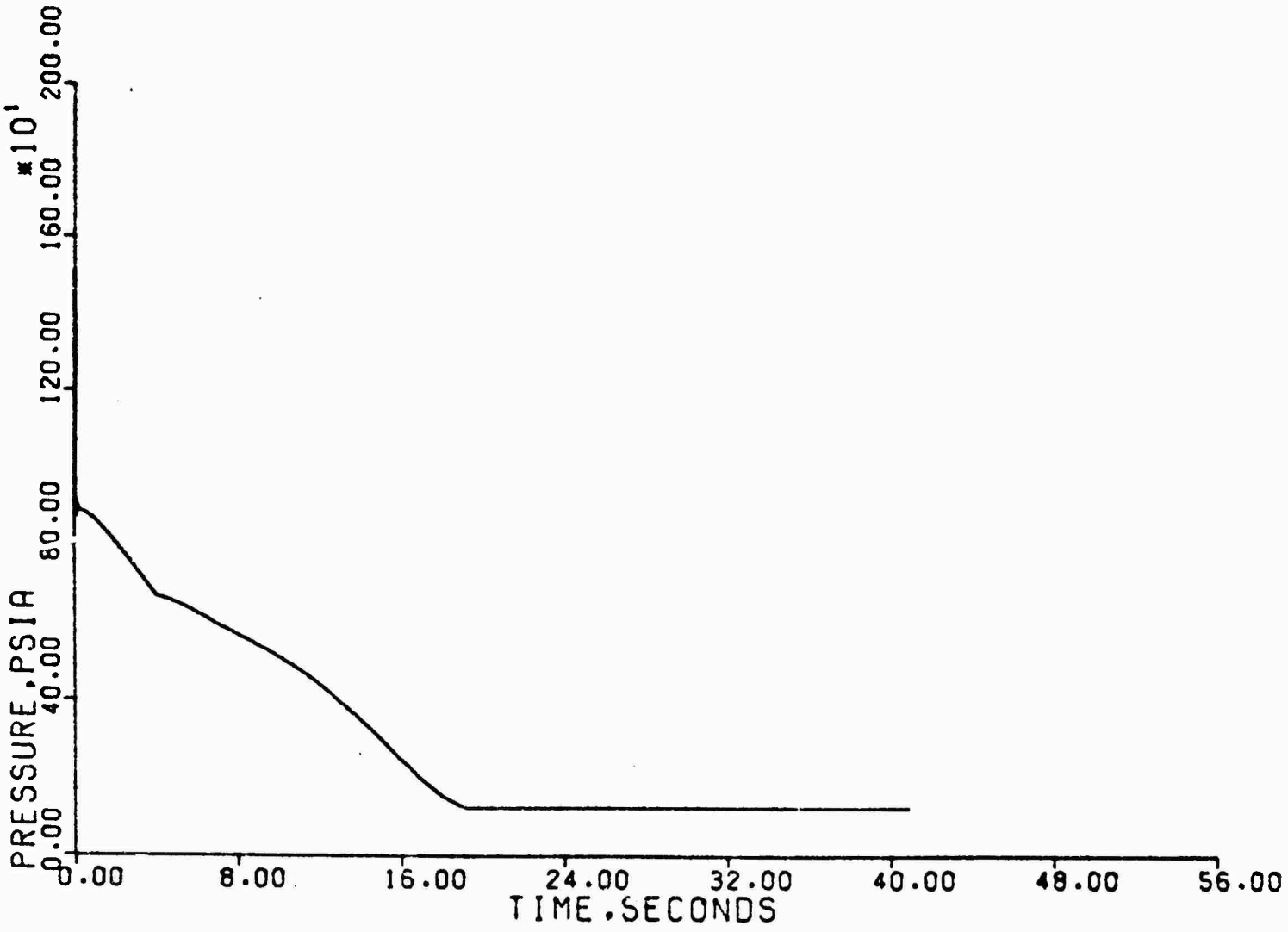

FIGURE 12B. 0.18 ft^2 PRESSURIZER SURGE LINE BREAK PRESSURE VS. TIME

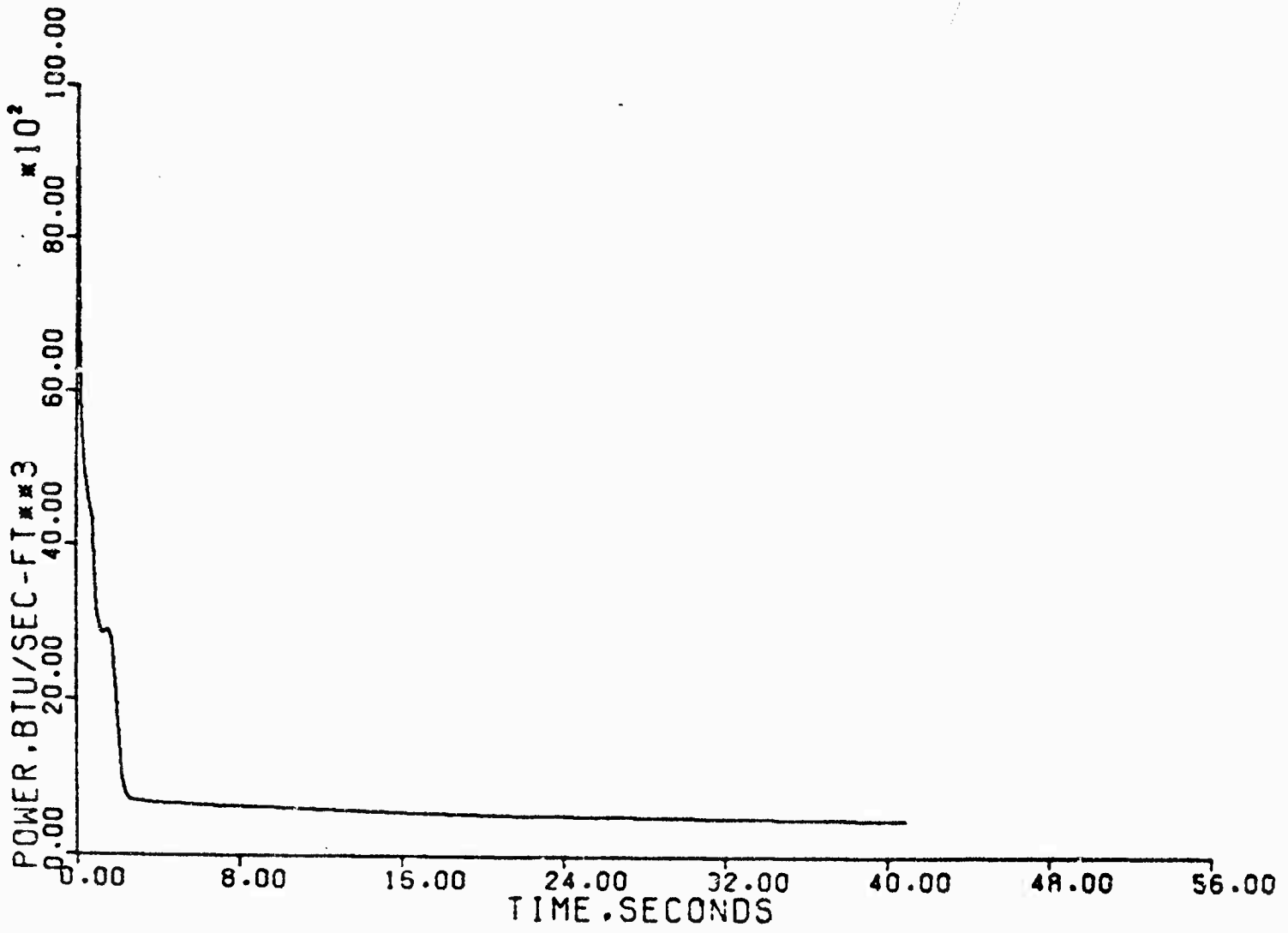

FIGURE 12C. 0.18 ft^2 PRESSURIZER SURGE LINE BREAK POWER LEVEL VS. TIME

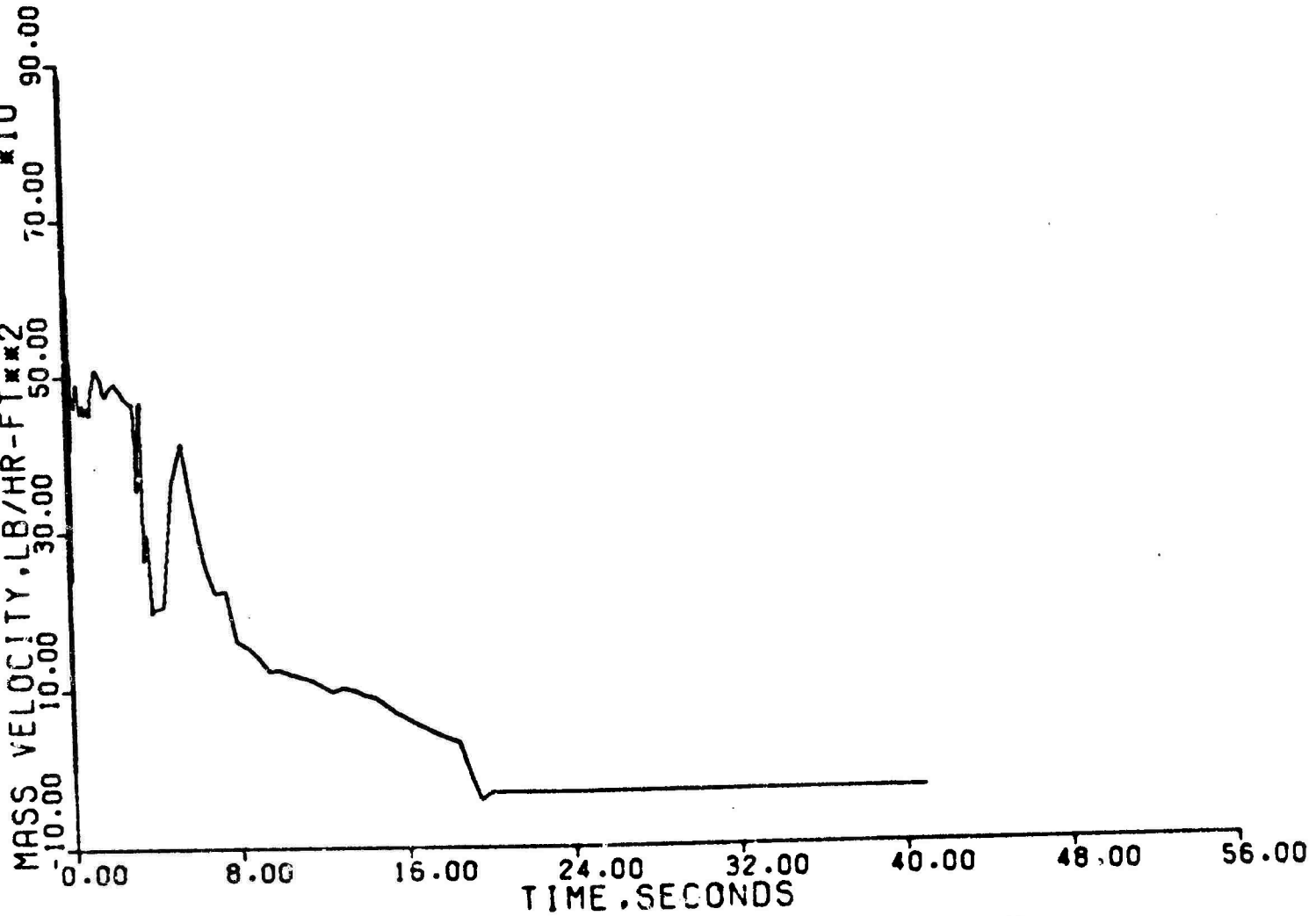

FIGURE 12D. 0.18 ft^2 PRESSURIZER SURGE LINE BREAK CORE FLOW VS TIME

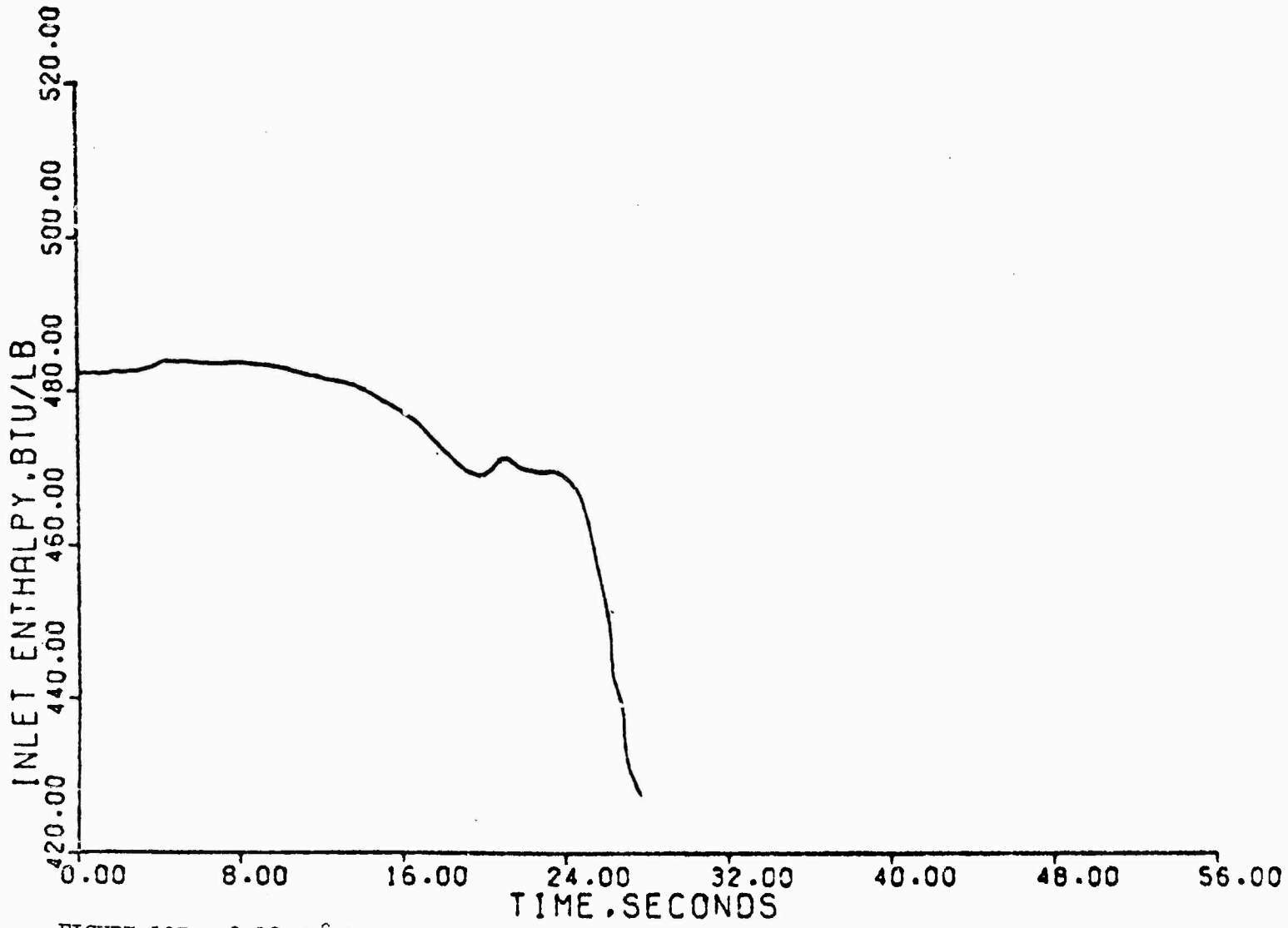

FIGURE 12E. 0.18 ft^2 PRESSURIZER SURGE LINE BREAK INLET ENTHALPY VS. TIME

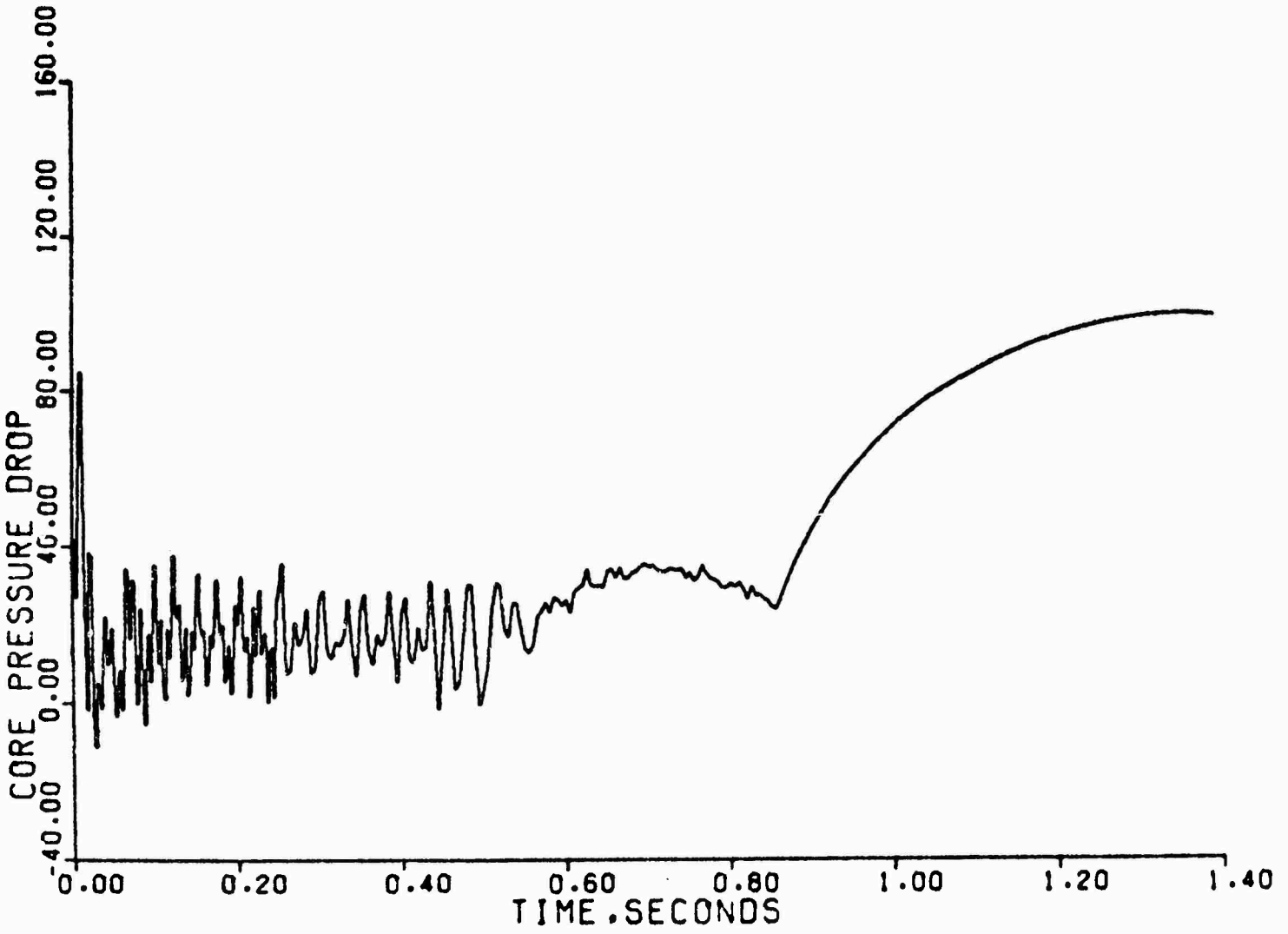

FIGURE 13. DOUBLE ENDED HOT LEG BREAK (SLOT) CORE PRESSURE DROP VS. TIME

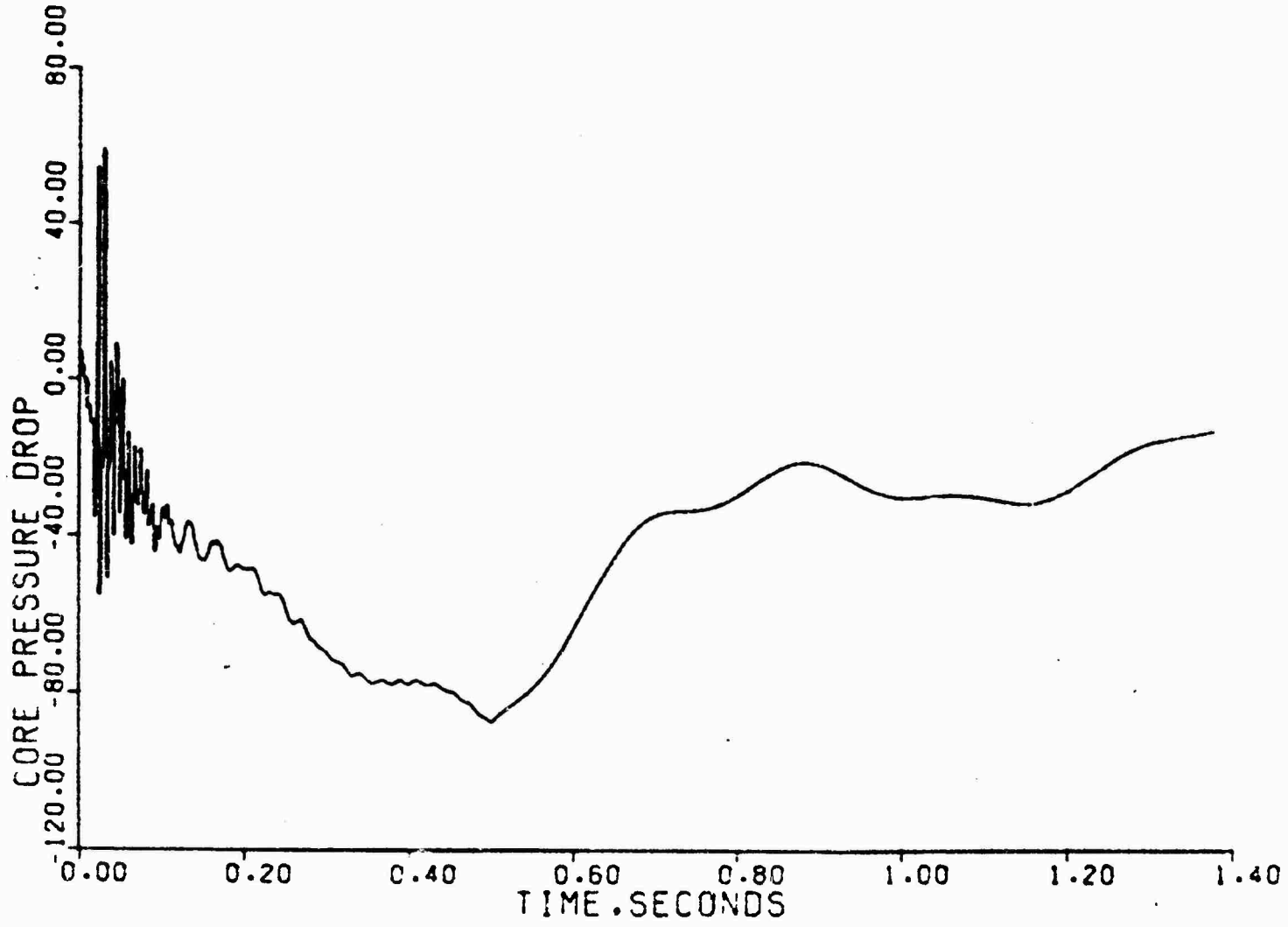

FIGURE 14. DOUBLE ENDED COLD LEG BREAK (SLOT) CORE PRESSURE DROP VS. TIME

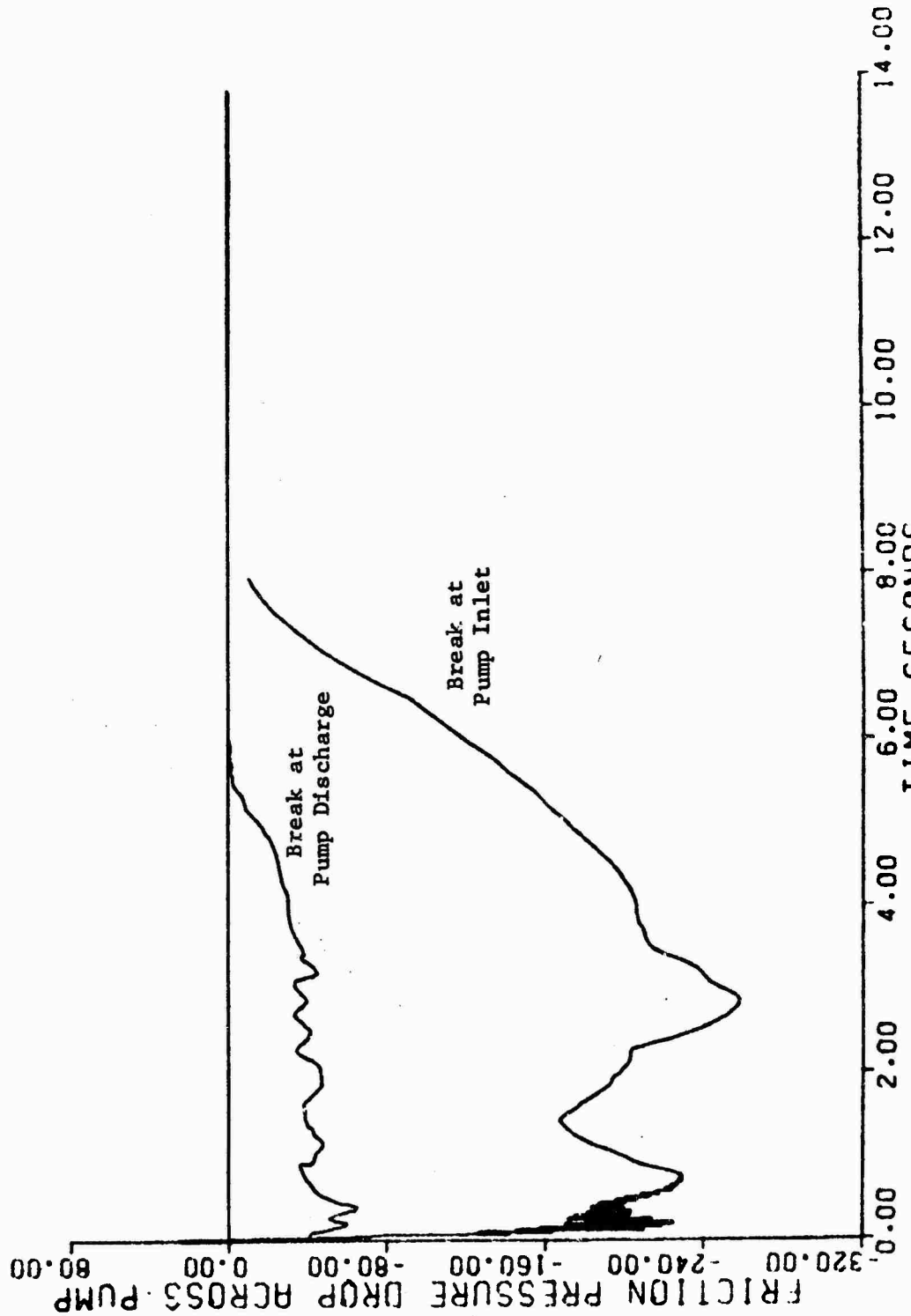

FIGURE 15. 0.6 DOUBLE ENDED COLD LEG BREAK (SLOT) FRICTION PRESSURE DROP ACROSS PUMP VS. TIME

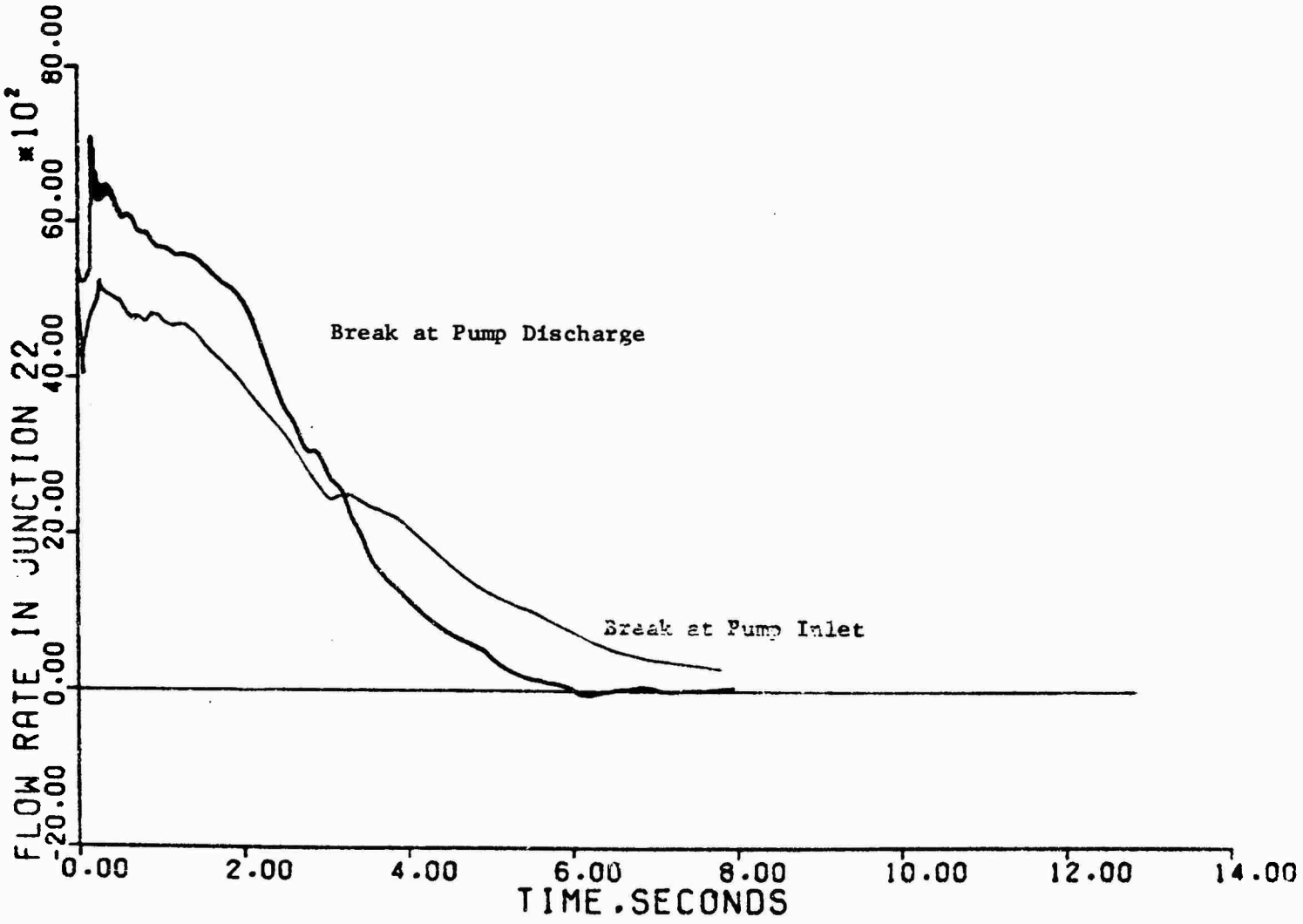

FIGURE 16. 0.6 DOUBLE ENDED COLD LEG BREAK (SLOT) BREAK FLOW RATE VS. TIME

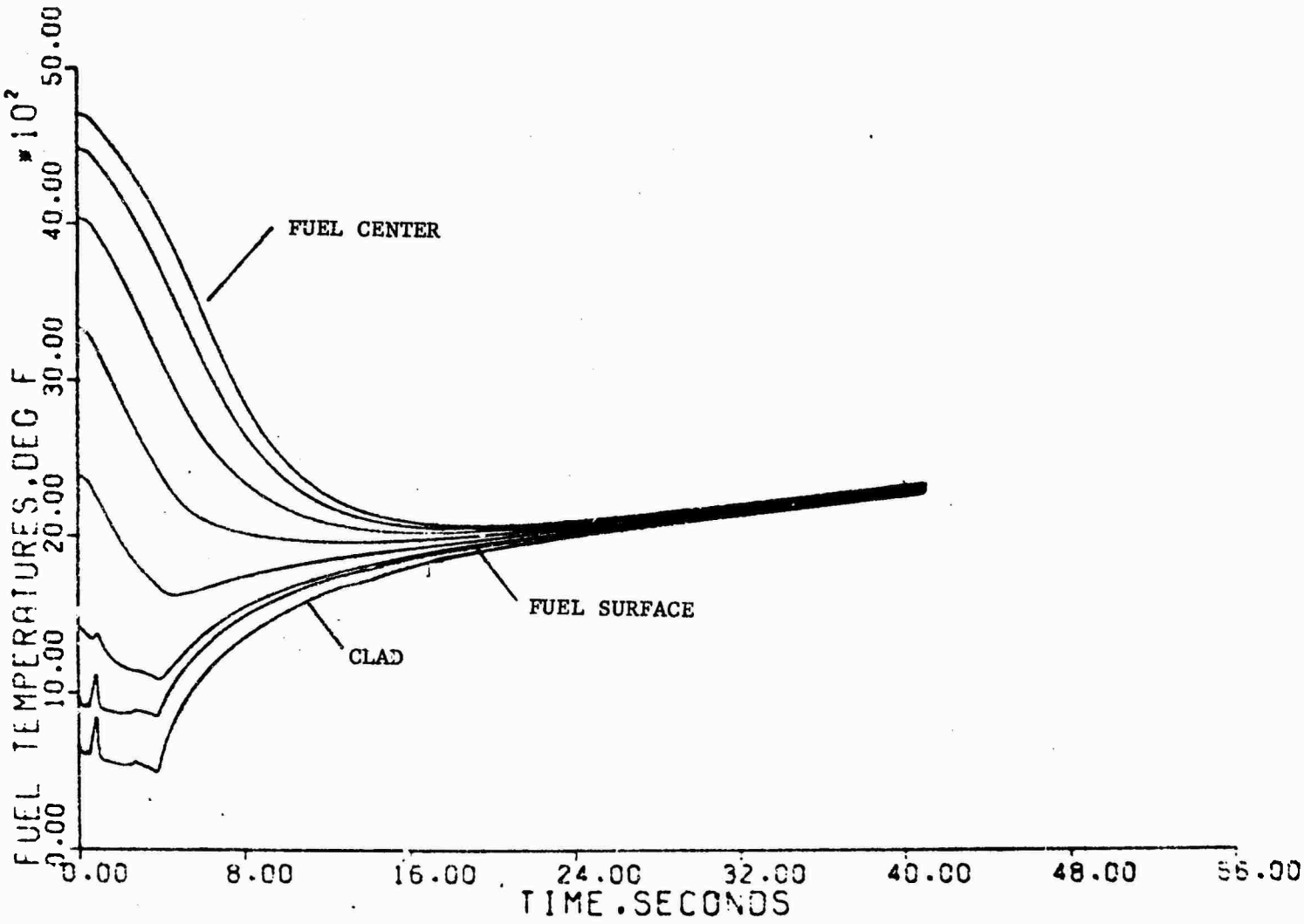

FIGURE 17A DOUBLE ENDED HOT LEG BREAK (GUILLOTINE)
CLAD AND FUEL TEMPERATURE AT HOT SPOT VS. TIME

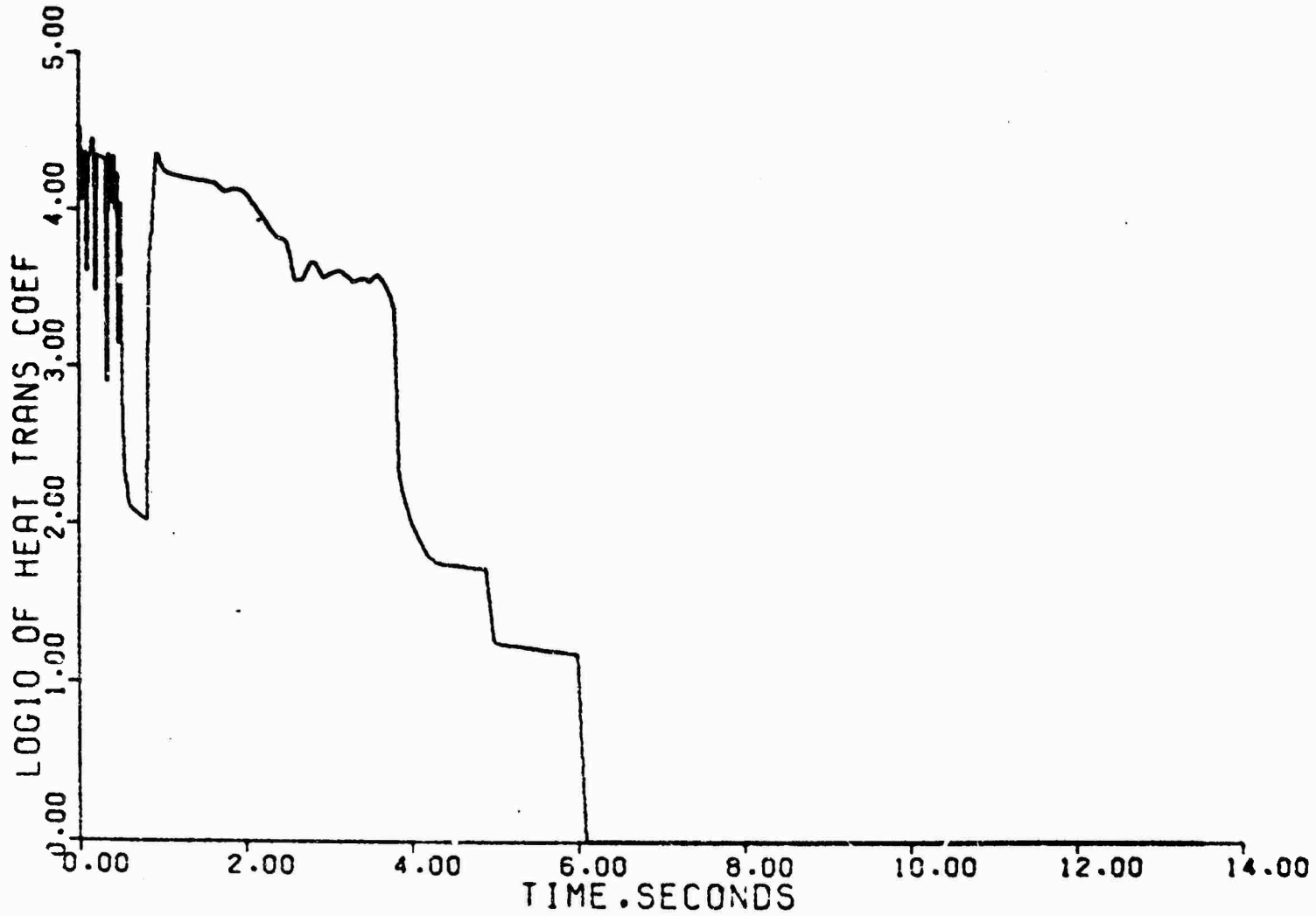

FIGURE 17B DOUBLE ENDED HOT LEG BREAK (GUILLOTINE)
HEAT TRANSFER COEFFICIENT AT HOT SPOT VS. TIME

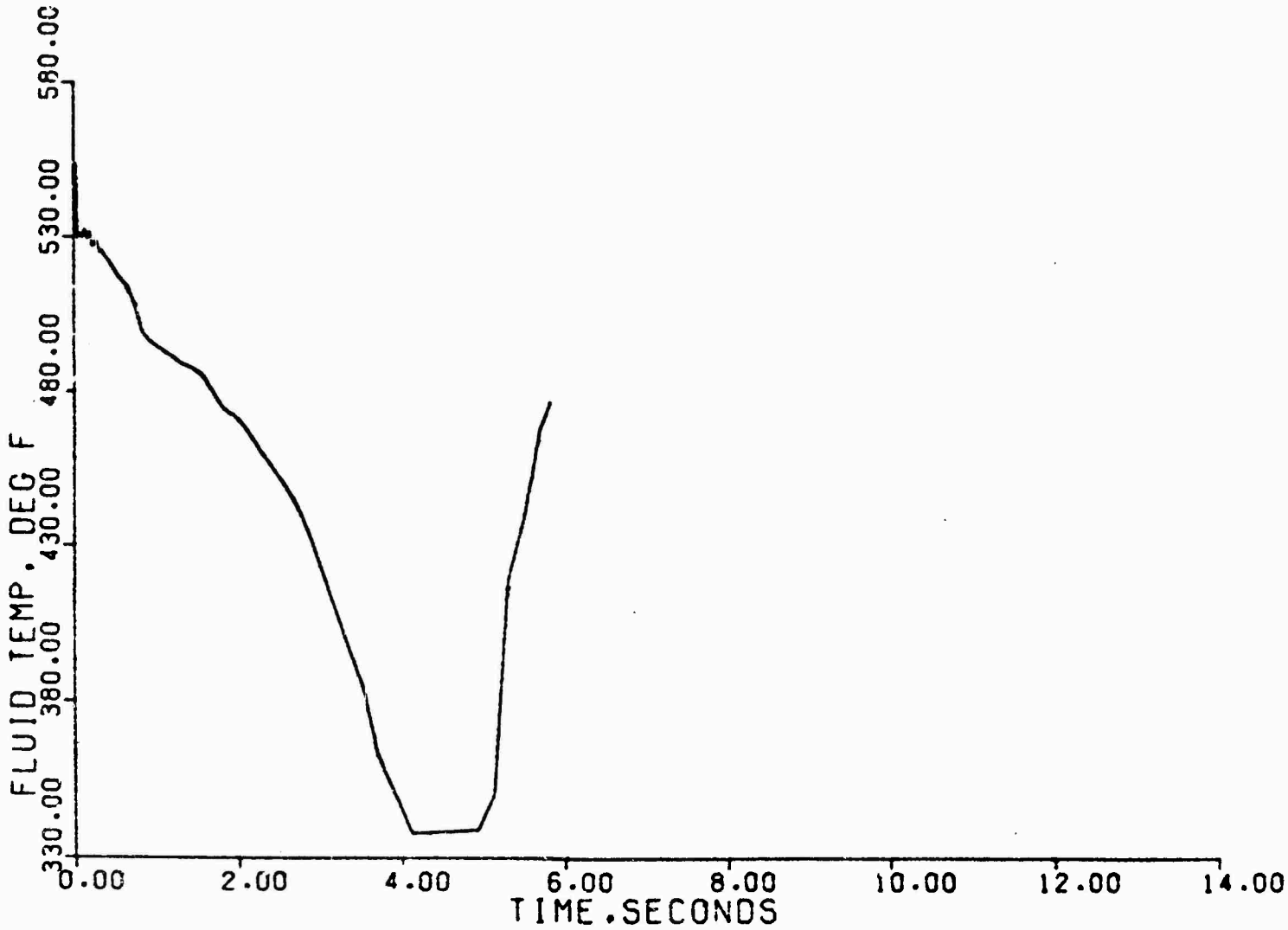

FIGURE 17C DOUBLE ENDED HOT LEG BREAK (GUILLOTINE)
FLUID TEMPERATURE AT HOT SPOT VS. TIME

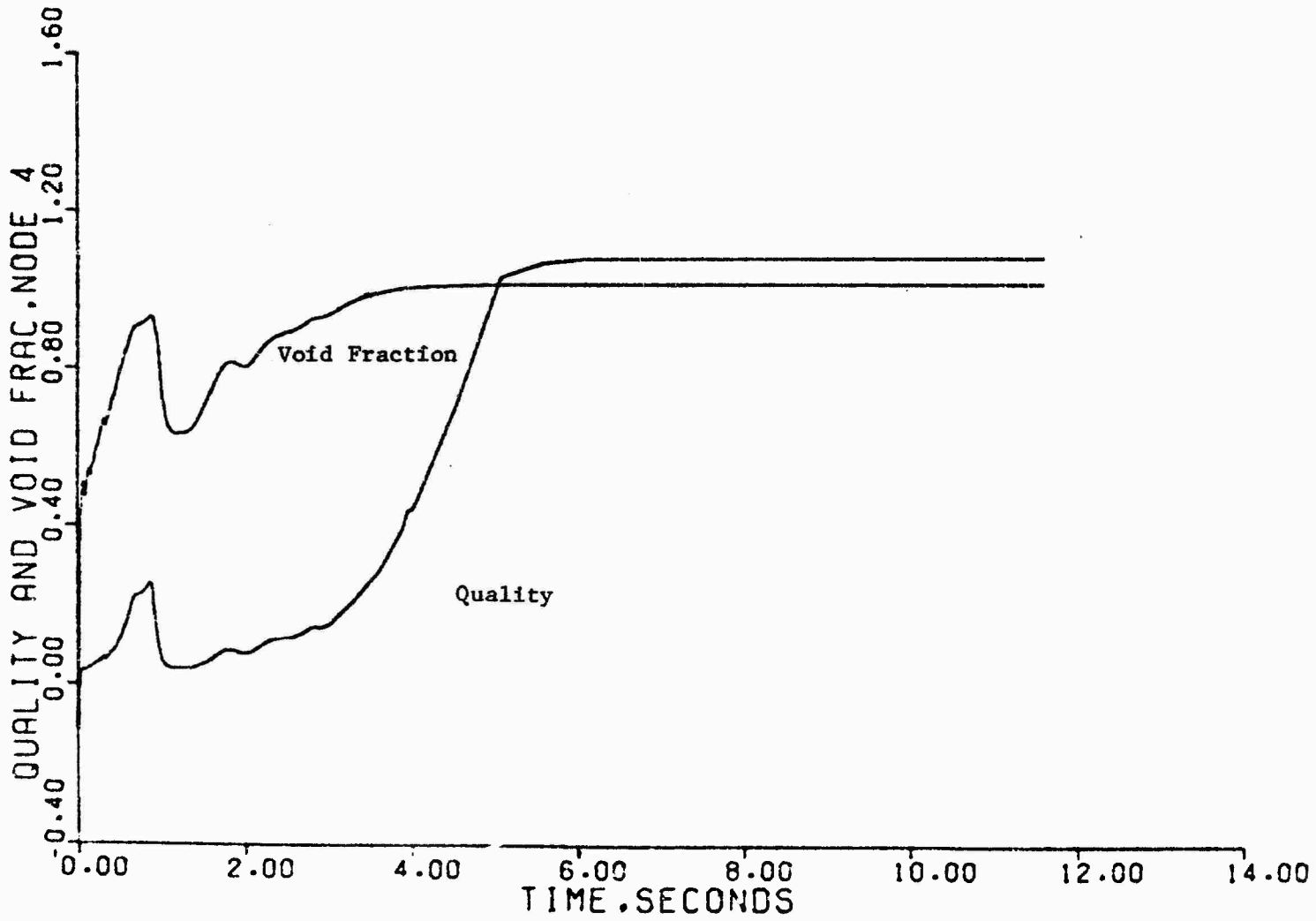

FIGURE 17D DOUBLE ENDED HOT LEG BREAK (GUILLOTINE)
QUALITY AND VOID FRACTION AT HOT SPOT VS. TIME

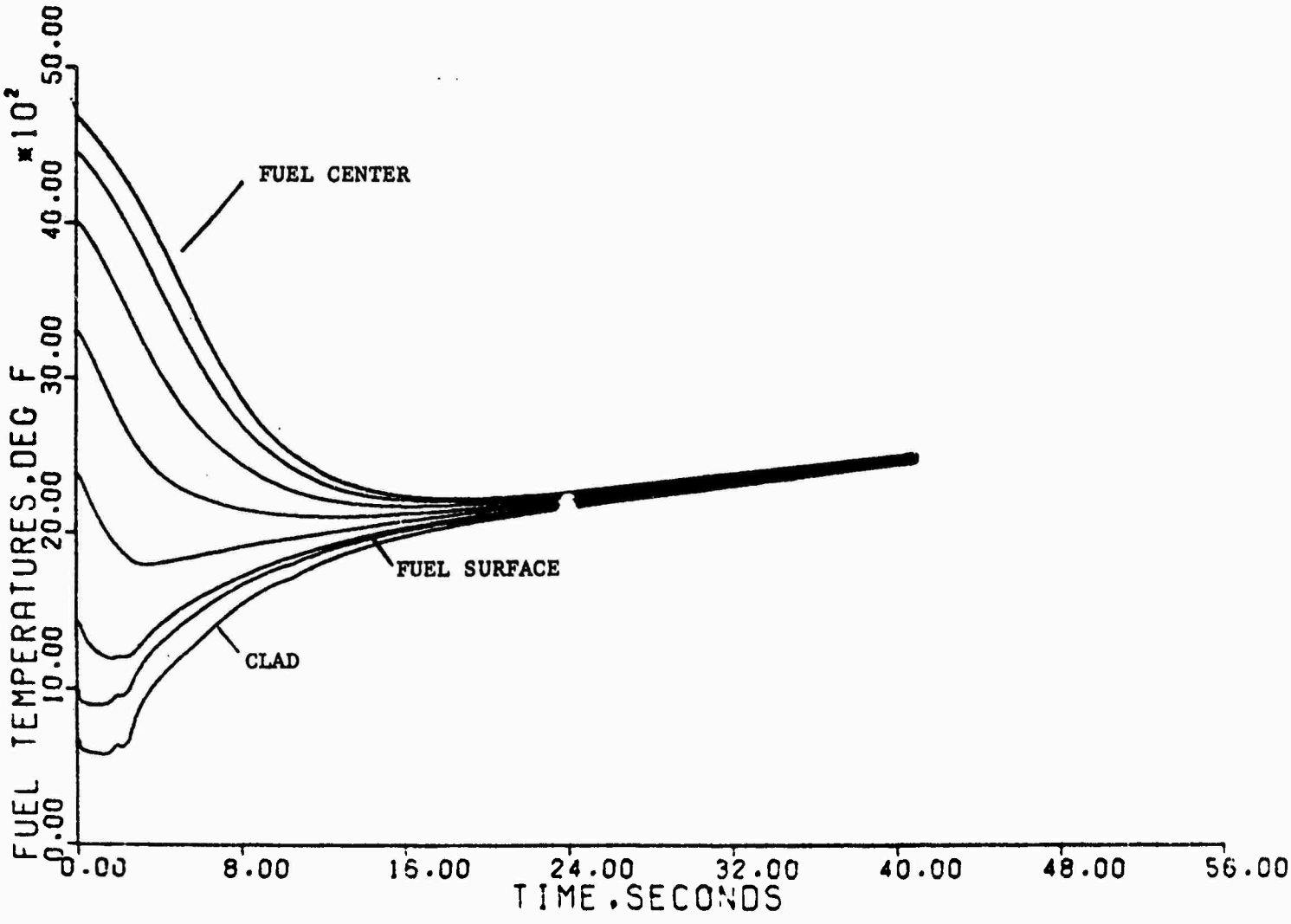

FIGURE 18A DOUBLE ENDED COLD LEG BREAK (GUILLOTINE)
FUEL AND CLAD TEMPERATURE AT HOT SPOT VS. TIME

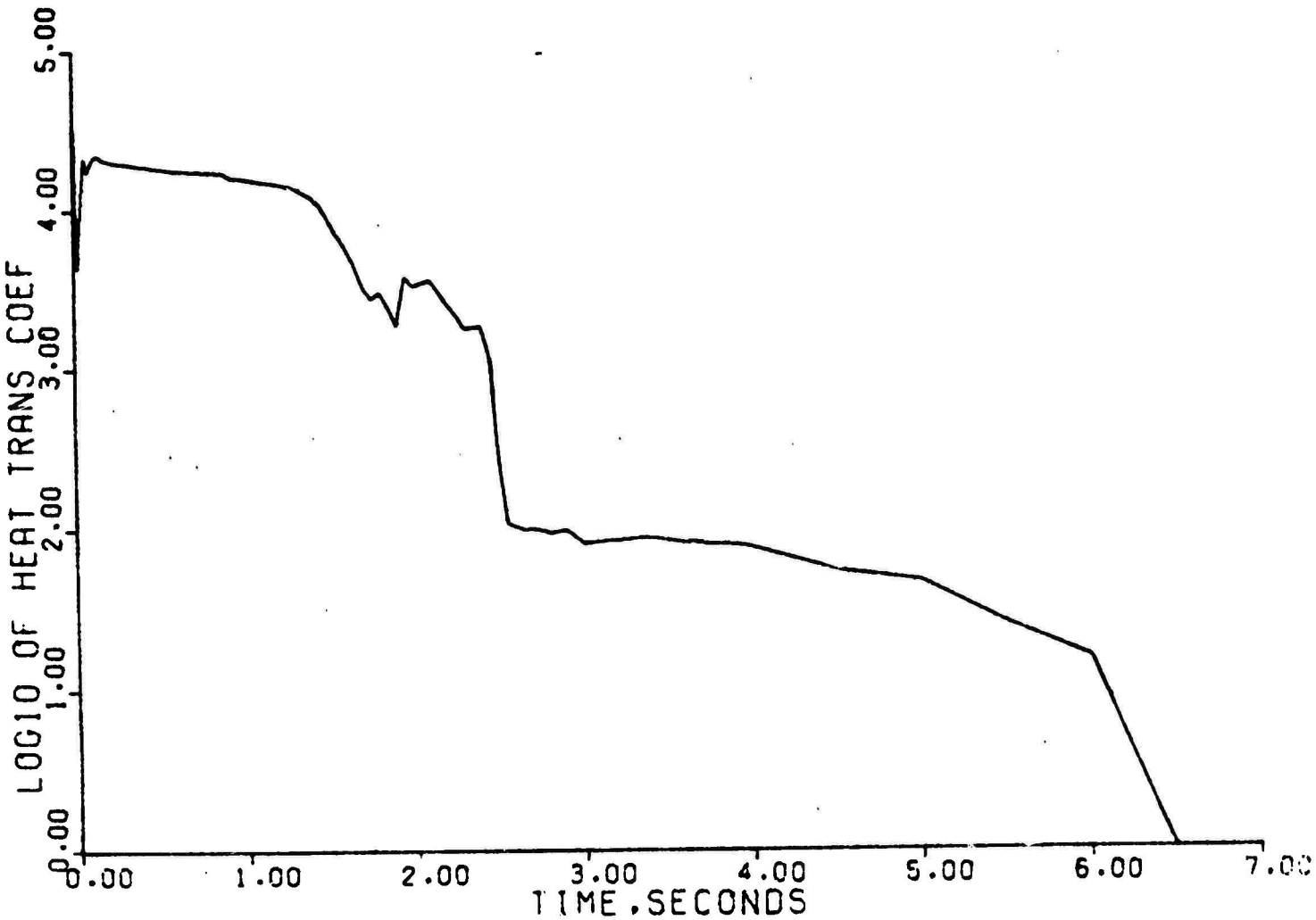

FIGURE 18B DOUBLE ENDED COLD LEG BREAK (GUILLOTINE)
HEAT TRANSFER COEFFICIENT AT HOT SPOT VS. TIME

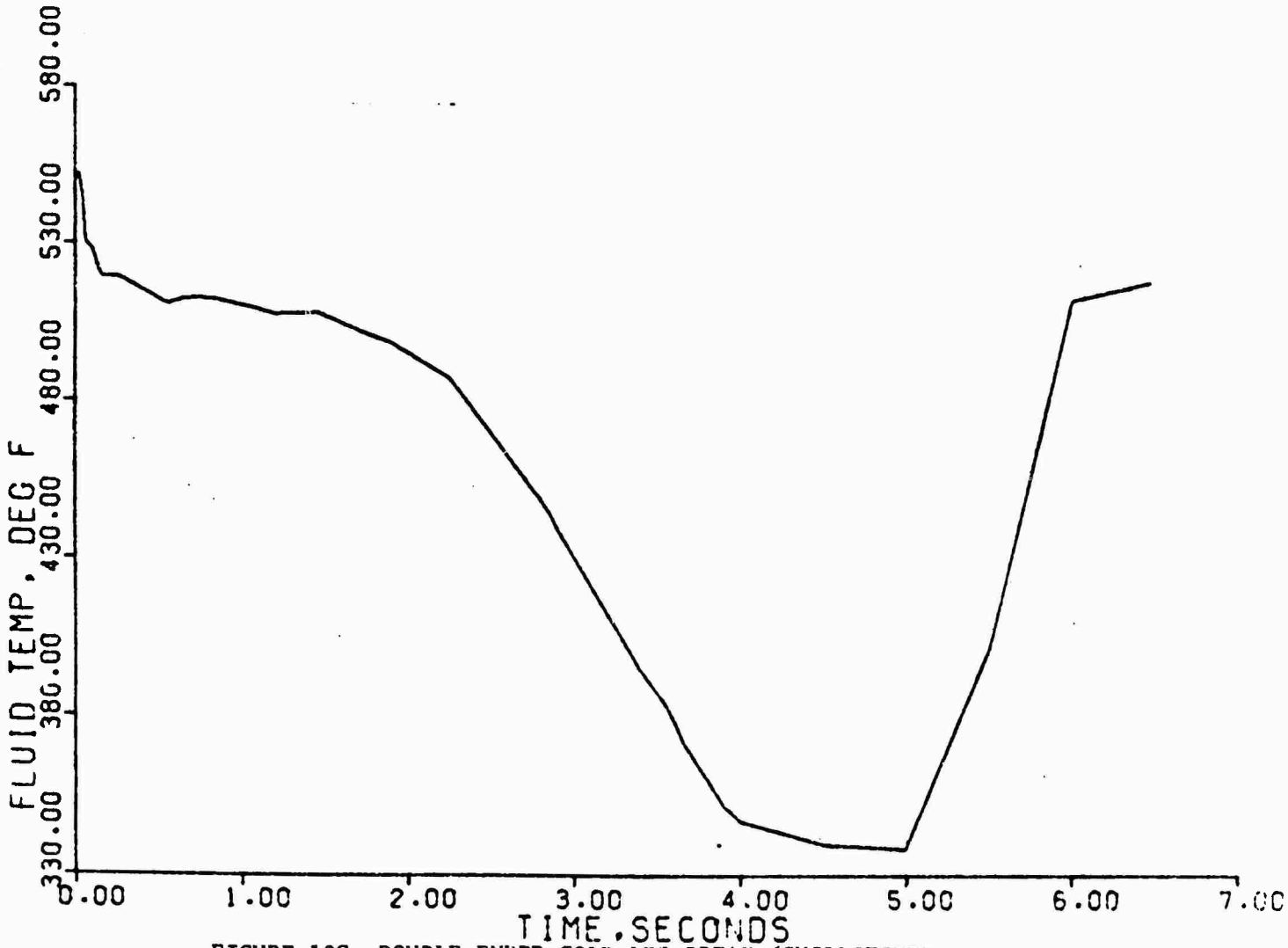

FIGURE 18C DOUBLE ENDED COLD LEG BREAK (GUILLOTINE)
FLUID TEMPERATURE AT HOT SPOT VS. TIME

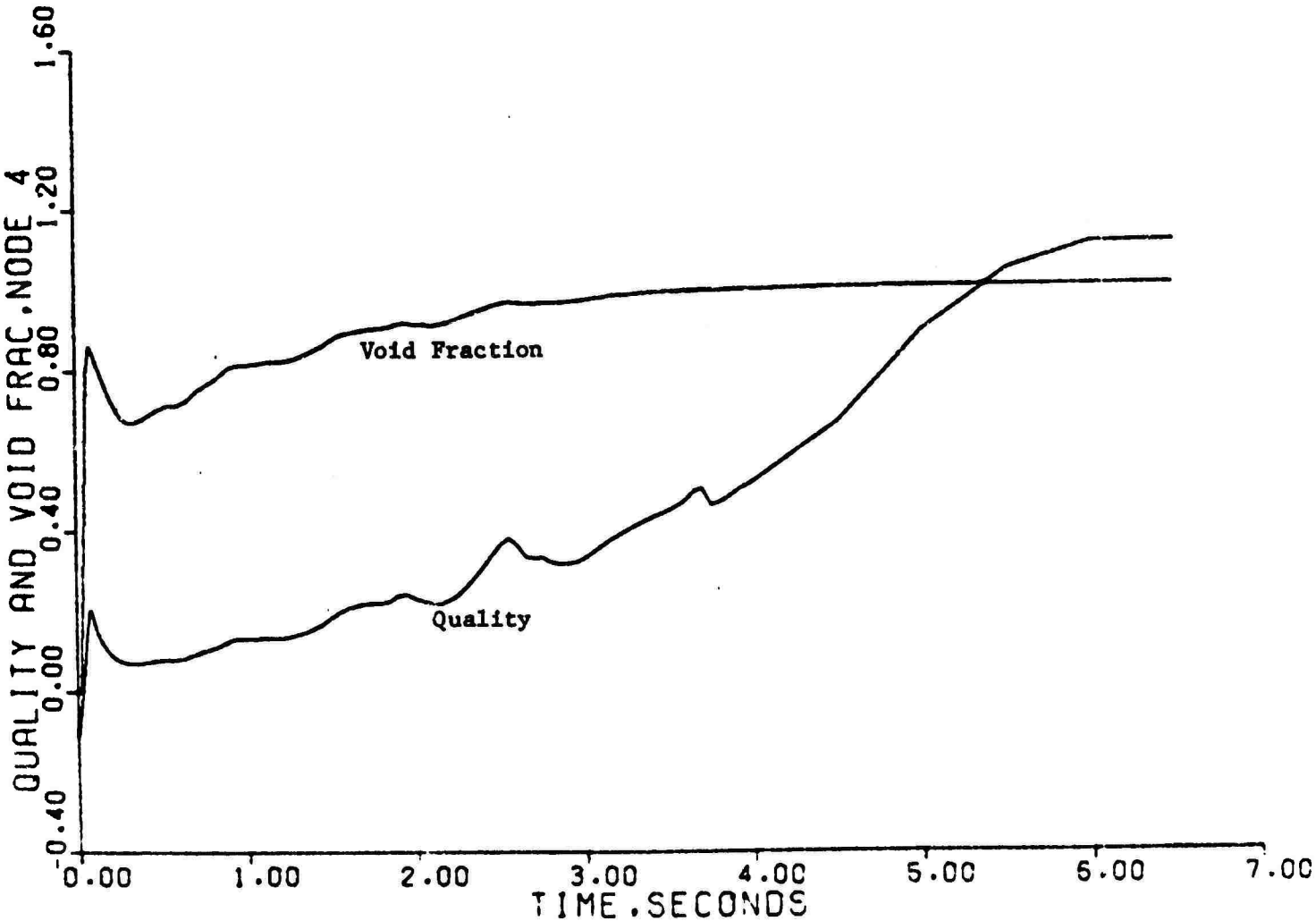

FIGURE 18D DOUBLE ENDED COLD LEG BREAK (GUILLOTINE)
QUALITY AND VOID FRACTION AT HOT SPOT VS. TIME

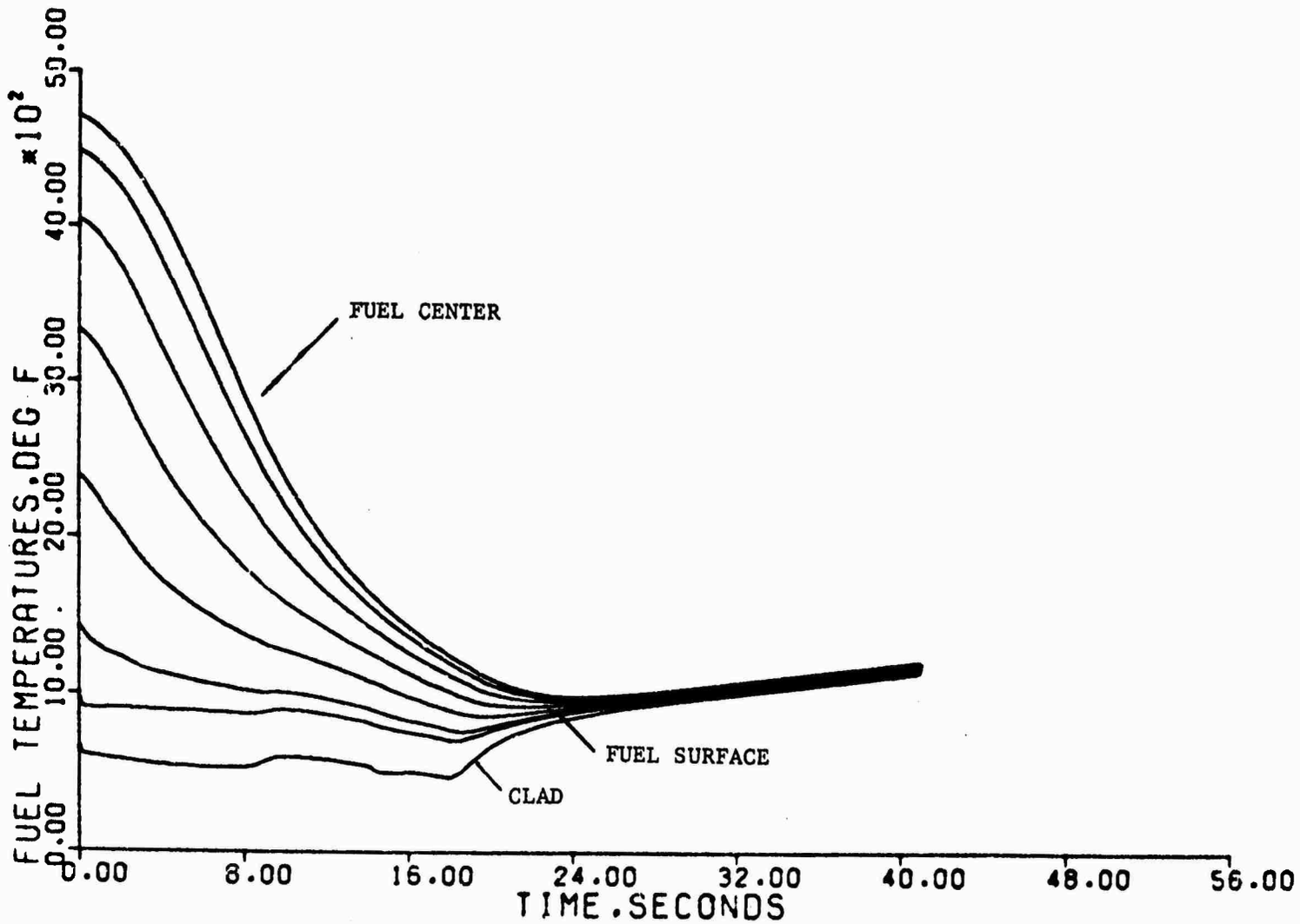

FIGURE 19A 0.18 ft^2 SURGE LINE BREAK
CLAD AND FUEL TEMPERATURE AT HOT SPOT VS. TIME

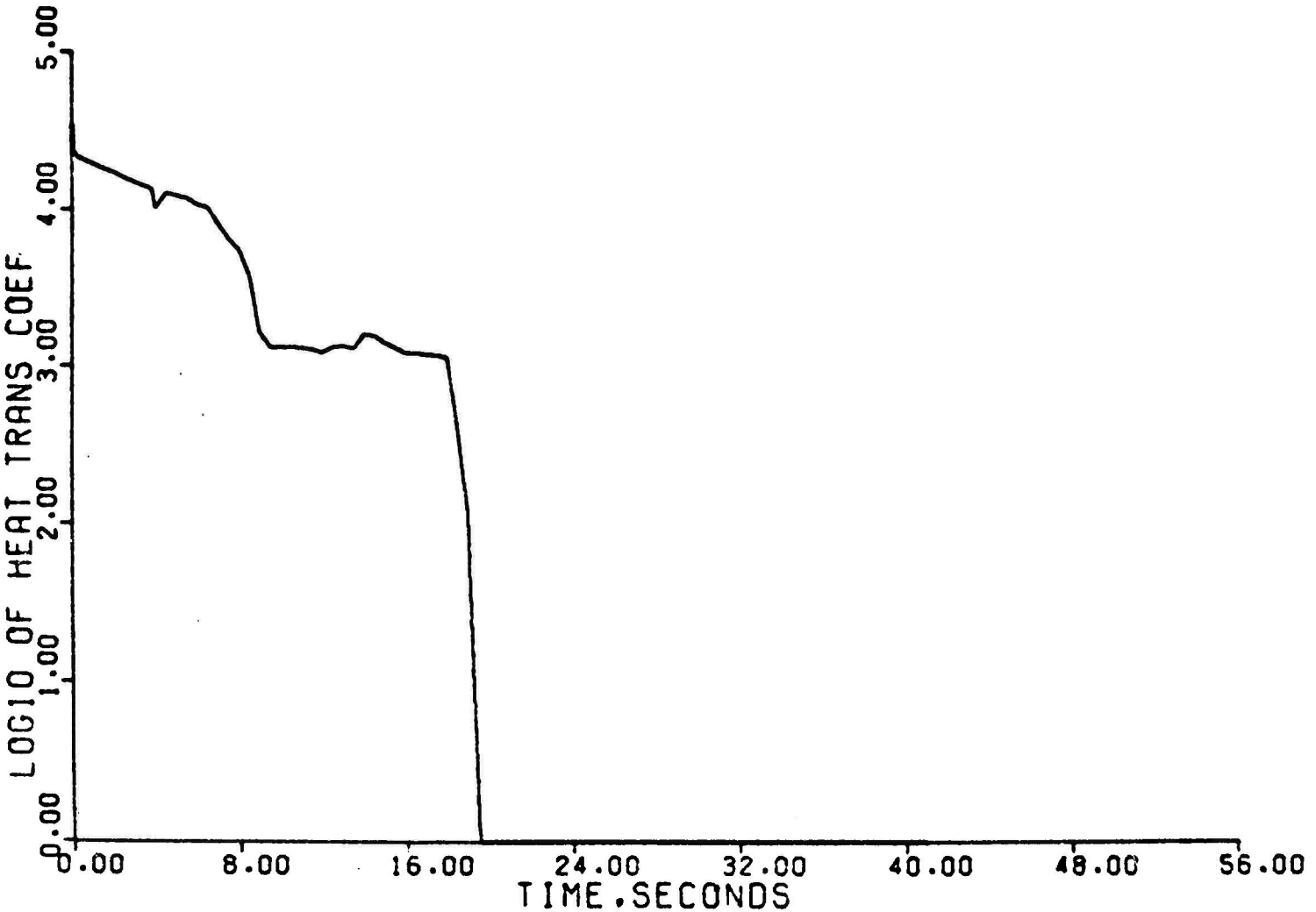

FIGURE 19B 0.18 ft^2 SURGE LINE BREAK
HEAT TRANSFER COEFFICIENT AT HOT SPOT VS. TIME

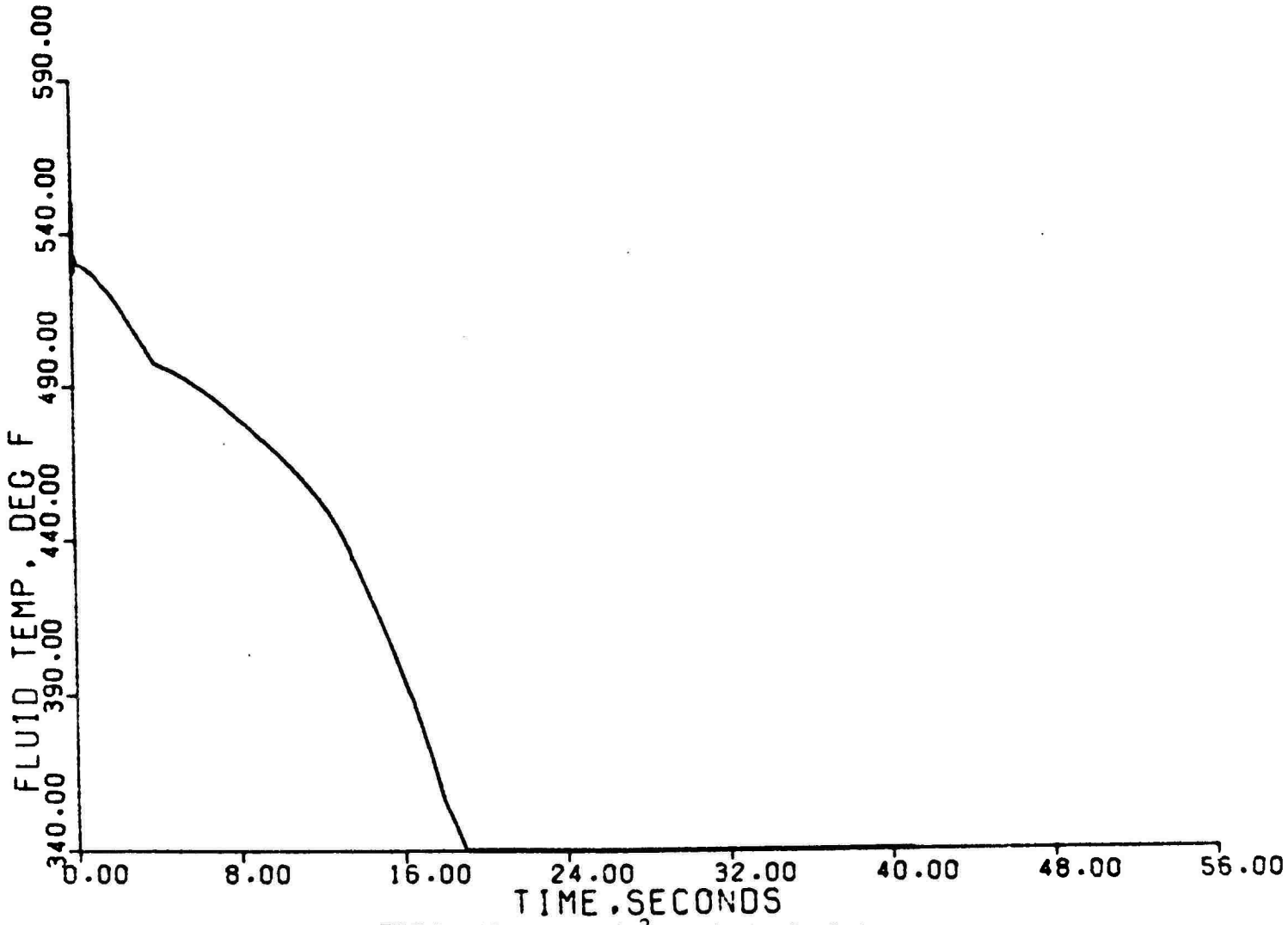

FIGURE 19C C 18 ft^2 SURGE LINE BREAK
FLUID TEMPERATURE AT HOT SPOT VS. TIME

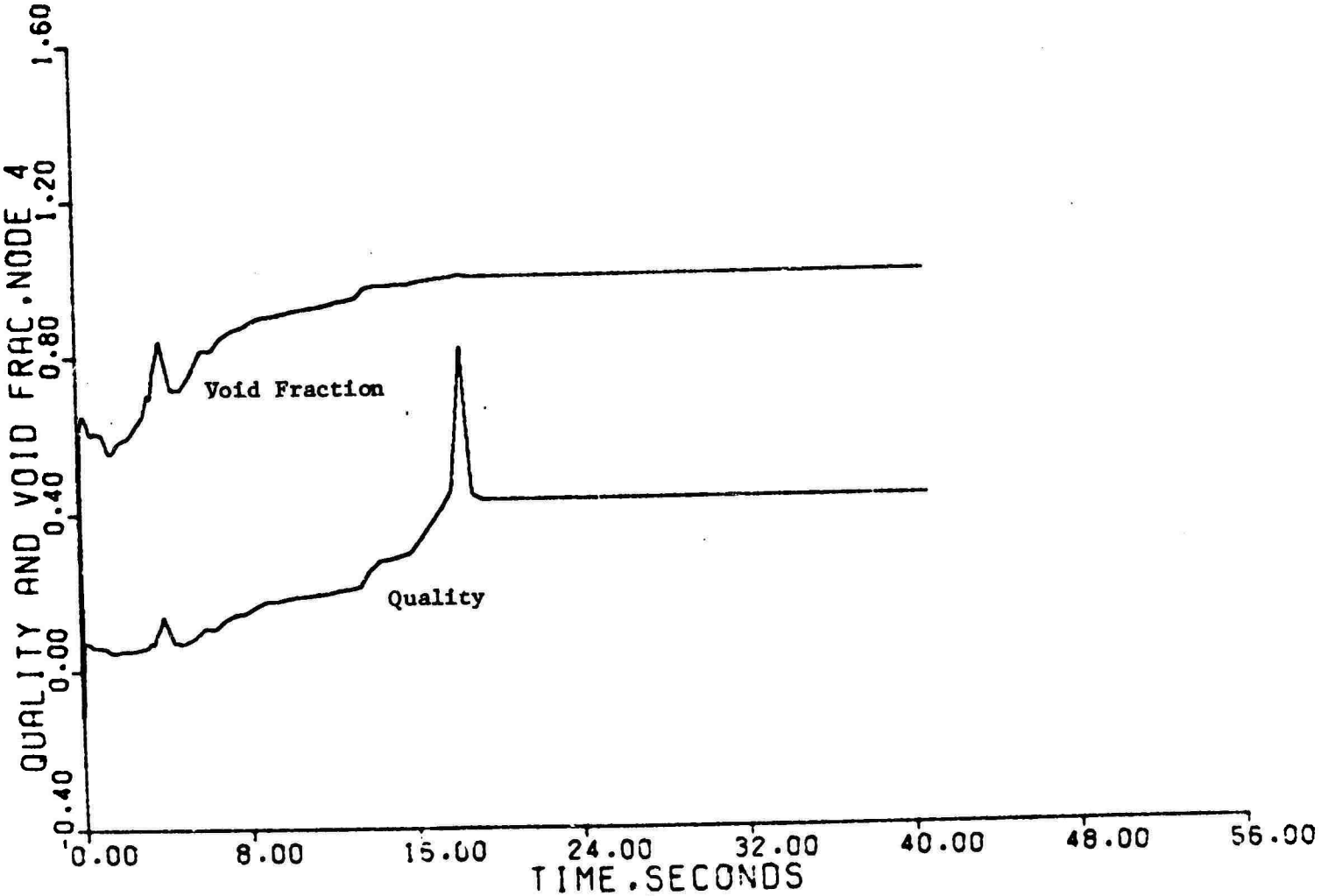

FIGURE 19D 0.18 ft^2 SURGE LINE BREAK
QUALITY AND VOID FRACTION AT HOT SPOT VS. TIME

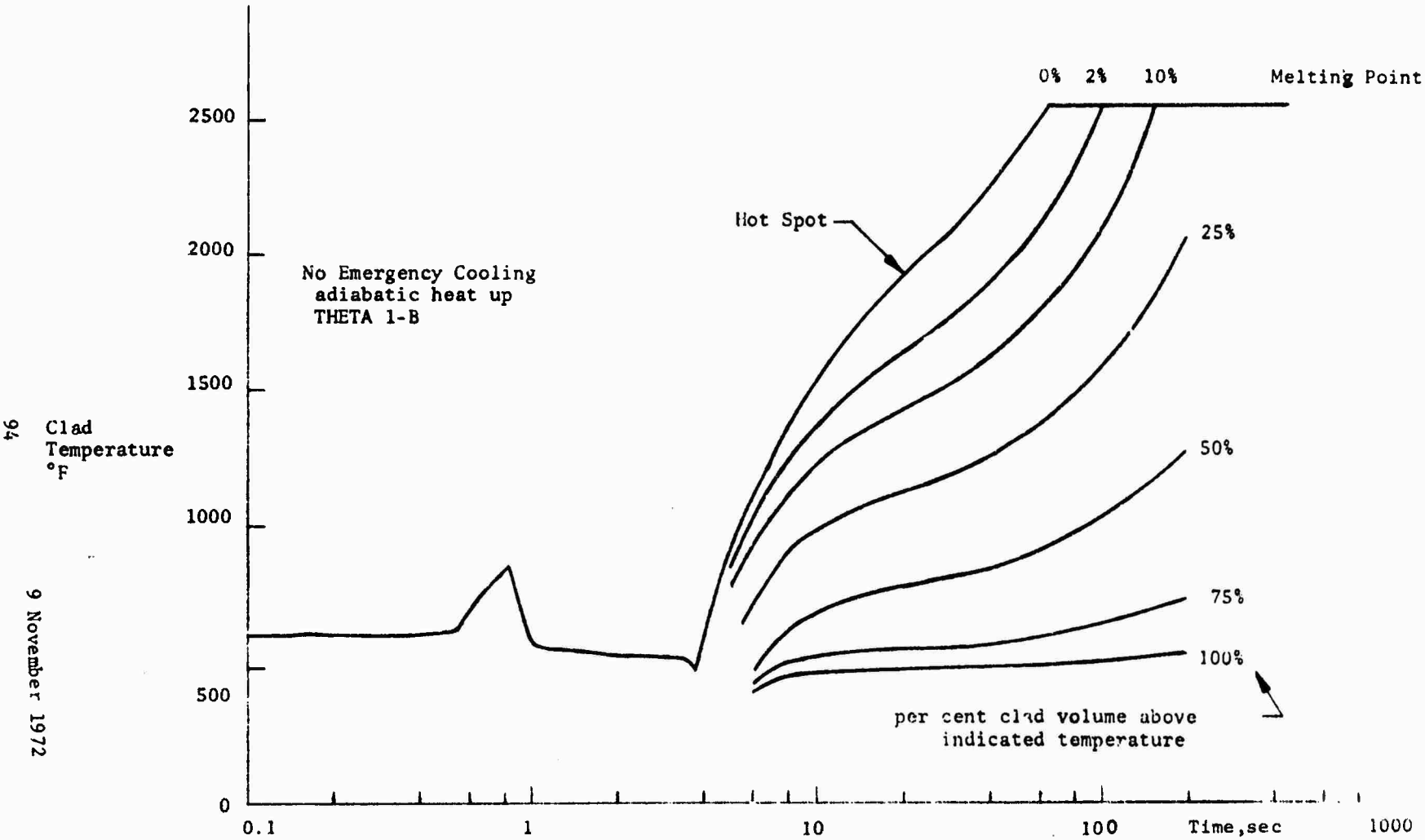

FIGURE 20. MH-1A DOUBLE ENDED HOT LEG BREAK GUILLOTINE
CLAD TEMPERATURE VS. TIME

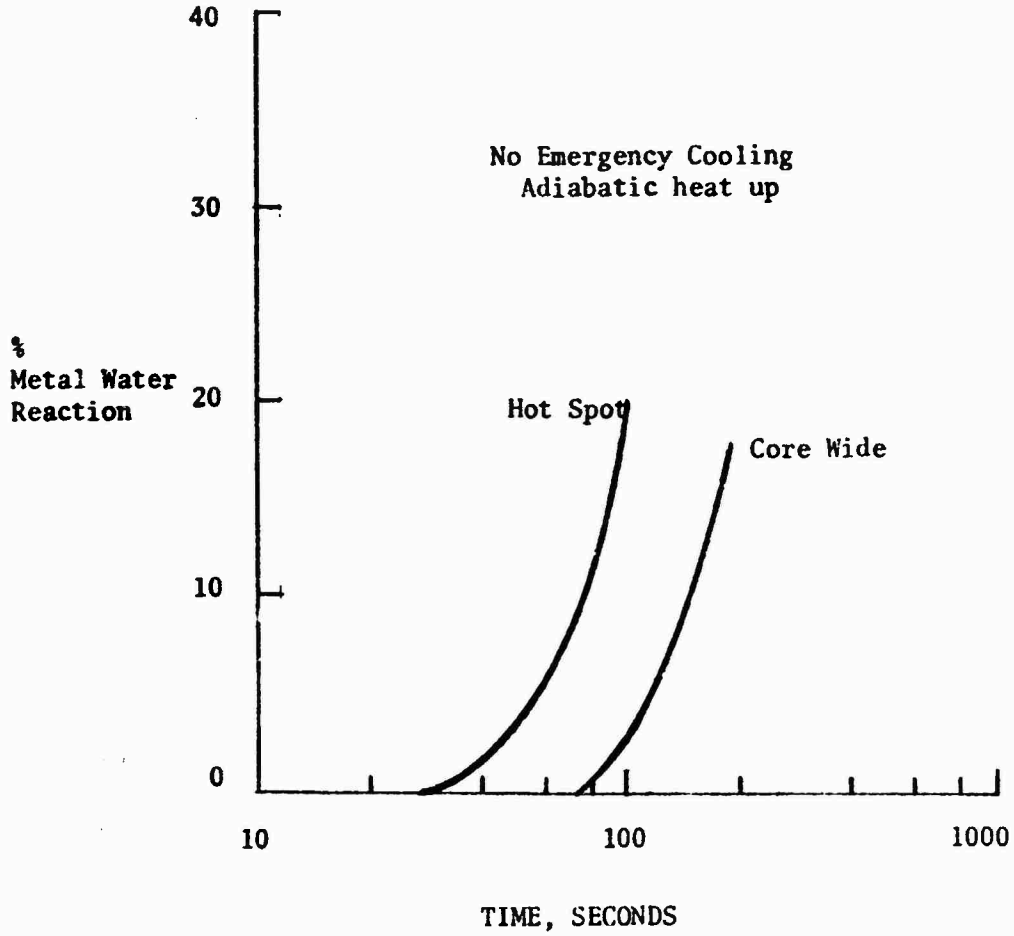

FIGURE 21. METAL WATER REACTION VS. TIME

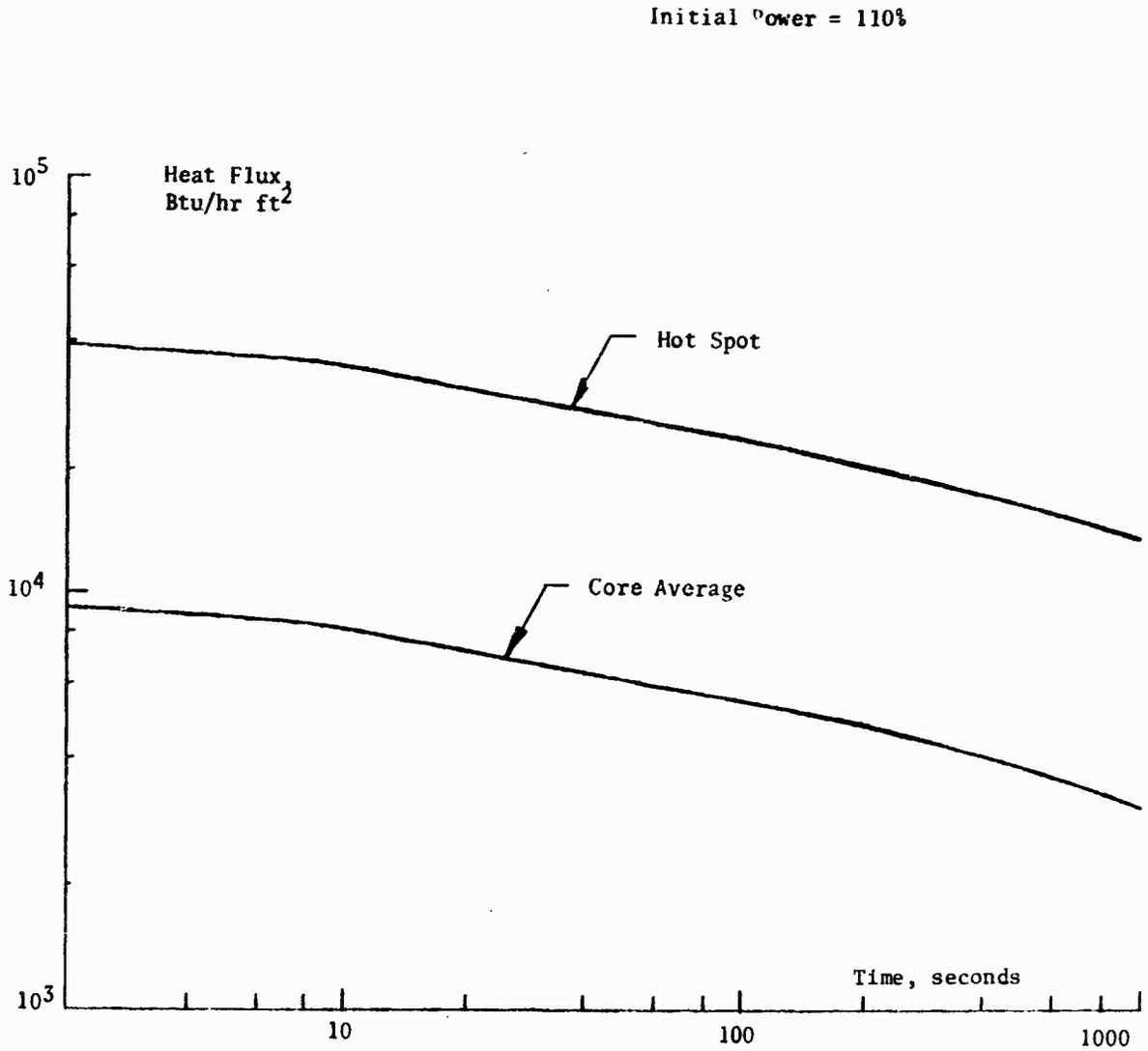

FIGURE 22. HEAT FLUX DUE TO RESIDUAL HEAT GENERATION VS. TIME AFTER SHUTDOWN

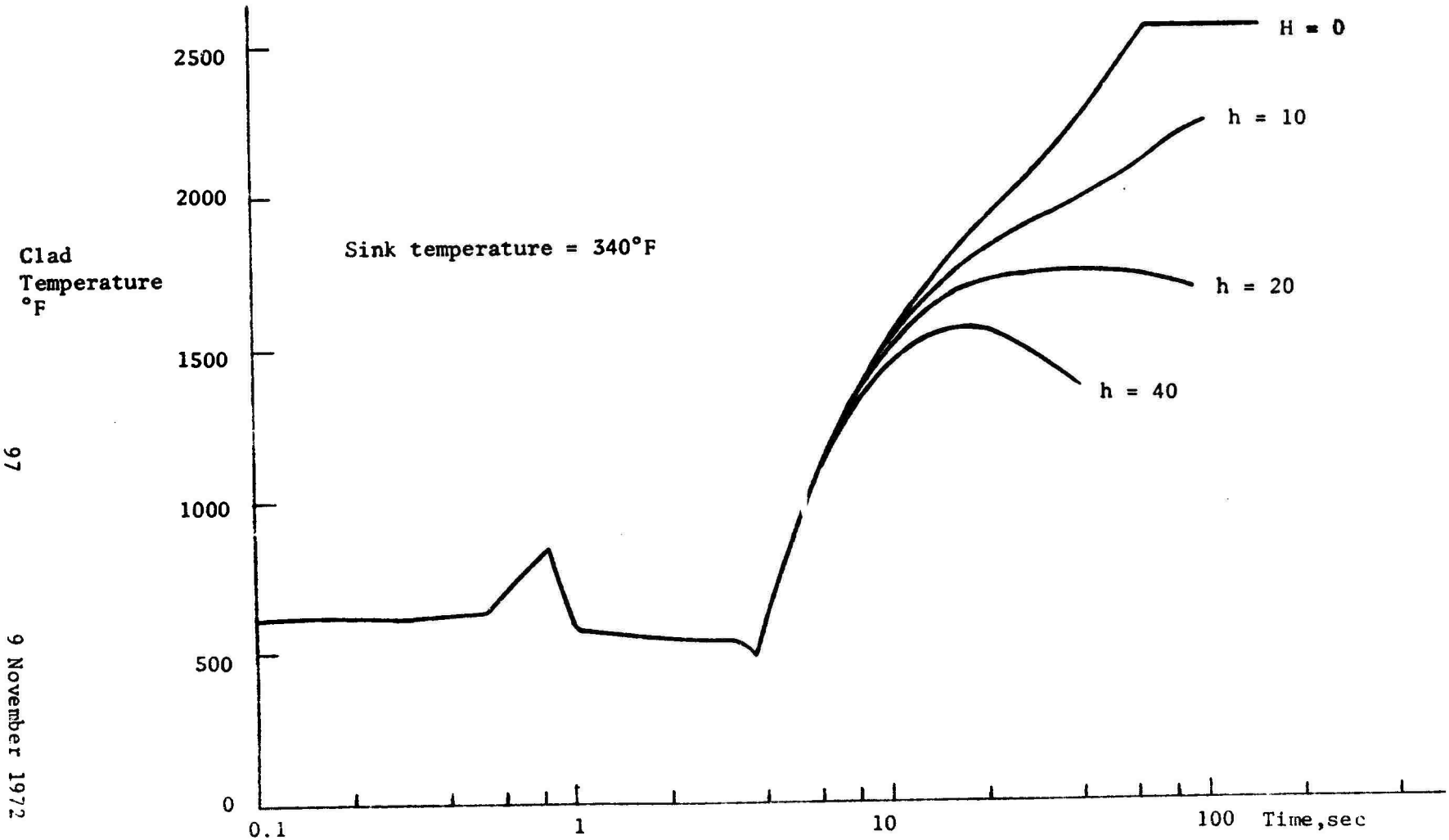

FIGURE 23. HOT SPOT CLAD TEMPERATURE VS. TIME FOR DOUBLE ENDED HOT LEG BREAK WITH VARIABLE HEAT TRANSFER COEFFICIENT

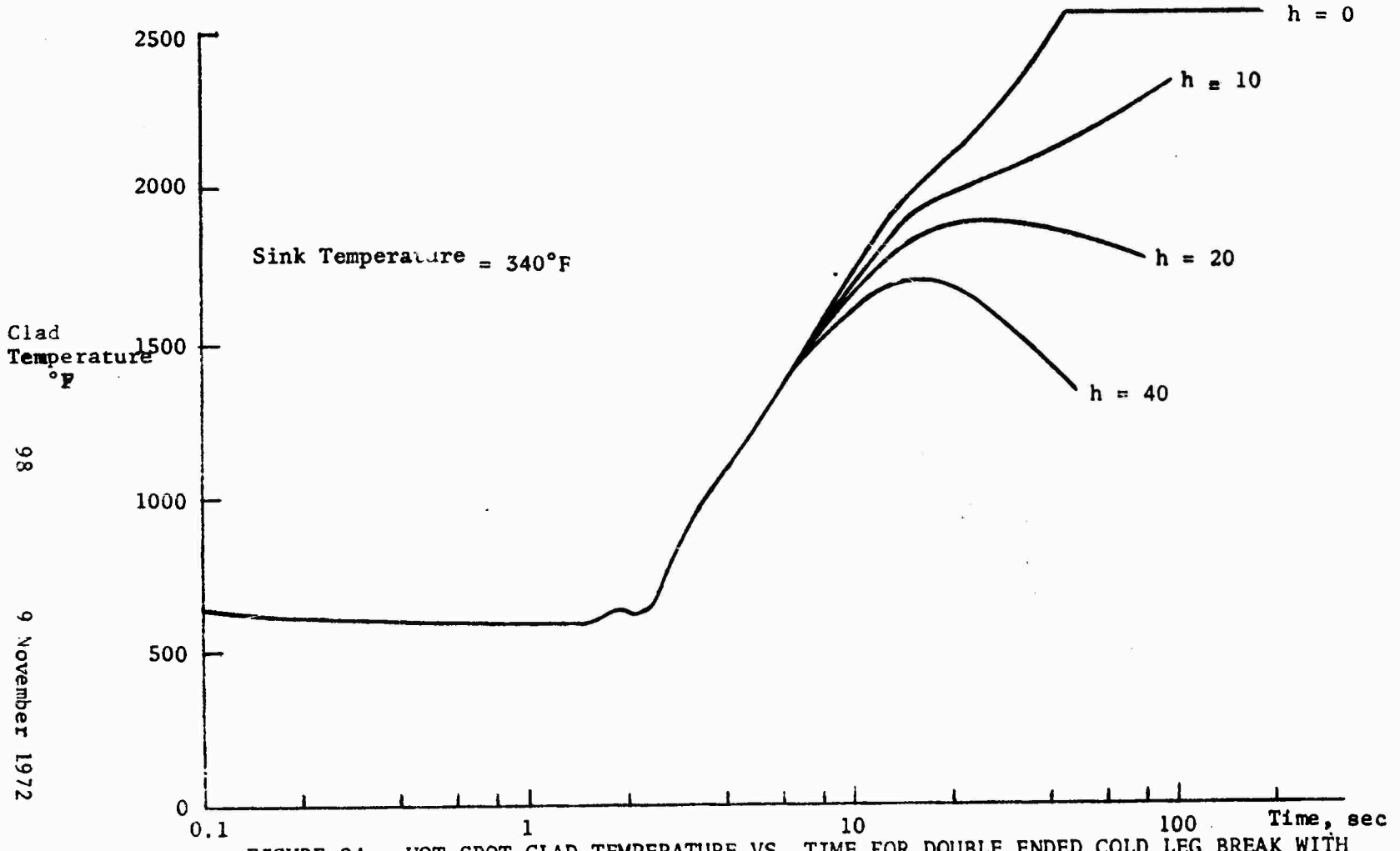

FIGURE 24. HOT SPOT CLAD TEMPERATURE VS. TIME FOR DOUBLE ENDED COLD LEG BREAK WITH VARIABLE HEAT TRANSFER COEFFICIENT

APPENDIX A

EMERGENCY CORE COOLING SYSTEM

The Emergency Core Cooling System presently installed in the MH-1A consists of emergency injection, coolant charging and decay heat removal functions performed by the Coolant Charging and Chemical Addition System. This system is activated in the event of a loss of coolant accident so as to:

a. Inject borated water into the reactor vessel in sufficient quantity to recover the core and to render the reactor subcritical with all rods withdrawn.

b. Provide emergency decay heat removal by injecting water into the reactor vessel immediately following loss of coolant.

c. Provide makeup with coolant charging pumps and long term core cooling.

A brief description of the major components and operation of the system in the event of a LOCA is presented below:

Emergency Coolant Injection. The emergency injection system is illustrated in Figure A-1. This system consists of an injection tank, twelve bottles of compressed gas, four solenoid valves, two check valves and associated piping. The emergency injection tank is a 350 cubic foot tank located on the platform deck in the reactor access compartment. The design pressure of the tank is 235 psig and design temperature is 125°F. The injection tank contains a minimum of 1000 gallons of borated water which is sufficient coolant volume to recover the core. The compressed gas is contained in twelve bottles located on the upper deck in the gas bottle storage room. The bottles are arranged in two banks of six, each bank connected to the injection tank by a line containing a solenoid valve. Upon coincident signals of low pressurizer pressure and high containment pressure, both solenoid valves open allowing the gas to pass through the pressure regulating valves and into the injection tank, thus providing the necessary pressure to force the borated water from the tank into the reactor vessel. Redundant solenoid valves assure that emergency coolant is provided if one of the valves in the pressurizing or coolant injection lines should fail.

Coolant Charging and Decay Heat Removal. The emergency coolant charging system consists of a 10,000 gallon emergency water storage tank located external to the containment vessel, piping and valves which connect the tank to the reactor vessel fill nozzle line, and two positive displacement charging pumps. Upon a LOCA actuation signal one charging pump is started automatically from the 450 volt emergency bus providing 8.5 gpm continuous makeup flow to the reactor vessel in addition to emergency coolant flow from the injection tank. There is sufficient water in the emergency water storage tank to remove the equivalent of the first five days of decay heat generation. Since the tank water can be replenished, the core can be kept submerged indefinitely. Electrical power for charging pumps is backed up by three independent diesel generators and the emergency diesel as well as onshore power when MH-1A is connected to a dependable power grid.

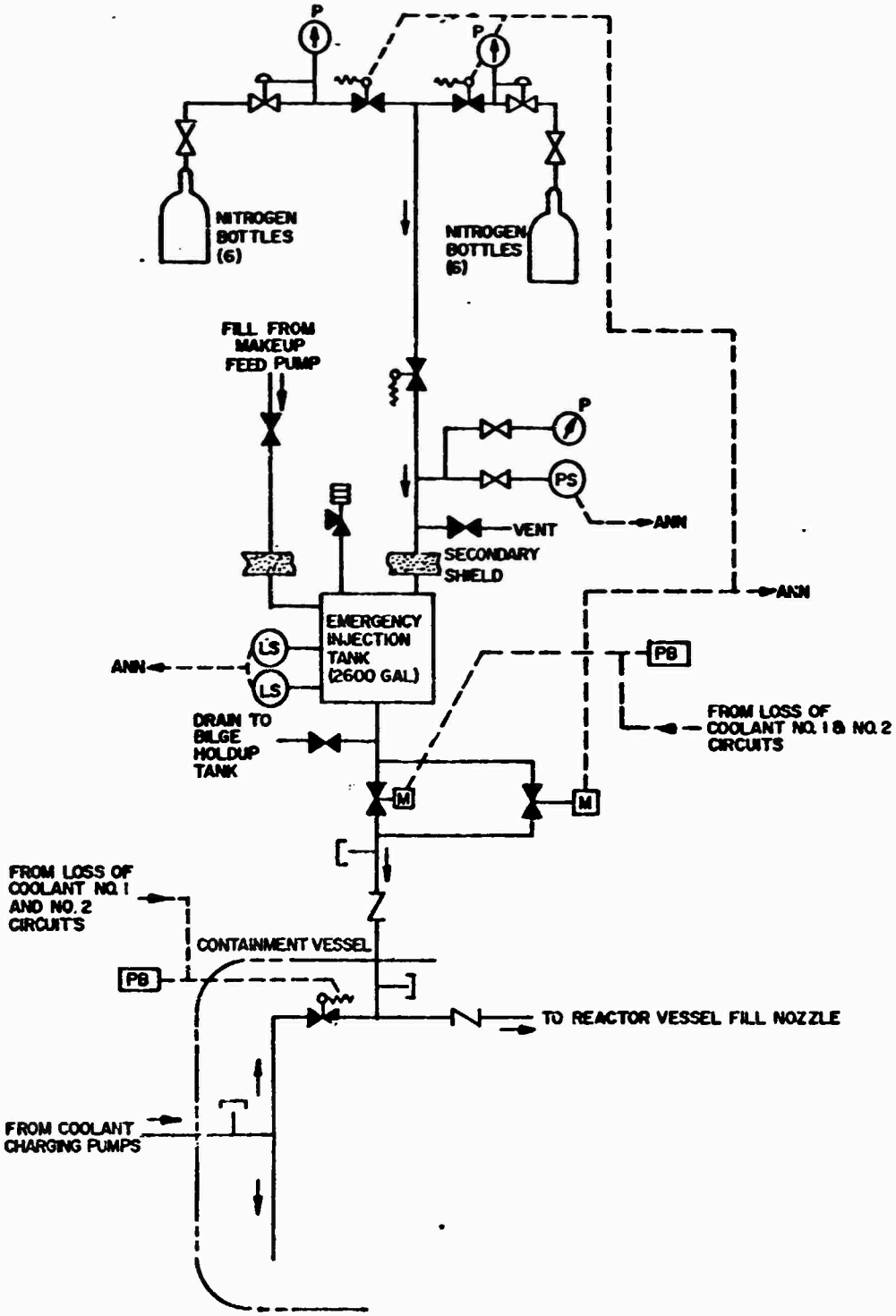

FIGURE A-1
EMERGENCY INJECTION COOLING WATER SYSTEM

APPENDIX B

PRIMARY SYSTEM GEOMETRY AND INITIALIZATION

RELAP-3 employs a one dimensional representation of the primary system in terms of fluid volume elements and junctions describing the plenums piping, reactor core, steam generator, pressurizer, and containment. Junctions can model pumps or check valves and can simulate leak or fill water sources. Input data describes the interconnection of system volumes, physical dimensions of the elements, and initial steady state conditions. Table B-1 briefly summarizes data for the MH-1A model representing a single ended hot leg slot break shown in Figure 1 of the main text. Other models are similar except for break type and location.

Appropriate data describing the initial steady state conditions in the system is supplied to the code. The initial pressure and temperatures distributions, mass flow rate, and power level are specified assuming that the power produced in the core is being removed by steam generator. Friction coefficient data required for the solution of the momentum equation is calculated internally in RELAP-3 based on the specified input pressure distribution and flow. If the initial flow through a junction is zero, then the friction coefficient is supplied. Similarly the resistance of the pumps after shutdown is provided as discussed in Appendix C.

The time dependent solution is determined in RELAP-3 by integrating the equations describing mass, energy, and momentum balances for each of the elements using the thermodynamic equations of state to obtain the fluid properties. The contents of volume elements during blowdown are assumed to be homogeneous. Fluid properties are considered uniform with the pressure occurring at the center of gravity. Various effects such as pump characteristics, reactivity feedback, choked flow, core and steam generator heat transfer, and safety injection are taken into account during the transient solution.

TABLE B-1

SUMMARY OF RELAP-3 INPUT DATA FOR MH-1A MODEL

SINGLE ENDED HOT LEG BREAK

Volume Data

Volume No.	Description	Volume (ft^3)	Elevation* (ft)	Initial Pressure (psia)
1	Reactor Inlet Plenum	64	0.0	1508
2	Core Volume 1	7.3	4.41	1507
3	Core Volume 2	7.3	5.14	1507
4	Core Volume 3	7.3	5.88	1507
5	Core Volume 4	7.3	6.62	1506
6	Reactor Outlet Plenum	74	7.36	1502
7	Hot Leg Piping	19	7.56	1500
8	Pressurizer	138	6.24	1500
9	Surge Line	4.9	7.78	1500
10	Steam Gen. Inlet	18	7.63	1498
11	Tube Volume 1	5.1	10.21	1497
12	Tube Volume 2	5.1	12.34	1496
13	Tube Volume 3	5.1	14.47	1495
14	Tube bends 4	7.3	16.60	1493
15	Tube Volume 5	5.1	14.47	1490
16	Tube Volume 6	5.1	12.34	1489
17	Tube Volume 7	5.1	10.21	1488
18	Steam Gen. Outlet	15	7.63	1485
19	Cold Leg Piping	16	7.63	1516
20	Reactor Downcomer	44	0.0	1508
21	Primary Containment	23016	0.0	15

*Dimension from reference level to lower elevation of volume

TABLE B-1 (cont'd)

SUMMARY OF RELAP-3 INPUT DATA FOR MH-1A MODEL

SINGLE ENDED HOT LEG BREAK

Junction Data

Junction No.	From Volume	To Volume	Minimum Flow Area (ft^2)	Junction Height (ft)
1	1	2	9.67	4.4
2	2	3	9.67	5.2
3	3	4	9.67	5.9
4	4	5	9.67	6.6
5	5	6	9.67	7.4
6	6	7	0.667	9.1
7	8	9	0.18	8.2
8	9	7	0.18	8.2
9	7	10	0.667	8.0
10	10	11	2.38	10.2
11	11	12	2.38	12.3
12	12	13	2.38	14.5
13	13	14	2.38	16.6
14	14	15	2.38	16.6
15	15	16	2.38	14.5
16	16	17	2.38	12.3
17	17	18	2.38	10.2
18	18	19	.473	8.1
19	19	20	.667	9.1
20	20	1	1.046	0.32
21	(Fill System)	20	0.0089	11.6
22	7	21	0.667	9.5

Initial Parameters

Power	49.5	MW_t
Coolant heating rate	1.69×10^8	Btu/hr
Flow rate	1080	lb/sec
Total mass	18,407	lb
Total energy	1.03×10^7	Btu

APPENDIX C

PUMP REPRESENTATION

The effects of the reactor coolant pumps on the system blowdown are represented in the analysis. The primary effects simulated include the pump head versus flow characteristics, pump cavitation, coastdown following pump trip, and flow resistance across the pumps after shutdown. The reactor coolant pumps in the MH-1A consist of two single stage centrifugal pumps connected in parallel by a piping volute assembly. Table C-1 shows the nominal speed pump head versus flow curve for parallel performance used to represent the primary pumps in RELAP-3. This curve is based on the manufacturer's test data (reference 3) conservatively extended to the range of flows encountered in a LOCA.

The loss of effectiveness of the pumps due to cavitation and flow coastdown (if pump trip is assumed) is evaluated in RELAP-3 from the following equation:

$$\Delta p_{Pump} = \frac{\rho_\ell}{144} \Delta p_{pump}(w) \cdot f_1 \cdot f_2 \qquad \text{(C-1)}$$

where:

$\Delta p_{pump}(w)$ = normal pump head from flow characteristic curve, ft

ρ_ℓ = fluid density at pump junction, lb/ft^3

f_1 = $1.0 - F_1 (P_D - P_1)^2$, loss of effectiveness $0 \leq f_1 \leq 1.0$

F_1 = cavitation constant (empirical)

P_D = pressure at inception of cavitation

= $P_v + F_2 \rho_\ell / 144$

P_v = vapor pressure at pump inlet, psia

F_2 = NPSH, ft

f_2 = pump coastdown multiplier

The term f_2 simulates the loss of effectiveness due to pump coastdown and is applied if loss of power to the pumps is assumed. If no pump trip occurs then f_2 remains equal to one. The coastdown multiplier for loss of power to both pumps was developed from an approximation of the pump characteristics and is consistent with flow coastdown reported in Reference 11. The shutdown resistance of the pumps following flow coastdown was determined from manufacturer's test data and is defined in RELAP-3 as:

$$k_s = \frac{[\Delta p \text{ pump}]\ \rho L}{|w_i|\ |w_i|}$$

where:

Δp pump = pump pressure differential, psi

ρ_L = coolant density at pump junction, lb/ft^3

w_i = average flow across pump junction, lb/sec

k_s = pump shutdown resistance

Table C-2 shows calculated shutdown resistances based on the above equation for various pump impeller conditions. Also shown are additional parameters used to represent the MH-1A coolant pumps in the analysis. The pump net positive suction head (NPSH) specified by the manufacturer was assumed and a conservative cavitation constant was selected so as to result in a rapid loss of effectiveness upon cavitation.

TABLE C-1

MH-1A NOMINAL SPEED PUMP HEAD VERSUS FLOW INPUT DATA
(Parallel Performance)

Flow gpm	Head ft
-8000	170
+2000	160
4000	152
6000	144
8000	132
10,200	110
12,000	80
14,000	44
16,000	0
100,000	0

TABLE C-2

MH-1A PRIMARY COOLANT PUMP DATA

Number of Pumps	2
Type	Centrifugal
Pump NPSH, ft	100
Cavitation constant (empirical)	.0018
Pump shutdown resistance* (490°F)	
Free rotors	5.0×10^{-4}
One locked rotor	7.9×10^{-4}
Two locked rotors	10.8×10^{-4}

*From equation C-2 based on manufacturer's test data.

APPENDIX D

REACTOR KINETICS

The reactor kinetics calculation in RELAP-3 is a point kinetics model with appropriate reactivity feedback effects. The standard reactor kinetics equations used in the program are:

$$\frac{dn}{dt} = \frac{\beta^*}{\ell^*}\left[\frac{\rho}{\beta^*} - 1\right] n + \sum_{i=1}^{6} \lambda_i C_i$$

$$\frac{dC_i}{dt} = -\lambda_i C_i + \frac{\beta_i^*}{\ell^*} n$$

where:

t = time, sec

n = reactor fission power, Btu/sec

ρ = total reactivity, $\Delta k/k$

β_i^* = effective delayed neutron fraction of the i^{th} group

β^* = effective delayed neutron fraction

λ_i = decay constant of i^{th} delayed neutron group, sec^{-1}

ℓ^* = neutron generation time, sec

C_i = precursors concentration for i^{th} delayed neutron group

Also included is a determination of gamma heating due to decay of the fission products. The total power is calculated as the sum of the contributions from the instantaneous fission rate and decay of the fission products. All power is assumed to be generated in the fuel elements, direct gamma heating of the coolant not being considered.

The major reactivity feedback effects included in the kinetics equations are contributions from control rod motion, moderator voids, moderator temperature, and Doppler broadening. The reactivity is input either explicitly as a function of time as with reactivity insertion due to reactor trip or implicitly through core feedback mechanisms determined from coolant density, coolant temperature, and fuel temperature for each core volume. The total reactivity is determined by summing up the individual contributions. The initial value of reactivity is assumed to be zero corresponding to a

steady-state equilibrium condition. Reactivity feedback from the moderator temperature and voids is expressed in terms of a linear negative feedback coefficient chosen so as to result in a conservative power transient during blowdown. Nonlinear Doppler feedback is input in the form of a curve of reactivity versus effective fuel element temperature based on the Doppler coefficient shown in Figure D-1. Table D-1 summarizes the reactivity coefficients and nuclear constants which were used to represent the MH-1A in the reactor kinetics calculations in RELAP-3. The dominant influence on the core power transient results from the moderator void feedback coefficient and this coefficient is input as a conservatively low negative value.

TABLE D-1

REACTOR KINETICS DATA FOR MH-1A CORE

ℓ^*	Mean neutron lifetime, sec	1.3×10^{-5}
β^*	Effective delayed neutron fraction	.007015
β_1	Effective Neutron Fraction for i^{th} Group	.00027
β_2		.00149
β_3		.00132
β_4		.00285
β_5		.00090
β_6		.00018
λ_1	Decay Constant for i^{th} Group, sec^{-1}	.0127
λ_2		.0317
λ_3		.115
λ_4		.311
λ_5		1.40
λ_6		3.87
α_T	Moderator Coefficient (BOL) dk/°F	
	zero power (68°F)	-0.6×10^{-4}
	full power (490°F)	-2.5×10^{-4}
α_D	Doppler Coefficient (See Fig. D-1) dk/°F (UO_2)	
	zero power (68°F, 0 MW)	-2.6×10^{-5}
	full power (490°F, 45 MW)	-1.6×10^{-5}
α_V (1)	Void Coefficient dk/% void	-2.2×10^{-3}

(1) Nominal value - reduced by 25% in analysis

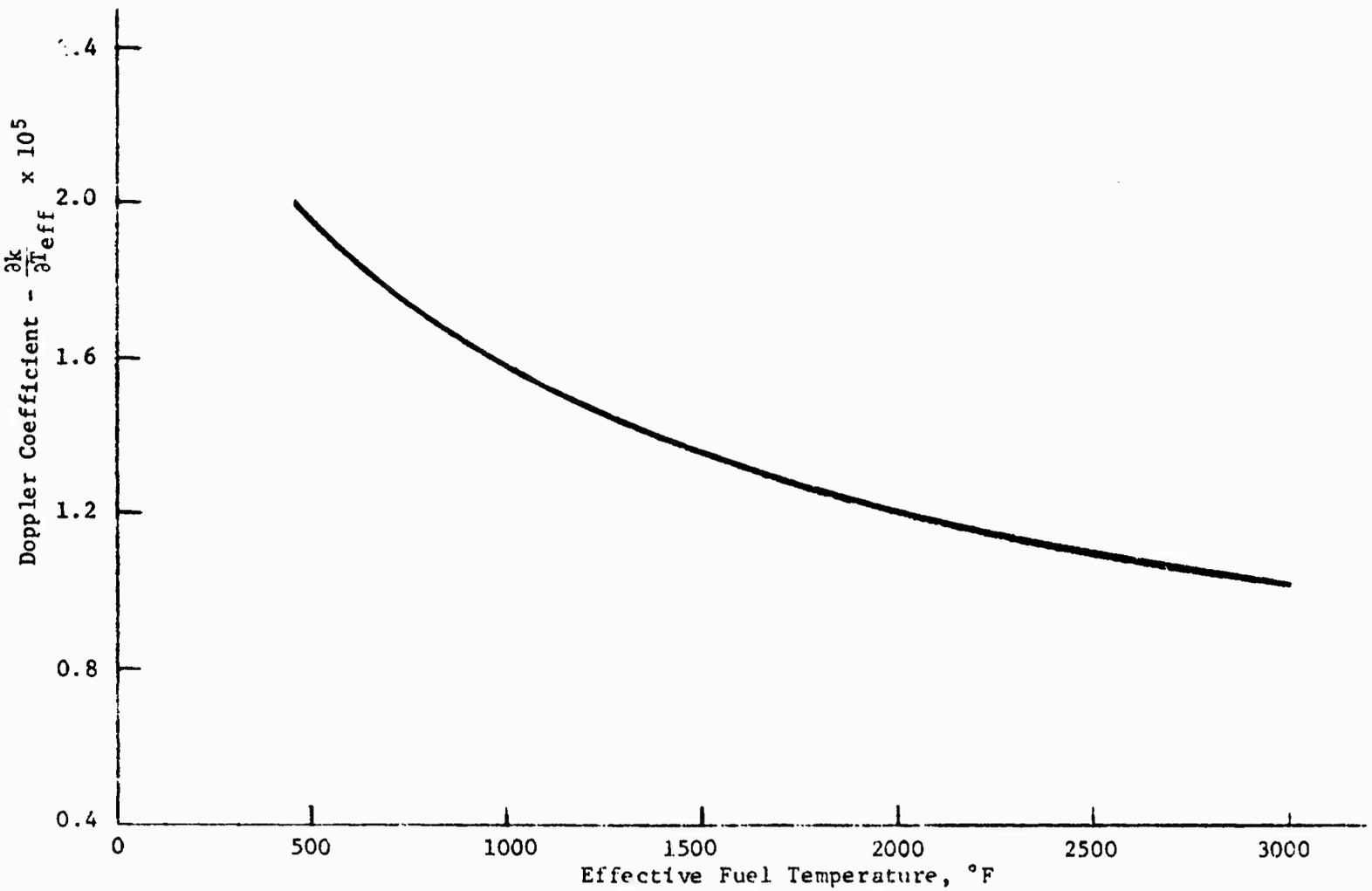

FIGURE D-1 DOPPLER COEFFICIENT VS EFFECTIVE FUEL TEMPERATURE

APPENDIX E

TIME STEP SIZE

RELAP-3 utilizes a forward finite difference approximation as its numerical advancement technique. Since the same time step size is used for all volumes and junctions, the stability of the solution is controlled by the most sensitive element of the model. The time step size must be smaller than the natural oscillation period of this element by a factor of 5 to 10 or numeric instabilities can result. An appropriate time step is given by:

$$\Delta t = (2\pi/na)\sqrt{V\,\ell/A}$$

where

n = 5 to 10

a = Velocity of sound in medium contained in volume

V = Volume of fluid

ℓ/A = Path inertia

In the analysis the most restrictive element was determined for each model and the time step for stability was calculated using the element dimensions and the acoustic velocity of the fluid in the element. A factor of $n = 10$ was used. The accuracy of the computer solution was verified by reducing the time step by one half and observing the calculated results. Comparison of the initial core flow rates and fuel temperatures showed no significant differences. Increasing the time step above the criterion resulted in numerical instability. Other cases used initial time steps consistent with the stability criterion with the factor $n = 10$ to reduce the time step below the natural frequency.

Later in the problem solution, other types of numeric instability due to mass and energy flow could occur. The time steps in this region of the problem were selected so as to prevent the fluid mass or energy transfer during a time increment from becoming large relative to mass or energy contents of the element.

APPENDIX F

FUEL ROD PROPERTIES

The variation of fuel rod properties with temperature was considered in the analysis. The high temperature property data incorporated in THETA 1-B is summarized in Table F-1 and Figures F-1 and F-2. The figures show the thermal conductivity and heat capacity of stainless steel and UO_2 fuel, respectively. Data for stainless steel was taken from Reference 23. The temperature dependent conductivity was based on composite data for austenitic stainless steel with the error considered $\pm$ 5 percent. Above 1330°F the thermal conductivity was conservatively assumed constant since the rate of increase may be limited by oxide formation. The heat capacity of the cladding was computed based on the chemical composition of the alloy assuming 18 percent chromium and 8 percent nickel with the remainder being iron. Heats of transformation corresponding to phase changes in Fe were assumed at temperatures of approximately 1400 and 1670°F. The melting temperature of the cladding was taken as 2550°F, the recommended lower limit for austenitic stainless steel. The UO_2 property data in THETA 1-B was based on the information in Reference 23. The correlations used in the code are reported in Reference 8.

TABLE F-1

HIGH TEMPERATURE PROPERTY DATA OF FUEL ELEMENT MATERIALS

		Stainless Steel (Ref. 23)	UO_2 (Ref. 8,23)
1.	Melting point, °F	2552-2659	5072
2.	Latent heat of fusion Btu/lb	Cr 121 Fe 119 Ni 129	67.5 $\pm$ 1.8
3.	Coefficient of thermal expansion in/in °F	1.12×10^{-5} mean coefficient (32 - 1832°F)	$3.72 \times 10^{-6}+1.787 \times 10^{-9}$ T T in °F (32-4082°F)
4.	Density @ 77°F, lb/ft^3	493	650 (95% theoretical density)
5.	Thermal conductivity Btu/hr ft°F	(32-1364°F) Fig. F-1	Fig. F-2
6.	Heat capacity, Btu/lb°F	Fig. F-1	Fig. F-2

///

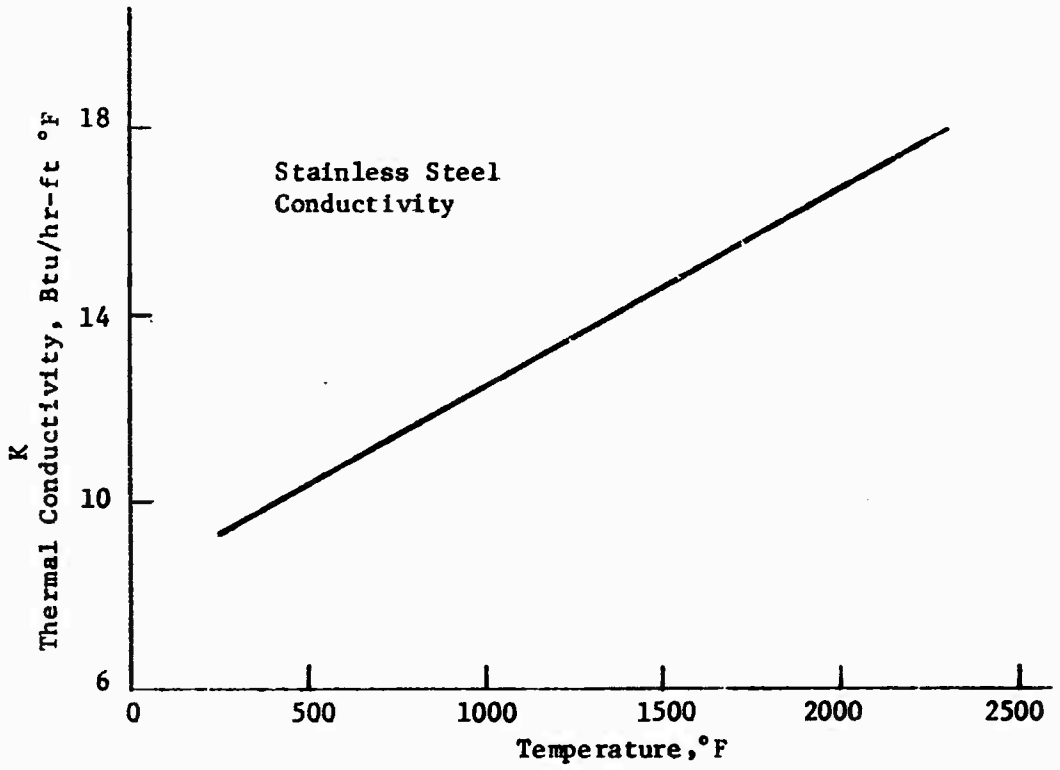

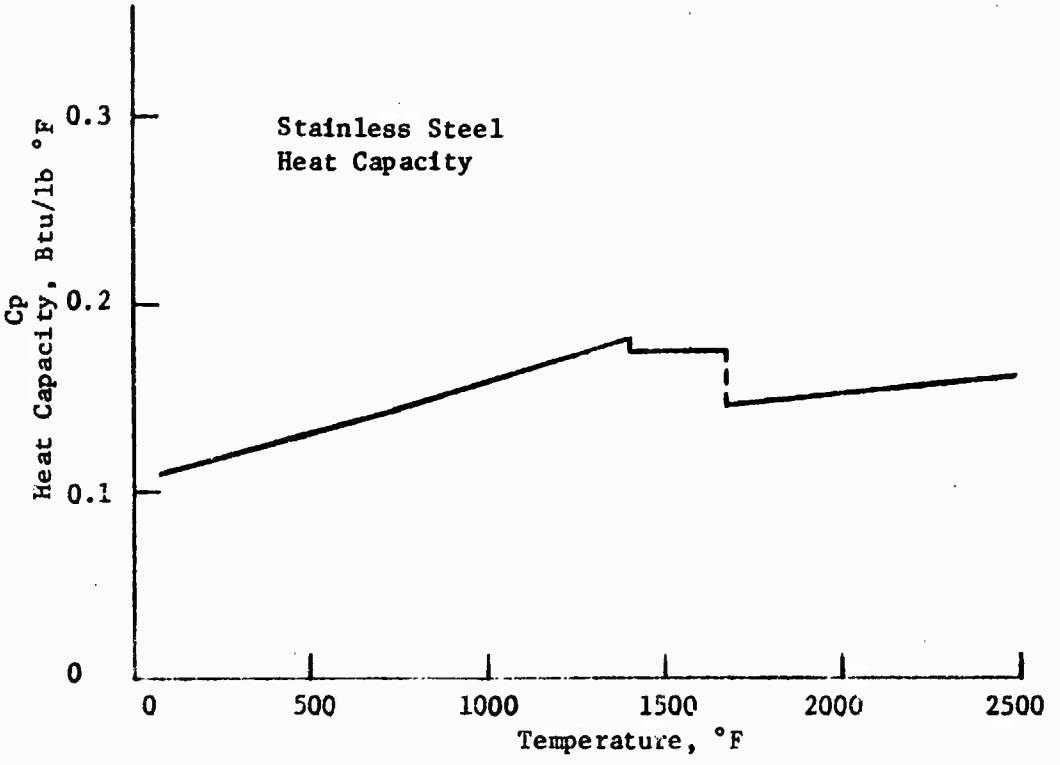

FIGURE F-1 STAINLESS STEEL CONDUCTIVITY AND HEAT CAPACITY VS TEMPERATURE

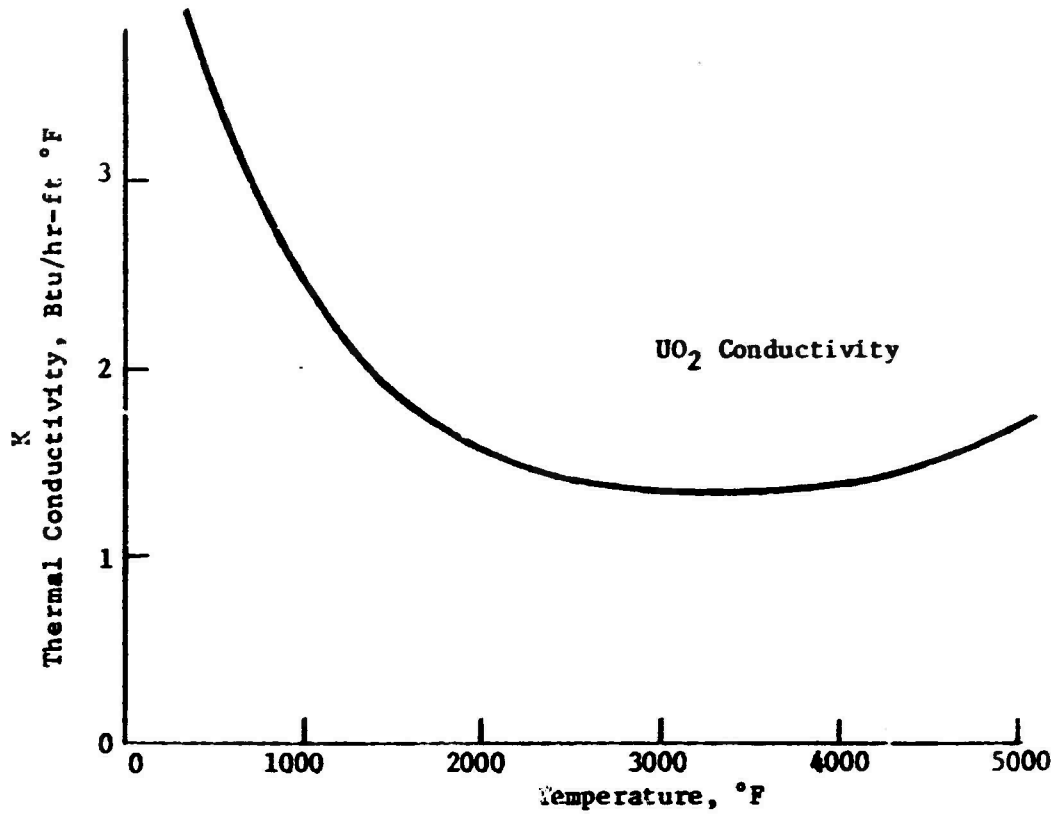

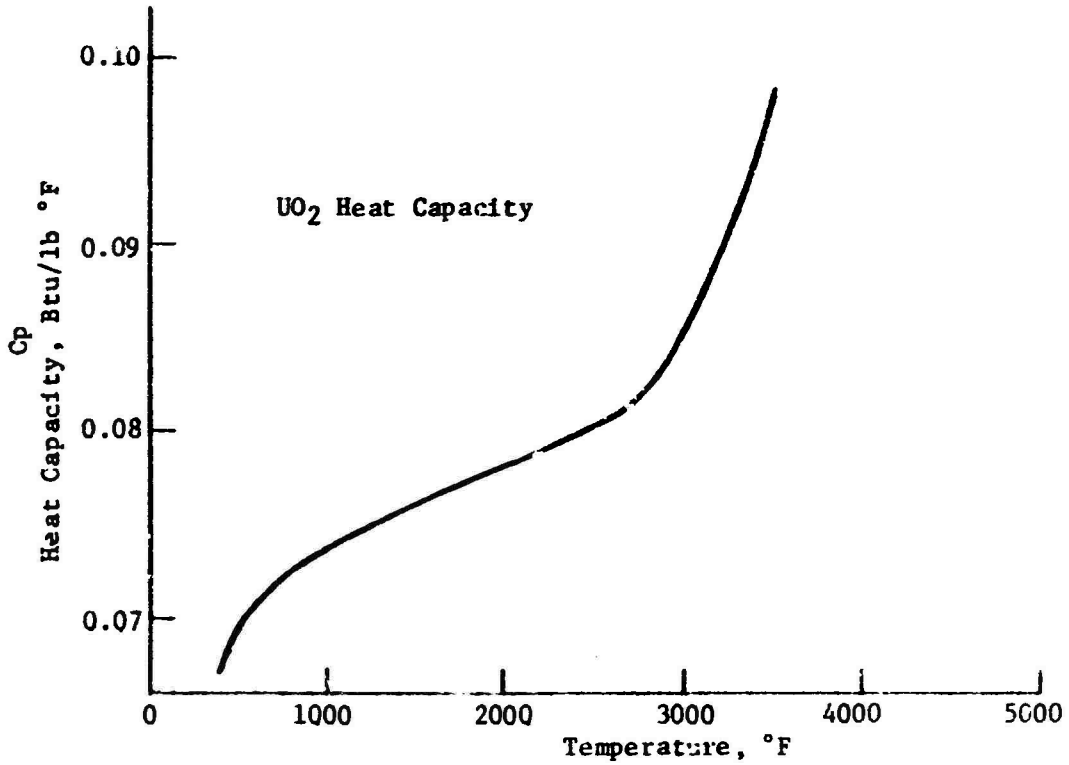

FIGURE F-2 UO_2 CONDUCTIVITY AND HEAT CAPACITY VS TEMPERATURE

APPENDIX G

METAL WATER REACTION

When raised to high temperatures in the presence of steam or water vapor, stainless steel cladding can react with steam to form metal oxides and hydrogen. This reaction is exothermic and the energy release can contribute to the clad temperature transient. The effects of the stainless steel - water reaction are represented in THETA1-B by means of the parabolic rate law. The reaction between stainless steel and steam proceeds relatively slowly at low temperatures, but the rate rapidly increases as metal approaches its melting temperature. The recommended equation for stainless steel (Reference 23) in terms of the weight gain due to oxidation of the clad above 1800°F is:

$$w^2/t = 2.4 \times 10^{12} \exp\left[\frac{84{,}300 \pm 2400}{RT}\right], \ mg^2\ (O)/cm^4 sec \qquad (G\text{-}1)$$

where w is the weight gain (oxygen) per unit surface area in mg/cm^2, t is the time in seconds, R is the gas constant in cal/mole °K, and T is the absolute temperature. The heat of reaction for the above process is about 254 cal/gm of stainless steel oxidized in the solid state (Reference 24). For purposes of analysis the major reaction product formed is assumed to be Fe^3O^4 although other oxides may be present. In THETA1-B the rate equation is expressed in terms of the amount metal reacted as follows:

$$\frac{dr}{dt} = \frac{K}{(r-r_o)} \exp(-\Delta E/RT), \ in/sec \qquad (G\text{-}2)$$

where: r = radius of unreacted metal in clad, in
r_o = original radius of unreacted clad, in
t = time, seconds
K = rate law constant, in^2/sec
ΔE = activation energy, cal/mole
R = gas constant, cal/mole °K
T = cladding temperature, °K

In the above relation, $(r-r_o)$ represents the oxide layer which retards the reaction in proportion to its thickness. The rate constant (K) is related to the pre-expotential factor of the rate equation (A) as follows:

$$K = \frac{A}{2\rho m^2 (2.54)^2}, \ in^2/sec \qquad (G\text{-}3)$$

where A is expressed in terms of mass of metal (Fe) reacted per unit surface area per sec quantity squared in gm^2/cm^4sec^2 and ρ_m is the density of stainless steel in gm/cc. At relatively high temperatures the reaction may be limited by the availability of steam at the oxide surface. For conservatism no steam limiting is permitted, in the analysis, i.e., the rate of reaction is assumed to equal the rate calculated by equation G-2. At temperatures approaching the melting point of stainless steel (~2550°F) a sudden rapid increase in surface area and reaction rate is observed. For engineering purposes it is conservatively assumed that 100 percent reaction occurs if the cladding reaches the melting temperature. Actually the percent reaction would again be limited by diffusion of steam to the reacting surface. Table G-1 summarizes the metal water reaction constants used in the analysis.

TABLE G-1

METAL WATER REACTION CONSTANTS

Material	Stainless Steel
Melting point, °F	2550
Density, gm/cc	8
Heat of reaction, cal/gm	254
Ratio of mass of Fe to mass of oxygen reacted	2.61
ΔE activation energy, cal/mole	84,300 ± 2400
K rate law constant, in^2/sec	1.985×10^4
R gas constant, cal/mole °K	1.987